Titre: Title:	Mixing Studies in a Co-Kneader
Auteur: Author:	Maria Magdalena Brito Bazan
Date:	2011
Type:	Mémoire ou thèse / Dissertation or Thesis
Référence: Citation:	Brito Bazan, M. M. (2011). Mixing Studies in a Co-Kneader [Ph.D. thesis, École Polytechnique de Montréal]. PolyPublie. https://publications.polymtl.ca/590/

UNIVERSITÉ DE MONTRÉAL

MIXING STUDIES IN A CO-KNEADER

MARIA MAGDALENA BRITO BAZAN

DÉPARTEMENT DE GÉNIE CHIMIQUE

ÉCOLE POLYTECHNIQUE DE MONTRÉAL

THÈSE PRESENTÉE EN VUE DE L'OBTENTION

DU DIPLÔME DE PHILOSOPHIAE DOCTOR (Ph. D.)

(GÉNIE CHIMIQUE)

JUIN 2011

UNIVERSITÉ DE MONTRÉAL

ÉCOLE POLYTECHNIQUE DE MONTRÉAL

Cette thèse intitulée:

MIXING STUDIES IN A CO-KNEADER

Présentée par: BRITO BAZAN Maria Magdalena

en vue de l'obtention du diplôme de: Philosophiae Doctor

a été dûment acceptée par le jury d'examen constitué de:

Mme. HEUZEY Marie-Claude, Ph. D., Présidente

M. TANGUY Philippe, Ph. D, Membre et directeur de recherche

M. FRADETTE Louis, Ph. D., Membre et codirecteur de recherche

M. AJJI Abdellah, Ph. D., Membre

M. HRYMAK Andrew N., Ph. D., Membre

To my parents, Edmundo and Mary.

To Estefania, Alexa and Alan.

ACKNOWLEDGEMENTS

I would like to express my gratitude to my advisor Prof. Philippe Tanguy. He has supported and guided me since I started to develop an interest in a scientific career, almost ten years ago. Thank you for believing in me and for trusting my capacity to lead this project.

Thank you to my co-advisor, Prof. Louis Fradette, for his counsel, advices and insights, and for his willing disposition.

The help and support I received from Mourad Heniche regarding the numerical part of this project is greatly acknowledged. I thank also his interest and encouragement during this time.

Thank you to the staff of the Department of Chemical Engineering at Ecole Polytechnique. To the team of technicians for their support regarding the experimental setup, particularly Jean Huard, Carol Pinchaud and Robert Delisle. To all past secretaries at the URPEI for their help during administrative procedures, Michelle Rozon, Marlene Bois and Josiane Archambault, and more recently Diane Pimparé. Thank you also to the past and present members of the URPEI.

The financial support of CONACYT (Mexico) during the realization of this project is greatly acknowledged.

Very special thanks to my “mexican connection” friends: Christian Rivera, Lionel Mendez and Enrique Mateos. I will never forget the time we shared here in Montreal filled with good moments, laughs, and your intensive courses on football and soccer. Thank you also for the support and help during difficult times. Thanks also to Hilda Garza for her friendship, daily visits to the office and cheers this last couple of years. I would also like to thank Julio Morales and Rodrigo Sanchez, for the many good times we shared.

I would like to thank Alfa Arzate and Monica Cordoba for their friendship, advices and for welcoming me into their family when I could not be with mine.

Thanks to Zoe Perin-Lavasseur and Mariya Marinova, for their company, words of encouragement and support during these last years. Thanks also to Xiao Wang for his good humor at the office and lab.

Thank you to my friends back in Mexico. Margot Crucet and Dafne Sanchez, thank you for always being there.

Lastly but most importantly, I would like thank my family. My father, Edmundo Brito, taught me by example to be passionate about my work. He planted the researcher seed in me by teaching me to always question things and he inherited me his love for engineering. My mother, Mary Bazan is my example of strength and perseverance. She has always known how to comfort me and she is simply the best mother I could have. Estefania and Alexa, because aside from being my sisters, they are also my friends, and Alan, my nephew for his great hugs and laughs. Thank you for everything you have given me, for your support, for believing in me and for your love.

RÉSUMÉ

Le mélange est une opération de base très utilisée dans plusieurs industries y compris celles du pétrole, des polymères, pharmaceutique, alimentaire, agricole, etc. Jusqu'à ce jour, les connaissances sur cette opération peuvent être encore considérées comme un art plutôt que basées sur des preuves scientifiques. Ainsi, de nombreux dispositifs de mélange utilisés dans la pratique industrielle sont toujours conçus et opérés en suivant une approche d'essai-erreur. Cela est aussi le cas des extrudeuses à vis. Toutefois, dans un environnement très concurrentiel où il y a une demande croissante de produits et procédés qui soient fonctionnels et innovateurs, la production de connaissances fondamentales sur la performance des outils de mélange comme le Co-Kneader doit être considéré comme un facteur clé.

Le Co-Kneader est une extrudeuse monovis modifiée. La vis à filet interrompu fait un mouvement de va-et-vient. En plus, le fourreau a des doigts de malaxage fixés à l'intérieur. La combinaison du mouvement réciproquant avec la présence des doigts de malaxage cause une action autonettoyante qui ne se trouve pas sur d'autres extrudeuses monovis. La vis du Co-Kneader est formée par des éléments interchangeables, ce qui donne la souplesse nécessaire pour modifier la configuration de la vis en fonction de l'application.

Une description fiable des mécanismes d'écoulement et de mélange dans le Co-Kneader est nécessaire afin de pouvoir évaluer les possibilités et les limites de cet outil de mélange. Ainsi, des descripteurs hydrodynamiques tels que patrons d'écoulement, profils de pression, efficacité de mélange et distribution des temps de séjour entre autres, ont été étudiés. La stratégie suivie dans cette étude a été d'abord de comprendre la performance du Co-Kneader d'un point de vue macromélange (c'est-à-dire, cause-effet des principales variables d'opération), puis examiner les mécanismes responsables de celui-ci. Une double approche méthodologique associée à cette stratégie a été mise en œuvre. Elle a comporté une partie expérimentale et une partie de modélisation de l'écoulement par dynamique des fluides numérique (CFD).

Un Co-Kneader transparent à l'échelle laboratoire a été spécialement conçu et construit pour les besoins de ce travail. Le fluide modèle utilisé est une solution aqueuse de sirop de maïs avec une viscosité newtonienne de 0.2 Pa·s. Les patrons d'écoulement ont été déterminés en suivant un traceur par une technique de décoloration rapide avec analyse d'images. La distribution de temps de séjour (DTS) a été estimée à partir des changements de conductivité produits par l'injection d'un traceur par impulsion. Le développent de la pression le long de la vis a été mesurée en utilisant des manomètres à tube ouvert placés près de l'entrée et à la sortie du système. La prédiction numérique du champ d'écoulement tridimensionnel non-stationnaire a été obtenue en résolvant les équations incompressibles de Navier-Stokes avec une méthode d'éléments finis. L'élément tétraédrique à 5-nœuds P1 +-P1 (MINI) a été utilisé pour calculer la vitesse et la pression.

Il a été constaté que la technique d'analyse d'images, pour la première fois appliquée à des systèmes en continus, donne un nouvel aperçu sur le mécanisme de mélange du Co-Kneader. Aussi elle peut être utilisée comme une méthode expérimentale simple afin de quantifier le degré de mélange vers l'arrière (backmixing). La DTS a été utilisée pour obtenir des coefficients de dispersion axiale. Dans un système entièrement rempli, le coefficient de dispersion augmente avec le débit et la vitesse de rotation de la vis. En outre, les doigts de malaxage et les interruptions dans le filet de la vis produisent des temps de séjour uniformément distribués autour de la moyenne. L'analyse de la distribution de longueur de trajectoires (DLT) montre que l'élément de mélange engendre un mélange axial tandis que l'élément de transport mélange dans la direction en aval du chenal de la vis (down-channel). Les résultats obtenus par CFD ont été validés par des résultats de pression expérimentale, démontrant être en accord. Les résultats de CFD suggèrent que les doigts de malaxage promeuvent des écoulements extensionnels dans les canaux de la vis. Les résultats présentés incluent des courbes caractéristiques adimensionnelles pour chaque type d'élément de vis, des coefficients d'efficacité extensionnelle, et pour la première fois une caractérisation du taux de cisaillement. Les résultats expérimentaux et de CFD présentés dans ce travail suggèrent clairement que le Co-Kneader peut être mieux conçu et opéré.

ABSTRACT

Mixing is a common basic operation in several industries including petroleum, polymer pharmaceutical, food, agriculture, etc. Up to the present day, our knowledge on this operation can still be considered more as an art rather than hard based scientific evidence. Thus, many mixing devices used in industrial practice are still being designed and operated following a trial-and-error approach and this is also the case of screw extruders. However, in a highly competitive environment where there is an increasing demand for more functional and innovative products and processes, generation of basic knowledge on the performance of mixing devices such as the Co-Kneader should be considered a key driver.

The Co-Kneader is a modified single screw extruder that has an oscillatory screw with sliced flights fitted into a barrel that has stationary pins. The combination of the reciprocating movement and the presence of the pins results in a self-wiping action not found on others single screw extruders. Interchangeable screw elements give the flexibility to change the screw configuration depending on the application.

To obtain a reliable description of the flow mechanisms and mixing in the Co-Kneader in order to assess the opportunities and limitations of this mixer, hydrodynamic descriptors like flow patterns, pressure drop, mixing efficiency and residence time distribution among others were studied. The strategy followed in this study was first to understand the Co-Kneader performance from a macromixing perspective (*i.e.,* cause-effect of main operational variables) followed by digging into the mechanisms responsible of it. A dual methodological approach associated to this strategy was implemented; experimental and computational fluid dynamics (CFD).

A transparent lab-scale modular Co-Kneader was specially designed and built for the purposes of this work. The model fluid was an aqueous solution of corn syrup with a Newtonian viscosity of 0.2 Pa·s. Flow patterns were determined by following a tracer pathway combining a fast

discoloration technique with image analysis. Residence Time Distribution (RTD) was estimated from a stimulus response technique based upon changes in conductivity after adding a tracer. The pressure build up along the screw was measured using open tube manometers placed near the inlet and at the exit of the system. The numerical prediction of the unsteady three-dimensional flow field was obtained by solving the incompressible Navier-Stokes equations with a finite element method. The 5-node P1+-P1 (MINI) tetrahedral element was used to approximate the velocity and the pressure.

It has been found that the image analysis technique, for the first time applied to continuous systems, gives new insight into the mixing mechanism of the Co-Kneader and may be used as a simple experimental method to quantify the degree of backmixing. RTD have been used to obtain axial dispersion coefficients. In a fully filled system, the dispersion coefficient increases with the flow rate and the screw speed. Furthermore, the pins and the slices in the screw generate evenly distributed residence times. Trajectory length distribution (TLD) analysis show that the mixing element yields axial mixing whereas the conveying element causes down-channel mixing. CFD results were first validated by means of experimental pressure vs. flow rate characteristic curves. The CFD results were found to be in good agreement with the experimental results. CFD results suggest that the pins in the barrel promote extensional flows in the screw channel. The presented results include dimensionless characteristic curves for each type of element, extensional efficiency coefficients, and for the first time a shear rate characterization. The combination of experimental and CFD original results from this work clearly suggest that the Co-Kneader can be better designed and operated.

CONDENSÉ EN FRANÇAIS

Le mélange de polymères est une opération très commune puisque la majorité de produits finis demandent l'incorporation de divers composants. Parmi eux on trouve des additifs, stabilisants, antioxydants, agents de renforcement, charges, ainsi que des mélanges et alliages de différents polymères de base. Les propriétés mécaniques, physiques, chimiques, ainsi que l'apparence du produit dépendent fortement de l'uniformité de la composition. De plus, il y a une demande croissante de nouveaux matériaux avec des propriétés adaptées pour satisfaire des besoins encore plus rigoureux et diversifiés. Les matériaux avec ces nouvelles propriétés peuvent s'obtenir plus simplement et de façon moins chère par des mélanges de différent polymères et charges, plutôt que par la conception chimique de nouvelles molécules de polymère. Dans un environnement très concurrentiel, des procédés plus fonctionnels et innovateurs son donc nécessaires. De cette façon, la production de connaissances fondamentales sur la performance des outils de mélange comme le Co-Kneader doit être considéré comme un facteur clé. L'objectif général de cette thèse est l'obtention d'une description fiable des mécanismes d'écoulement et de mélange dans le Co-Kneader ainsi que la clarification de l'impact des variables du procède sur la capacité de mélange de la machine. Tout ça pour pouvoir faciliter la mise en œuvre de nouveaux profils de vis spécialement conçus pour une application quelconque.

Les extrudeuses à vis, où la majorité des opérations de transformation des polymères sont effectuées, peuvent être considères comme des mélangeurs en continu. Cependant, dans certains cas, le mélange est très inefficient et pour l'améliorer certaines modifications sont effectuées sur la vis ou bien sur le fourreau. Le Co-Kneader est une extrudeuse monovis modifiée. La vis a un seul filet interrompu et fait un mouvement de va-et-vient. En plus, le fourreau a des doigts de malaxage fixés à l'intérieur. La combinaison du mouvement réciproquant avec la présence des doigts de malaxage cause une action autonettoyante qui ne se trouve pas sur d'autres extrudeuses monovis. La vis du Co-Kneader est formée par des éléments interchangeables, ce qui donne la souplesse nécessaire pour modifier la configuration de la vis en fonction de l'application.

Le Co-Kneader est connu pour avoir un écoulement complexe en raison de son principe de fonctionnement (c'est-a dire, l'oscillation et le mouvement de rotation). Cependant, il n'y a pas d'études expérimentales de visualisations rapportées dans la littérature. D'autre part, les études portant sur la modélisation de l'écoulement font des simplifications importantes telles que l'omission de l'oscillation de la vis ou bien des doigts de malaxage. En général, les études publiées sur le Co-Kneader sont rares par rapport aux autres outils de mélange comme les extrudeuses monovis et les bivis. Donc, pour que cette machine ne soit plus utilisée de façon empirique et pour que ces capacités et ces limites soient identifiées, elle doit être mieux connue et comprise.

Dans le but d'atteindre l'objectif principal de cette thèse, la méthodologie de recherche de ce projet est divisée en trois objectifs spécifiques: i) développer des techniques de visualisation qui permettront d'observer le mécanisme de mélange dans le Co-Kneader ainsi que déterminer les effets des conditions d'opération, ii) évaluer les caractéristiques hydrodynamiques du Co-Kneader en utilisant un modèle numérique tridimensionnel incluant autant le mouvement d'oscillation comme les doigts de malaxage, et iii) mieux caractériser l'hydrodynamique et les capacités de mélange de chaque type d'élément de vis.

La stratégie de recherche suivie dans cette étude a été d'abord de comprendre la performance du Co-Kneader d'un point de vue macromélange (c'est-à-dire, cause-effet des principales variables d'opération), puis examiner les mécanismes responsables de celui-ci. Une double approche méthodologique associée à cette stratégie a été mise en œuvre. Elle a comporté une partie expérimentale et une partie de modélisation de l'écoulement par dynamique des fluides numérique (CFD).

Un Co-Kneader transparent à l'échelle laboratoire a été spécialement conçu et construit pour les besoins de ce travail. Le rapport L/D du Co-Kneader est égal à 11 et le diamètre intérieur du fourreau est de 50.8 mm. Le mouvement caractéristique du Co-Kneader consiste d'un aller-retour pour chaque tour de vis. L'amplitude de cette oscillation est de 7.5 mm. Les dents de malaxage forment trois rangées placées tout au long du fourreau. Chaque doigt de malaxage est cylindrique,

avec un diamètre de 4.2 mm et 7.4 mm de long. Il existe différents types d'éléments de vis disponibles pour ce type d'extrudeuse. Dans cette étude nous avons utilisé des éléments de transport (EZ) et des éléments de mélange (KE). L'élément EZ a un seul filet et une seule interruption. L'élément KE a deux filets et trois interruptions. Une configuration de doigts de malaxage correspond à chaque élément. Donc la répartition des doigts le long du fourreau dépend du profil de vis utilisé. L'élément EZ a un seul doigt de malaxage chaque deux interruptions et l'élément KE a deux doigts de malaxage dans chacune des trois rangées d'interruptions. Le profil de vis étudié compte deux sections de transport dont chacune est formée par 5 éléments EZ, et une section de mélange placée entre les deux, formée de 8 éléments KE. Le fluide modèle utilisé a été une solution aqueuse newtonienne de sirop de maïs de 82% (viscosité = 0.2 Pa s; densité = 1270 kg/m^3). Les conditions d'opération utilisées étaient les suivantes: vitesse de rotation de 50 à 100 tr/min, débit massique de 5 à 30 kg/h.

Les patrons d'écoulement ont été déterminés en suivant un traceur par une technique de décoloration rapide avec analyse d'images. La technique de décoloration se base sur le changement de couleur selon le pH, d'un fluide qui contient un indicateur acide-base (dans ce cas bromocrésol). Une fois le traceur injecté, les expériences ont suivi le changement de couleur de pourpre (couleur dans des conditions alcalines) à jaune (couleur dans des conditions acides) à mesure que le mélange a eu lieu. Chaque expérience a été enregistrée sous format vidéo. La méthode d'analyse d'images consiste à quantifier la quantité de fluide mélangé à travers le temps selon la couleur des pixels dans chaque image prélevée de la vidéo filmée. De cette façon, des courbes de mélange sont obtenues. Dans cette thèse, cette méthodologie est appliquée pour la première fois sur un système en continu, puisqu'elle est généralement utilisée pour l'analyse de mélange dans des cuves agitées.

La distribution de temps de séjour (DTS) a été estimée à partir des changements de conductivité produits par l'injection d'un traceur par impulsion. La sonde de conductivité installée sur le montage expérimental a suivi la conductivité locale en fonction du temps. L'accumulation de pression le long de la vis a été mesurée en utilisant des manomètres à tube ouvert placés près de l'entrée et à la sortie du système.

La prédiction numérique du champ d'écoulement tridimensionnel non-stationnaire a été obtenue en résolvant les équations incompressibles de Navier-Stokes avec une méthode d'éléments finis. L'élément tétraédrique à 5-nœuds P1 +-P1 (MINI) a été utilisé pour calculer la vitesse et la pression. En raison du mouvement complexe du Co-Kneader et visant à simplifier les conditions limites du système, une méthode de domaine fictif connue comme méthode d'éléments finis virtuels (Virtual Finite Element Method VFEM) a été employée. Dans le cadre du VFEM, un maillage unique est nécessaire pendant les calculs et la vis est représentée par un ensemble de points de contrôle mobiles qui agissent comme des contraintes cinématiques. Suite à cette approche, le profil de vis complet a été constitué par environ 135 000 points de contrôle. D'autre part, la géométrie représentant le domaine fluide a été composée d'un maillage 3D cylindrique avec une section annulaire, dans lequel la forme des doigts de malaxage a été soustraite. La géométrie du modèle a les mêmes dimensions que le dispositif expérimental. Le maillage non structurées 3D final a été composé d'environ 1 million d'éléments ce qui a donné un système de près d'un demi million d'équations.

Comme prévu, les courbes de mélange dépendent des conditions d'opération: à mesure que la vitesse de rotation de la vis augmente, le temps de mélange diminue. Pour une même condition, les courbes de mélange obtenues après l'analyse d'images présentent de très petites variations, ce qui signifie que la technique est aussi robuste pour les systèmes en continu que pour les cuves agitées. Trois régions différentes liées aux sections de la vis (deux sections de transport avec une section de mélange entre les deux) ont été clairement identifiés dans les courbes de mélange. En ajustant un modèle statistique linéaire aux courbes de mélange, un taux de mélange a été défini. Ce taux estime l'augmentation dans le temps de la zone mélangée suivant la direction axiale pour chaque section de la vis. Les résultats montrent clairement qu'il y a un changement brusque du taux de mélange en fonction de la section de vis et des débits. Il a été constaté que la technique d'analyse d'images, pour la première fois appliquée à des systèmes en continu, donne un nouvel aperçu du mécanisme de macro-mélange dans le Co-Kneader. En outre, elle peut être utilisée comme une méthode expérimentale simple pour quantifier le degré de mélange vers l'arrière (backmixing).

L’analyse de la DTS a montré les tendances attendues, à mesure que le débit et la vitesse de rotation augmentent, le temps de séjour moyen diminue. Un comportement similaire a été observé en ce qui concerne la variance des distributions autour de la moyenne; à mesure que le débit et la vitesse de rotation augmentent, la variance diminue. Le modèle de dispersion axiale a permis une estimation du coefficient de dispersion axiale. Il a été constaté que pour un système complètement rempli, le coefficient de dispersion augmente linéairement avec le débit et la vitesse de la vis. En comparant la DTS du Co-Kneader avec celle d’une extrudeuse monovis, il a été trouvé que contrairement à la monovis, le Co-Kneader génère des temps de séjour uniformément distribués autour de la moyenne. Ce comportement est attribué à l’effet des interruptions dans le filet et des doigts de malaxage. Aussi, comparé à un mélangeur statique le Co-Kneader a une DTS plus élargie.

Afin de vérifier l'exactitude du modèle numérique, les résultats obtenus des simulations ont été comparés avec les mesures de pression expérimentales et ils ont été jugés en bon accord. L'erreur relative calculée entre les résultats expérimentaux et les résultats numériques dans tous les cas est inférieure à 8%. Des courbes caractéristiques adimensionnelles de débit versus différence de pression ont été générées à partir des simulations numériques. Il a été démontré que l'élément de transport a une plus grande capacité de pompage que l'élément de mélange Toutefois, comparativement à une monovis théorique, ces deux éléments ont une très basse capacité de pompage. Ces résultats confirment pourquoi en pratique, le Co-Kneader est couplé avec une extrudeuse de décharge. Les résultats de ce travail suggèrent que la faible capacité de pompage du Co-Kneader est due à la présence des interruptions dans les filets de la vis.

L'effet local des doigts de malaxage a été analysé à partir des champs de vitesse obtenus avec la CFD. Il a été constaté que le débit est divisé et recombiné d'un canal à l'autre quand les doigts de malaxage se trouvent au milieu d’une interruption de filet, ce qui favorise l’écoulement vers l’arrière (backflow) et le mélange distributif. Aussi dans cette position, il a été démontré que l’écoulement semble accélérer plus entre doigts de malaxage adjacents. Lorsqu'il n'y a pas de doigts de malaxage entre les interruptions du filet, l’écoulement suit simplement la direction en

aval du canal (down-channel). De la même façon au milieu du canal, l'écoulement normal est perturbé quand il y a un doigt de malaxage. Les résultats de CFD suggèrent aussi que les doigts de malaxage favorisent les écoulements extensionnels.

Les analyses de la DTS et de la distribution de longueur de trajectoires (DLT) présentées dans ce travail ont été obtenues par une technique de suivi de particules, où le mouvement de traceurs sans masse est dominé uniquement par le champ d'écoulement. Une approche élément-par-élément couplée à un schéma de tirs prédicteur-correcteur a été choisie pour obtenir le chemin suivi par une particule. Les trajectoires utilisées pour les analyses de la DTS et de la DLT ont été obtenues en utilisant 300 tirs par élément. La DTS numérique a été obtenue en calculant le temps pris par chacun des traceurs pour se rendre du point d'injection jusqu'au plan de sortie. Environ 1000 particules ont été injectées dans chacun des plans analysés. Les résultats numériques du temps de séjour moyen ont été comparés avec des valeurs expérimentales et ils se sont montrés en accord. Les DLT ont été obtenues en même temps que les DTS. On obtient les DLT en calculant la longueur de la trajectoire parcourue à partir du plan d'injection jusqu'au plan de sortie par chaque particule fictive. L'analyse de la DLT a montré que l'élément de mélange engendre un mélange axial tandis que l'élément de transport mélange dans la direction en aval du chenal de la vis (down-channel). Dans ce travail, l'analyse de la DLT a été effectuée pour la première fois sur une extrudeuse et elle s'est avérée être un outil complémentaire à l'étude des mécanismes de mélange dans le Co-Kneader.

Afin d'évaluer l'efficacité du mélange dispersif à l'intérieur du Co-Kneader, l'efficacité extensionnelle α a été obtenue. Ce paramètre quantifie les composantes rotationnelles et élongationnelles du champ de vitesse. Il a été démontré que la section de mélange a une valeur de α légèrement supérieure par rapport aux sections de transport. En termes de magnitude il n'y a pas de différence significative entre les valeurs moyennes de chaque élément $\alpha_{m\text{–KE}}$ et $\alpha_{m\text{-EZ,}}$ les deux étant comprises entre 0,51 et 0,53. En outre, il a été constaté que la valeur de $\alpha_{m\text{–KE}}$ et $\alpha_{m\text{-EZ}}$ demeure relativement constante en variant le débit à vitesse constante.

Le taux de cisaillement $\dot{\gamma}$ a été obtenu tout au long du Co-Kneader en diverses positions angulaires de la vis ainsi que pour différentes conditions d'opération. Les différences entre les éléments de vis ont été clairement démontrées. Le taux de cisaillement moyen est plus élevé dans les éléments de mélange et il reste constant sur tout le long de la section. Au contraire, sur les sections de transport, il y a de grandes oscillations sur les valeurs de $\dot{\gamma}$ où les valeurs plus élevées se trouvent à l'emplacement du seul doigt de malaxage qui a cet élément. Une analyse plus détaillée de l'élément de mélange a révélé que la valeur moyenne de $\dot{\gamma}$ est plus élevée lorsque le doigt de malaxage est à la position initiale de 0° (c'est à dire au milieu de l'interruption du filet) et elle diminue à mesure que le doigt de malaxage se déplace entre les filets de vis. Elle atteint à nouveau la valeur maximale quand le doigt termine son passage, après 120°. Ce cycle est répété trois fois, ce qui correspond à la géométrie de l'élément de mélange (trois doigts de malaxage et trois interruptions du filet). Parce que l'élément de transport a un seul doigt de malaxage, la valeur de $\dot{\gamma}$ n'est pas autant affectée par la position de la vis.

Afin de traiter les variables géométriques et d'opération ainsi que leur impact sur $\dot{\gamma}$, une valeur moyenne du taux de cisaillement produit dans chaque élément de vis a été obtenue en utilisant l'approche classique de Metzner-Otto. Le taux de cisaillement est alors proportionnel à la vitesse de la vis avec la constante de proportionnalité $K_{s.}$ Les valeurs estimées de $K_{s.}$ pour les elements de transport et de mélange est de 18 et 23 respectivement. Une valeur plus élevée de K_s pour l'élément de mélange est expliqué par le plus grand nombre de doigts de mélange trouvés sur cet élément.

D'après les résultats obtenus dans ce travail on peut conclure que les nouvelles techniques dirigées à caractériser et quantifier le mécanisme de mélange tels que l'analyse de DLT et la méthode expérimentale de visualisation couplée à l'analyse d'images, ont été appliquées avec succès pour la première fois sur un mélangeur en continu. Ces méthodes ont permis de décrire le mécanisme de mélange du Co-Kneader, qui c'est avéré être principalement dans la direction axiale, ainsi que de clarifier comment les conditions d'opération impactent le mélange axial et l'écoulement vers l'arrière (backflow). Par le biais du modèle 3D numérique qui prenait en

compte toutes les caractéristiques géométriques et mécaniques du Co-Kneader, il a été possible de mieux évaluer l'impact fourni par les doigts de malaxage sur l'écoulement global ainsi que sur les capacités de mélange de la machine. Il a été trouvé que en dehors de provoquer la division et recombinaison de l'écoulement dans les canaux de la vis, ils favorisent aussi l'écoulement extensionnel où, le cas contraire, il y aurait seulement de l'écoulement de cisaillement. La caractérisation des éléments de vis les plus couramment utilisés a été faite par l'analyse de la DTS et du taux de cisaillement produit par chaque élément individuel. Cette information peut être utilisée vers la conception de nouveaux profils de vis spécialement créés pour combler les besoins d'une application particulière.

Dans l'ensemble, les résultats expérimentales et de CFD suggèrent que l'extrudeuse Co-Kneader peut être mieux conçue et opérée. La stratégie suivie dans ce travail a permis l'analyse détaillée de la performance hydrodynamique du Co-Kneader. Cette analyse pourra alors aider identifier et examiner les mesures convenables, tels que l'implémentation de nouveaux profils de vis et de conditions d'opération optimales, pour la conception et l'amélioration des procèdes.

TABLE OF CONTENTS

LIST OF TABLES

LIST OF FIGURES

NOTATION

Symbol	Description	Units
A	Area	m^2
C_0	Initial zero value from conductivity probe	Dimensionless
C_∞	Final stable value from conductivity probe	Dimensionless
C_i	Output from conductivity probe	Dimensionless
D	Diameter	m
D_{ax}	Axial dispersion coefficient	m^2/s
D_b	Inside diameter of barrel	mm
D_o	Outside diameter of screw	mm
e	Flight thickness	mm
h	Bin width	Dimensionless
H	Screw channel depth	mm
K_{ch}	Shear rate constant from single screw channel	Dimensionless
K_{pin}	Shear rate constant from pin-flight gap	Dimensionless
K_s	Shear rate constant from Metzner-Otto relationship	Dimensionless
l	Trajectory length	m
L_{ax}	Axial length	m
L_e	Length of screw element	mm
L_h	Helical or down-channel length	m
l_m	Mean trajectory length	m
L_s	Length of flight slices	mm
m	Slope on mixing curve	Dimensionless
M	Mixed pixels	%
M	Mixing index	Dimensionless
m_r	Mixing rate	Dimensionless
n	Number of data points	Dimensionless
N	Screw speed	rpm
P	Pressure	Pa

P*	Dimensionless pressure	Dimensionless
Pe	Peclet number	Dimensionless
Q	Flow rate	kg/h
Q*	Dimensionless flow rate	Dimensionless
R	Radius	m
s	Width of screw slice	mm
S_0	Amplitude of screw stroke	mm
s_z	Gap between pin and screw flight	mm
t	Time	s
t_m	Mean residence time	s
u	Mean axial velocity	m/s
v	Velocity	m/s
V	Volume	m^3
W	Screw channel width	mm

Greek symbols:

Symbol	**Description**	**Units**
α	Extensional efficiency	Dimensionless
$\dot{\gamma}$	Shear rate	1/s
δ	Relative error	%
φ	Flight angle	°
μ	Newtonian viscosity	Pa s
θ	Dimensionless time	Dimensionless
ρ	Density	kg/m^3
σ^2	Variance	s^2
σ_l^2	Length variance	m^2
τ	Shear stress	Pa
ω	Oscillation frequency	1/s
ξ	Dimensionless normal coordinate	Dimensionless

LIST OF APPENDIXES

CHAPTER 1
INTRODUCTION

1.1 Mixing in the Polymer Processing Industry

The purpose of mixing is to reduce composition non-uniformities in systems comprising two or more substances. It constitutes an essential step in many industries because the quality and properties of products depend on the effectiveness of mixing the different components involved. In the polymer processing industry, end products depend upon the regular incorporation of a lot of components; among them are additives, stabilizers, antioxidants, fillers, reinforcing agents, as well as blends and alloys of different base polymers. Mechanical, physical, chemical, and appearance properties are thus strongly dependent on composition uniformity. Examples of mixing operations in polymer processing production lines are (Rauwendaal, 1998a):

- Homogenization, where blending of virgin polymers with color concentrates take place.
- Reactive extrusion, where polymerization reaction and extrusion occurs simultaneously. Examples are free radical grafting or polycondensation (*e.g.* Nylon).
- Reinforcing and filling of critical and difficult-to-handle compounds (*e.g.* thermoplastics, rubbers or thermosets) with other materials (*e.g.* fiber glass, carbon tubes, nanocomposites) to improve and enhance their properties.

1.1.1 Mixing mechanisms

In general, mixing of two or more components can be achieved by three different types of motion:

- Molecular diffusion, which is driven by a concentration difference between the different species present in the mixture and occurs spontaneously.
- Eddy motion, which is the result of turbulent mixing.

- Convection, which involves the spatial movement of fluid particles from one location to another.

Molten polymers are very viscous fluids, with viscosities ranging from 100 Pa·s to 100 000 Pa·s. This results in laminar flows where the fluid moves in adjacent layers that slide over each other without lateral mixing. In these conditions turbulent mixing is non-existent and molecular diffusion occurs very slowly; therefore convective motion is the dominant mixing mechanism. Convective mixing in polymer processing is achieved by imposing deformations such as shear and elongation, which results in an increase of the interfacial area separating the components. This mixing mechanism is called *distributive* or *extensive mixing*. Reorientation and randomization of the interfacial elements throughout the volume is also necessary to effectively achieve distributive mixing. Some mixing components, like solid agglomerates (*e.g.* Silica, carbon black, and pigments), viscoelastic polymer blobs or droplets, exhibit cohesive strength. Therefore in order to reduce the size of these cohesive components, stresses have to be applied. This mixing mechanism is known as *dispersive* or *intensive mixing*. **Figure 1–1** shows the combined effect of the two mixing mechanisms.

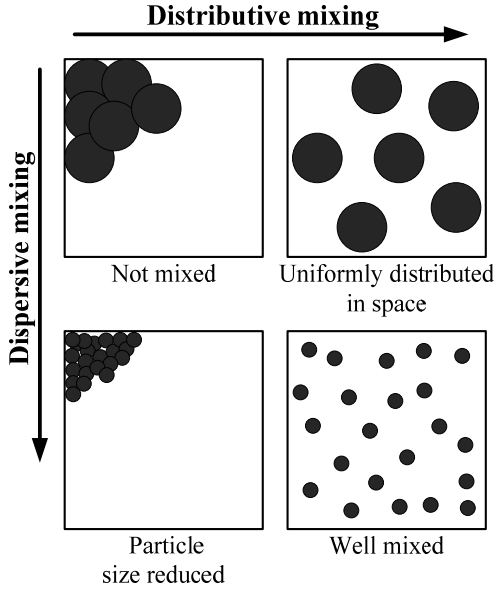

Figure 1–1. Schematic of dispersive and distributive mixing.

1.2 Polymer Mixing Technology

Numerous types of equipment exist to carry out mixing operations involving polymeric materials. The classification of the different mixing machinery (Tadmor & Gogos, 2006) is presented in **Figure 1–2**.

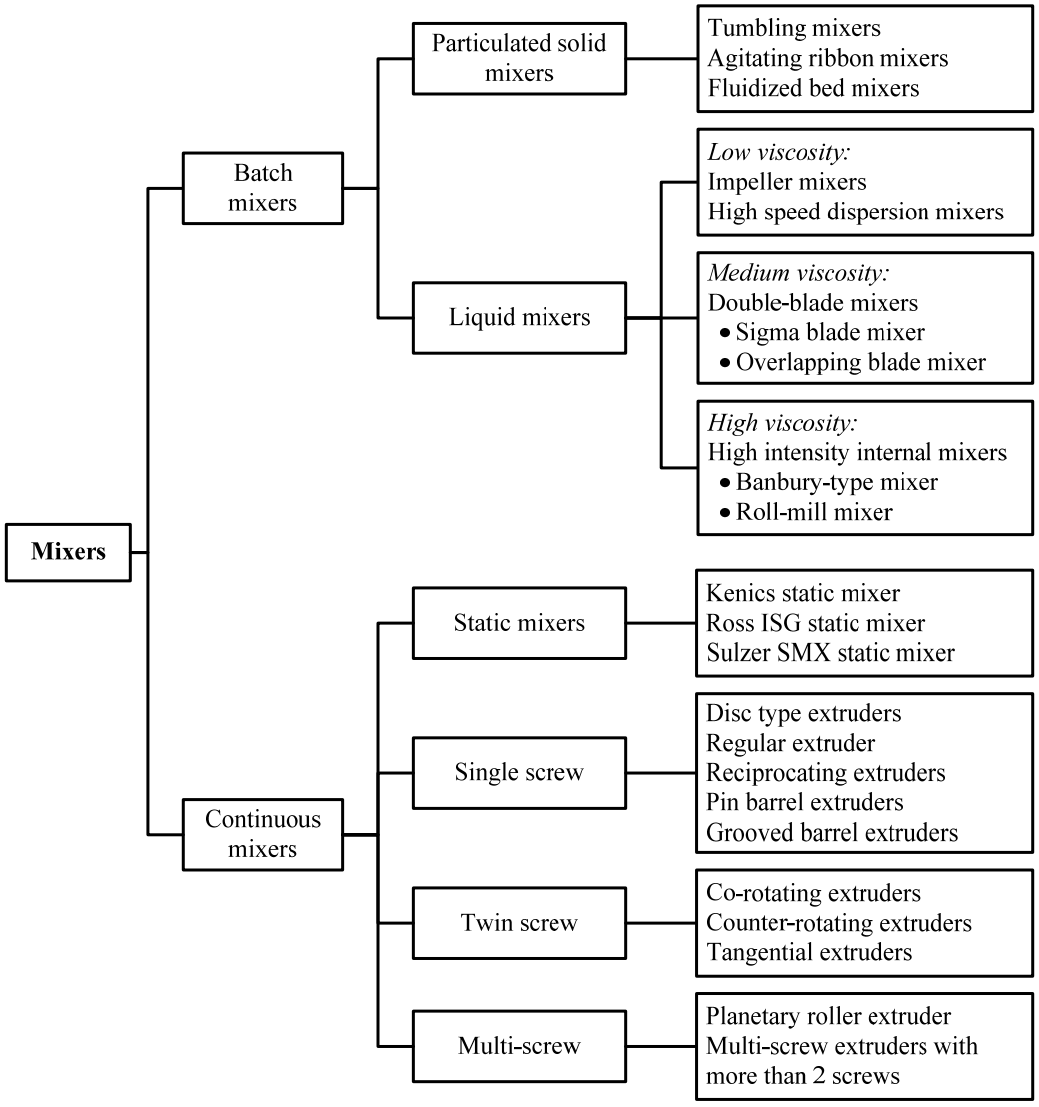

Figure 1–2. Classification of mixers.

The first classification is based on the way they operate, whether they are continuous or batch mixers. Batch mixers can then be classified into particulate solid mixers or liquid mixers.

Moreover, liquid mixers can be subdivided according to the mixture viscosity range in which they are used. Continuous mixers include static mixers as well as screw extruders. Screw extruders are further classified depending on the number of screws; they can be single, twin or multi screw extruders. The most used in the industry are single and twin screw extruders.

1.2.1 Twin screw extruders

Various types of twin screw extruders are available. The differences among them concern their design and operating principles. Twin screw extruders can be classified according to the direction of rotation. If both screws rotate in the same direction they are known as a co-rotating twin screw extruders. If they rotate in different directions they are known as a counter-rotating twin screw extruders. Depending on the distance between both screws they can be separated, tangential, partially intermeshing or fully intermeshing. The different configurations are showed in **Figure 1–3**. The design of the extruder depends on the application. Each of them has different functional characteristics like throughput, mixing capacity, pressure development, residence time distribution, etc. Very often mixing elements are added to the screw to enhance the mixing action.

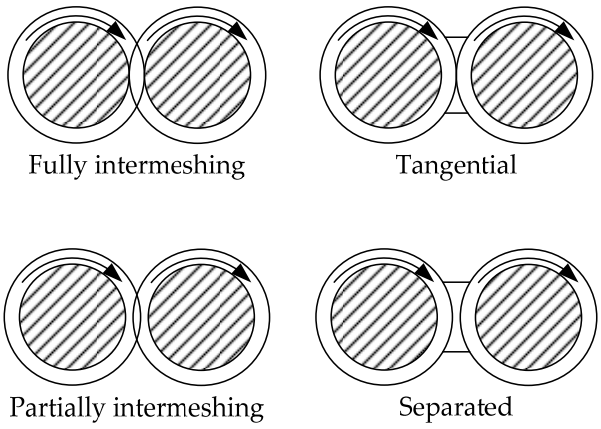

Figure 1–3. Twin screw extruders with different degree of intermeshing.

There is a lot of operational experience regarding intermeshing co-rotating twin screw extruders. They are widely used because of the flexibility in the selection of screw configurations, efficient mixing capability (best for distributive mixing) and self-wiping effect (Sakai, 2009). In the case of counter-rotating twin screw extruders, distributive mixing is better when they are non-intermeshing, and dispersive mixing is better when they are intermeshing (Rauwendaal, 1998a).

1.2.2 Single screw extruders

Regular single screw extruders are the most common type of extruders in polymer processing. Because they are not very good mixers as such, different devices or adaptations are made to the screw in order to enhance the mixing action. Depending on the desired type of mixing to be achieved, whether it is dispersive or distributive, is the kind of mixing section added. **Figure 1–4** shows some examples of mixing elements used in single screw extruders.

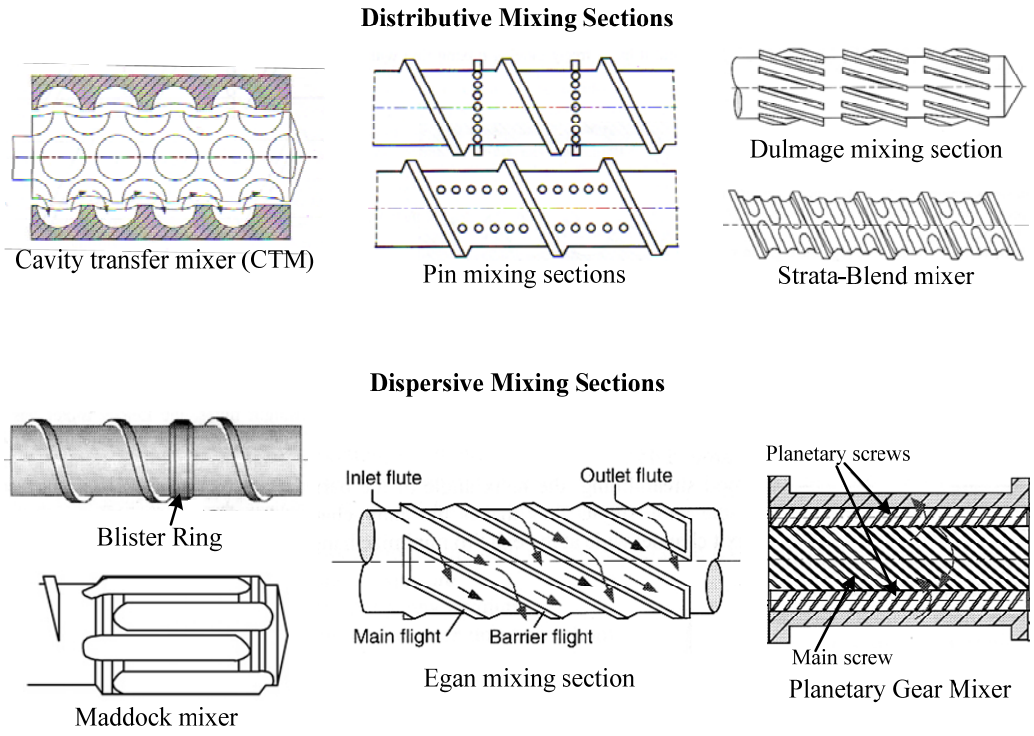

Figure 1–4. Mixing sections for single screw extruders (from Rauwendaal (1998b))

1.2.3 The Co-Kneader

The Co-Kneader (**Figure 1–5**), also called “List/Buss Kneader” or “Kokneter”, was invented in 1945 by Heinz List (1950). It is a special type of single screw mixer since it combines simultaneously the usual rotational motion with a reciprocating action. The screw has slices in the flights and it is fitted into a barrel that has stationary pins. The combination of the reciprocating movement and the presence of the pins results in a self-wiping action not found on any other single screw extruder.

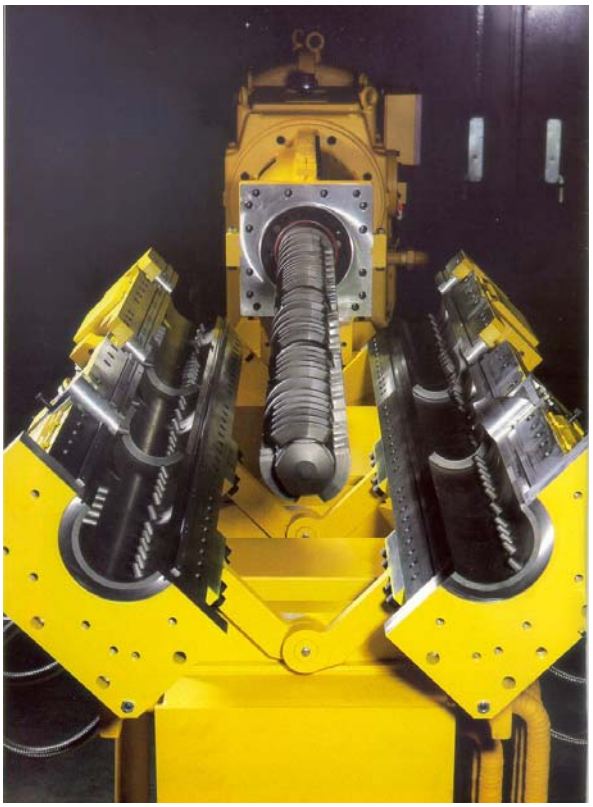

Figure 1–5. Industrial Co-Kneader (Buss brochure)

Good dispersive and distributive mixing capabilities have been attributed to the Co-Kneader, which makes it very suitable for compounding applications. It has been stated that the highly effective mixing action of the Co-Kneader allows a very short machine length, typically about 11D. When compared to a typical length of 30D-50D for twin screw extruders it becomes clear that the mixing efficiency of a Co-Kneader per unit axial length is substantially better than both

single and twin screw extruders (Rauwendaal, 2009). However, even though it was invented many years ago there are few studies available regarding this mixer and still less that have focused on the mixing mechanism or on the flow patterns.

1.3 Motivation of the study

Up to the present day, our knowledge on mixing operations can still be considered more as an art rather than hard based scientific evidence. Thus, many mixing devices used in industrial practice are still being designed and operated following a trial-and-error approach. This is still the case of screw extruders, and especially of the Co-Kneader. Additionally, there is an increasing demand for new materials with tailored properties designed to meet more rigorous and diversified requirements. These new properties can be simply and cheaply designed into materials by blending and compounding different polymers and fillers, rather than chemically designing new polymeric molecules. In a highly competitive environment, more functional and innovative processes are needed. In light of this, generation of basic knowledge on the performance of mixing devices such as the Co-Kneader should be considered a key driver.

1.4 General Objective

The general objective of this project is to develop a reliable description of the flow mechanisms and mixing in the Co-Kneader and to clarify how process variables impact the mixing capacity of the machine in order to facilitate the implementation of tailored screw profiles according to the application.

CHAPTER 2
LITERATURE REVIEW

2.1 The Co-Kneader Mixer

The Co-Kneader is a continuous mixer that has a single screw that both rotates and oscillates. The screw has interrupted flights and there are stationary pins along the walls of the barrel. This geometry, together with the combination of the rotational and axial movement of the screw, promote distributive mixing (Elemans, 2009). The Co-Kneader was invented in 1945 by Heinz List (1950) and nowadays it is distributed by Buss AG in Switzerland. White & Lyu (1998) present a summary of the development of the modern Co-Kneader since its origins.

2.1.1 Geometry

The single screw of the Co-Kneader is fitted in a clam shell barrel that has stationary pins. (**Figure 2–1**). The pins are placed along the length of the barrel forming three rows at 120° from each other. While the screw rotates it also reciprocates, making one complete forward and return stroke for every revolution. The magnitude of the stroke is about 15% of the screw diameter (Rauwendaal, 1998a).

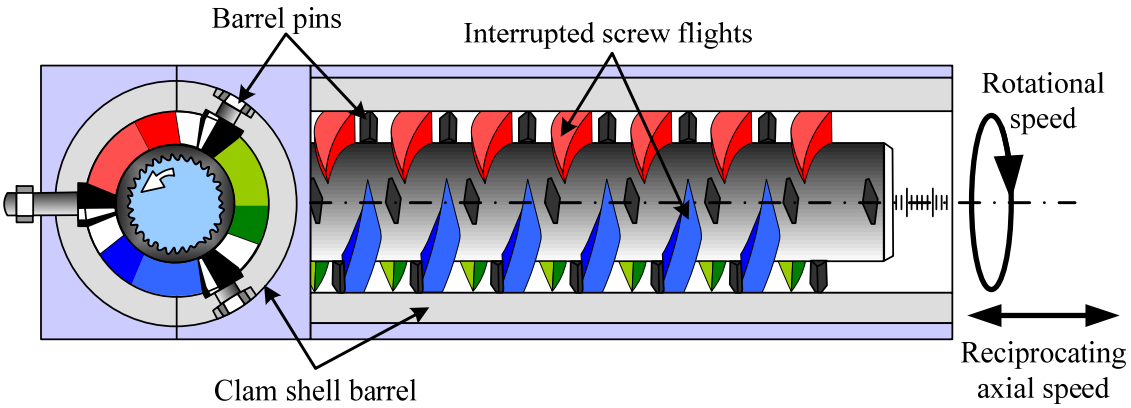

Figure 2–1. Schematic of a Co-Kneader (from Buss AG)

Since there are many clearances in the screw flights, high pressures cannot buildup. Additionally, the oscillatory motion of the screw relative to the barrel causes great pressure and throughput fluctuations (Elemans & Meijer, 1990). To tackle these problems, either a discharge extruder or a gear pump is used to guarantee constant pressure at the die.

The Co-Kneader is commercially available in a range of screw diameters from 30 mm to 200 mm and the process length can vary from 8 to 20 *L/D*, giving an output range of 10-4000 kg/hr.

2.1.1.1 Modular Screw Elements

The screw of the Co-Kneader consists of interchangeable elements that are assembled into a shaft. There are different types of elements that can be placed along the screw shaft in any desired position depending on the application. The most common are:

- Conveying screw elements: Known as EZ elements (from German: *Einzugsbüchse*) (**Figure 2–2a**), they have one flight, one screw slice, and two rows of one pin

- Mixing (kneading) screw elements: Known also as KE elements (from German *Knetbüchse*) (**Figure 2–2b**) they have two flights, three parallel screw slices, and three rows of two pins. The KE elements are for dispersive and distributive mixing of the molten polymer (Rauwendaal, 1991b). The closed-channel mixing elements, known as GS elements (from German *Gangschliessbüchse*) (**Figure 2–2c**) are a variation from the KE element. They also have two flights; however one has three slices and the other only one. This element has three rows of two pins. Its purpose is to prevent the backflow of the molten polymer.

- Restriction ring adapters: Known as ST elements (from German *Stauring*) (**Figure 2–2d**), they are used in conjunction with restriction rings (**Figure 2–4b**).

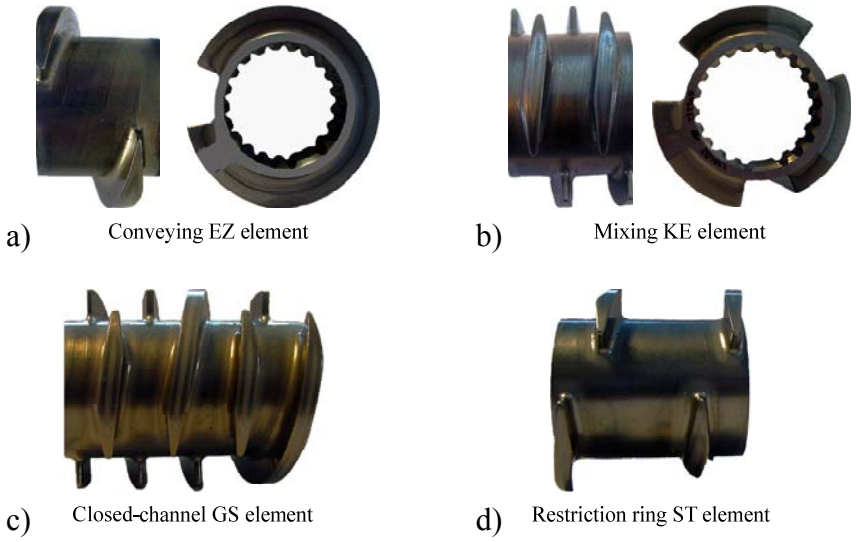

Figure 2–2. Modular screw elements: **a)** Conveying EZ element; **b)** Mixing KE element; **c)** Closed-channel GS element; **d)** Restriction ring ST element.

2.1.1.2 Pins

The pins are fixed along the barrel wall forming three parallel rows. Each pin is interchangeable. Since each screw element has a different pin configuration, the distribution of the pins along the barrel depends on the screw profile. They are usually diamond-shaped although in small size Co-Kneaders they are cylindrical; they can be solid (**Figure 2–3a**) or hollow (**Figure 2–3c**) as well. Hollow pins are used to place thermocouples (**Figure 2–3c.*i***) along the screw axis or as feed ports for injecting liquids (**Figure 2–3c.*ii***). There are also blank pins (**Figure 2–3b**), which are used to cover the perforations on the barrel where pins are not needed.

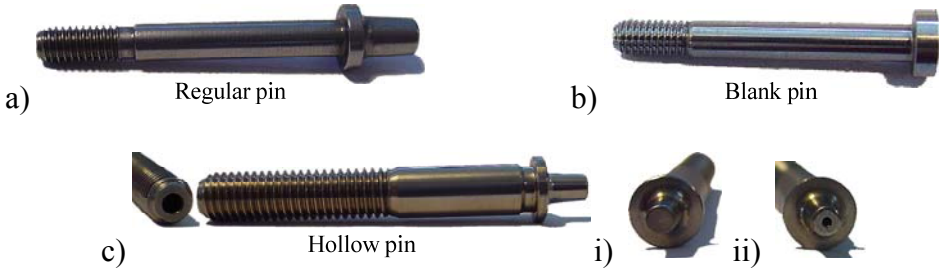

Figure 2–3. Types of pins: **a)** Regular pin; **b)** Blank pin; **c)** Hollow pin for ***i)*** thermocouple and ***ii)*** injection of fluids.

2.1.1.3 Barrel Liners

The clam-shell barrel of the Co-Kneader consists of segmented liners. The liners have perforations of different size depending on whether the pin is solid or hollow (**Figure 2–4a**). They are also changed as they wear out. Restriction ring liners (**Figure 2–4b**) act like barriers fitted into the barrel (White *et al.*, 2003). They are used to increase the degree of filling of the KE elements placed upstream and therefore they improve the mixing action (Rauwendaal, 1998a). They are also used in sections preceding openings in the barrel such as side-feed or vent ports (Elemans, 2009). Restriction rings are available in different sizes, thus varying the annular gap between the restriction ring and the screw root.

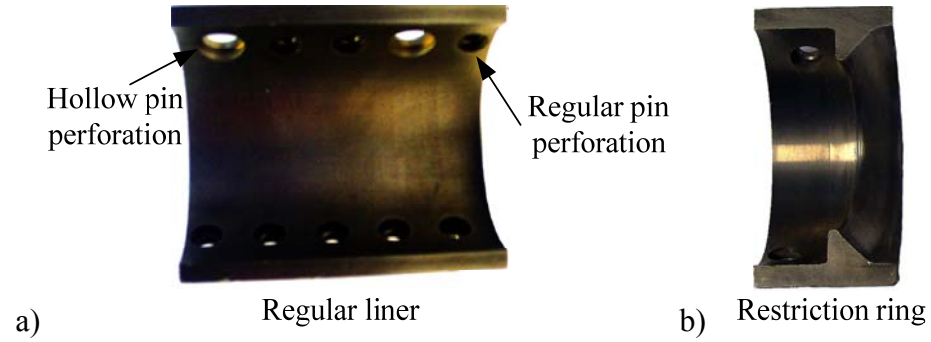

Figure 2–4. Types of barrel liners: **a)** Regular liner; **b)** Restriction ring.

2.1.2 Operating Principle

The rotational and reciprocating motions of the Co-Kneader cause the pins to move, relative to the screw, in a sinusoidal way through the flight clearances of the screw. Rauwendaal (1991b) explains this motion in detail and the important aspects are described next. **Figure 2–5** illustrates the trajectories of the pins relative to a screw flight segment, which is shaded in the figure. The screw and the barrel surface are shown unrolled into a flat plane and the conveying direction of the material is from right to left. After a quarter of a screw turn (**Figure 2–5b**) the pin has wiped

the upper left flank of the shaded flight segment and the material that passed between the pin and the flight has been sheared. After another quarter of a turn (**Figure 2–5c**) the upper right flank of the flight is wiped and the other pins push the material back into the screw channel behind the slots creating backflow. This backflow causes efficient radial and axial mixing (Rauwendaal, 1991b). At 270° (**Figure 2–5d**) the lower left flank is wiped, and when the full screw turn is completed at 360° (**Figure 2–5e**), the lower right flank is wiped. Each time the pin passes near the flanks the material is sheared (**Figure 2–6**) and the wiping action reduces the stagnation of material. This process is the same for all the flight segments in the screw and the entire screw surface is covered by the pins as shown in **Figure 2–5f**.

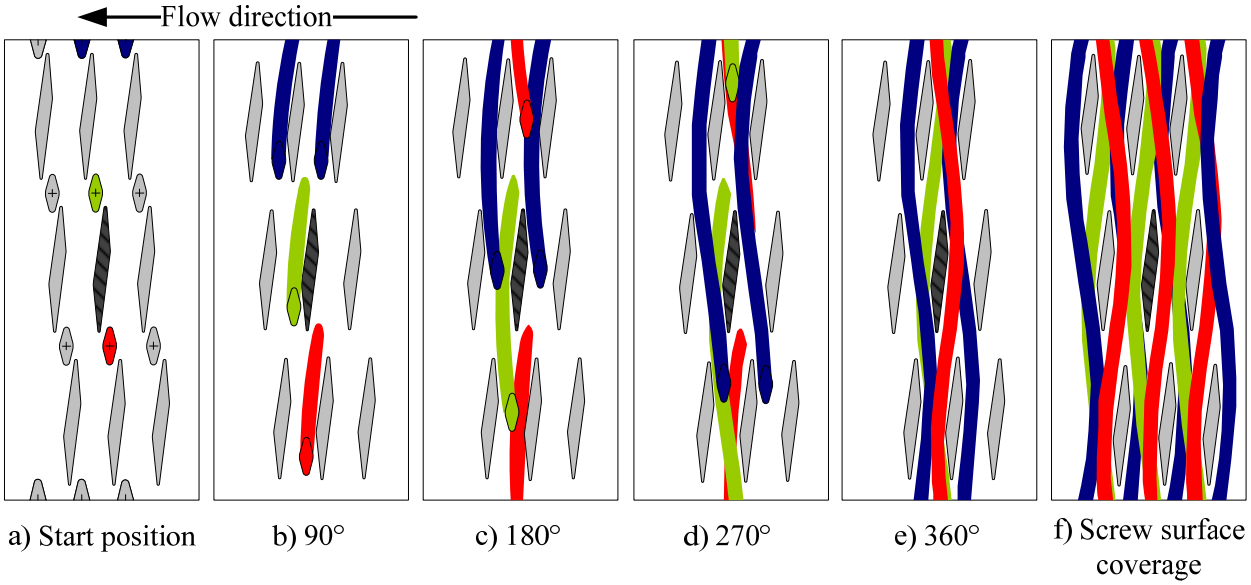

Figure 2–5. Trajectories of stationary pins relative to the shaded flight (from Buss AG)

The heat transfer in the Co-Kneader is also enhanced due to the self-cleaning action of the screw and barrel, and thus the chance of material degradation is reduced. This is particularly useful in reactive processing and when working with thermally sensitive polymers. Self-cleaning action is usual in intermeshing twin-screw extruders however the Co-Kneader is the only single screw extruder that has certain sections completely self-wiping. This characteristic allows the Co-Kneader to be used in applications where conventional single-screw extruders could not possibly be used (Rauwendaal, 1991b).

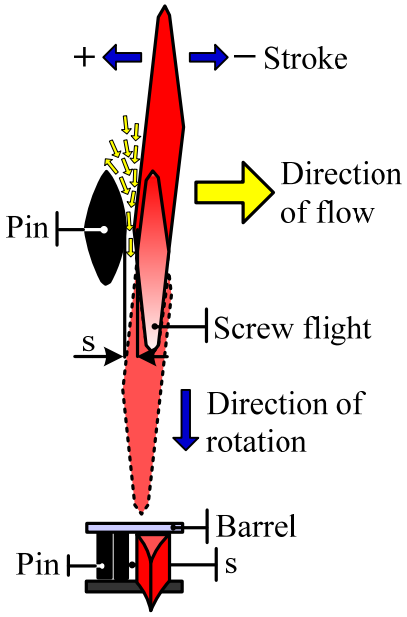

Figure 2–6. Diagram of shear flow between the pin and the flight segment (from Buss AG)

An up close diagram of the shear flow taking place when a pin is passing by a screw flight segment is shown in **Figure 2–6**. According to Buss AG, the shear rate in the Co-Kneader is exclusively dependent on the screw speed and of a geometrical constant. The minimum gap width between the barrel pin and the screw flight is represented by *s*, which is defined by the following Buss AG relationship as

$$s = c_{geom} \cdot D \tag{2.1}$$

The shear rate is defined as

$$\dot{\gamma} = \frac{\pi \cdot D \cdot N}{60 \cdot s} \tag{2.2}$$

The combination of **Equation 2.1** and **Equation 2.2** results in

$$\dot{\gamma} = \frac{\pi \cdot D}{60 \cdot c_{geom} \cdot D} \cdot N = c_{BUSS} \cdot N \qquad (2.3)$$

where $\dot{\gamma}$ is the shear rate, s is the gap width, c_{geom} is a geometric constant given by the manufacturer, D is the diameter of the screw, and N is the screw speed. Buss AG sustains that according to this relationship the shear rate in the Co-Kneader depends only on the operational speed of the extruder. This would only be true for a fixed geometry.

2.1.3 Applications

There are over 3 000 Co-Kneader mixers working worldwide and it is considered to be a good extruder in processing thermally sensitive materials like PVC compounds and thermosets powder coatings (White *et al.*, 2003). Filled and reinforced engineering plastics can be processed in a Co-Kneader. Examples of this are PA, PBT, PET, PC, PP, among others. It is also used in the manufacturing of polymeric blends and alloys, colored and additives masterbatches as well as in the food industry.

2.2 Mixing Mechanism in the Co-Kneader

The first attempt to explain the distributive mixing action of the Co-Kneader was that of Jakopin & Franz (1983). In their work, they made a qualitative analysis of the number of striations per *L/D*. They calculated that the total number of striations per *L/D* was 2^{12}.

Booy & Kafka (1987) studied the flow in an elemental channel (**Figure 2–7**). They determined that in a mixing zone of 8 *L/D*, a screw speed of 60 rpm and a flow rate of 1 575 kg/hr, the fluid is split approximately 60 times. They also affirm that this number of striations is proportional to the screw speed and the *L/D* ratio, but inversely proportional to the flow rate. Also, they observed that the flow is split and recombined by the rows of sliced flights and that this action constantly

shuffles fluid elements, resulting in the reorientation of the interfaces. According to the authors, this process is what causes the mixing action in the Co-Kneader.

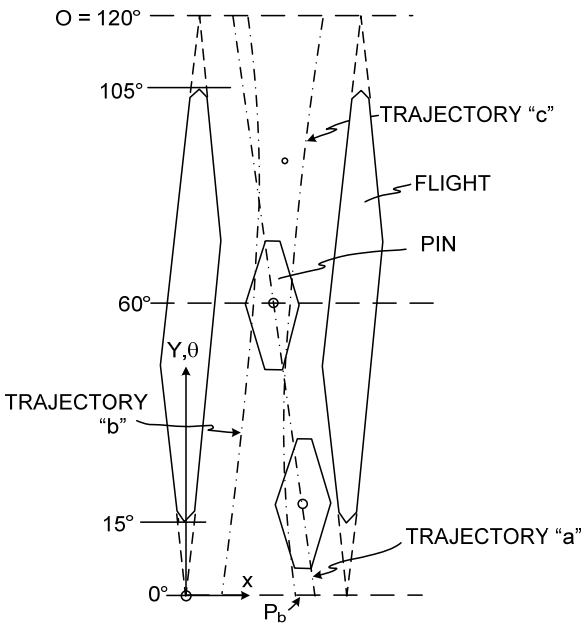

Figure 2–7. Elemental channel studied by Booy & Kafka (1987).

Elemans & Meijer (1990) took another approach. They stated that in order to have a more comprehensive model of the mixing quality, the degree of fill in the screw elements had to be known first. They formulated two expressions for the number of reorientations n_r in a screw element, one for a completely filled element

$$n_r = \frac{1.5p \cdot \pi^2 D^2 H(\tan\varphi)(1-ne)N}{Q} \tag{2.4}$$

and another for the case of partially filled screw elements

$$n_r = \frac{1.5p \cdot \pi D L_f H(1-ne)N}{Q} \tag{2.5}$$

where p is the number of pins, D the diameter, L_f the filled length, H the channel depth, φ the angle of the flight, n the number of flights, e the relative flight width, N the screw speed and Q the volumetric throughput. They made the calculation for a completely filled mixing element of L = 27 mm, D = 46 mm, working at N = 240rpm and with Q = 20kg/h, and obtained n_r=128.

The striation count is often used to obtain the total interfacial area between different flow components. Since an increase of the interfacial area is a direct result of the laminar mixing process, the striation count can be used as a measure of the effectiveness of mixers. However, in order to be valid, this approach requires a characteristic flow direction and a uniform strain history. In flows where there is not a single characteristic direction, this measure is not enough since it only gives a sense of the amount of mixing but nothing about the distribution of the mixture (Bigio & Stry, 1990).

2.3 Experimental Studies

There are relatively few experimental studies of the flow in the Co-Kneader even though it has been commercialized during the past 60 years. Various papers have been focused on the application of the machine in compounding processes (Stade, 1977, 1978; Todd, 1987). There have been melting experiments (Lyu & White, 1998) and measurements of temperature profiles (Lyu & White, 1997c). The rest of the studies, detailed in the following sections, cover hydrodynamic aspects of the machine such as pumping characteristics, RTD, and comparative mixing studies with other mixing equipment.

2.3.1 Pumping Characteristics and Filled Lengths

The first experimental work carried out to understand the working mechanisms of the extruder was performed by Elemans & Meijer (1990). The results reported were obtained in a modular

laboratory Co-Kneader of 46 mm of diameter and 600 mm long that was fitted in a Plexiglas cylinder. The experiments were performed using conveying, mixing and closed-channel mixing screw elements, with and without pins. Different processing conditions were studied like screw speed (150-250 rpm) and output (10-25 kg/h). The Newtonian fluids used for the experiments were silicon oil (μ = 1Pa·s) and paraffinic oil (μ = 0.2Pa·s) under isothermal conditions. A special die at the end of the extruder was used in order to avoid pressure and output variations resulting from the screw oscillation. Local pressure differences were measured directly by means of a series of open manometers installed along the barrel. By obtaining throughput versus pressure characteristic curves, it was found that the conveying element had a much larger capacity than the two mixing elements. Also, it was concluded that the presence of the pins affected very little the pumping abilities of all the screw elements. Filled axial lengths were determined by direct observation of the material distribution through the transparent barrel. No distinct influence of the pins on the filled length was observed.

Lyu & White (1995) reported experiments done in a modular Co-Kneader of 46 mm of diameter and L/D = 16 connected to a crosshead extruder of L/D = 5 and D = 45 mm. The experiments were made with polypropylene. Two different screw configurations were investigated and they were formed by conveying elements, mixing elements and restriction rings. They observed that the Co-Kneader gave a fluctuating output but they eliminated it by coupling a crosshead extruder at the end. They also obtained filled lengths. The results were used to validate a mathematical model.

2.3.2 Residence Time Distributions

Elemans & Meijer (1990) measured the RTD in the Co-Kneader using polyvinyl chloride (PVC) with titanium dioxide ($Ti0_2$) particles as tracers. They took samples at the end of the extruder at a given interval of time and detected the amount of tracer in them via X-ray fluorescence. They presented dimensionless plots with the values of the cumulative response. They found that at greater speeds the mean residence time in the machine was reduced.

Lyu & White (1998) report RTD results obtained in a partially filled system with polystyrene and aluminum flakes as tracers. The results showed that as the feed rate increased the residence time decreased and the distribution was narrowed. Additionally, as the screw speed increased the residence time distribution narrowed and tended to lose its long tail.

Troelstra (1998) analyzed the axial mixing in the Co-Kneader by means of the axial dispersion model. Experiments to obtain the RTD were performed using water and two syrups with viscosities of 5 and 21 Pa·s. The experiments were carried out in a system having D = 46mm and L/D = 15 using dye as tracer. It was demonstrated that the axial dispersion model could well represent the experimental data. Furthermore, it was found that for a partially filled system the axial dispersion coefficient increased linearly with the screw speed but was not affected by the flow rate.

Hoppe *et al.* (2002) conducted RTD experiments using polystyrene in a Co-Kneader of D = 46mm and L/D = 11. They investigated the effect of the tracer by using two kinds: free anthracene and anthracene grafted on the polymer. They found that only the grafted anthracene tracer could characterize the actual flow of the polymer in the extruder since it had the same rheological behavior as that of the unmodified polymer. The RTDs with grafted tracer were found to be always bimodal, which was attributed to the backflow of the polymer caused by the oscillation of the screw. They also found that for a partially filled Co-Kneader, the variance of the RTD increased when the feed rate was increased as well. Based on the experimental data, they developed an RTD model for the particular Co-Kneader screw configuration they studied. The model consisted of a combination of ideal reactors such as continuous stirred tanks and plug flow reactors. The predicted RTD was in good agreement with experiments.

One of the first comparative studies of residence time distributions was made by Shon *et al.* (1999). They compared the RTD of a Co-Kneader, a continuous mixer, a modular intermeshing co-rotating and counter-rotating twin screw extruders. For the experiments they used polypropylene with aluminum flakes in different screw configurations and with different operating conditions. They found that in every machine when the outflow was increased the

residence time decreased and the RTD narrowed. The same tendency was observed when screw speed increased. Their results also showed that the intermeshing counter-rotating twin screw extruders had the shortest residence time and narrowest RTD. On the other hand the Co-Kneader had the longest residence time and the broadest RTD, which according to the authors could mean that the kneader had the best distributive mixing.

2.3.3 Mixing and Compounding

Shon & White (1999) did a comparative study of glass fiber breakage in a Co-Kneader, a co-rotating and counter-rotating twin screw extruders. The study included a comparison using three different screw configurations varying in terms of mixing severity. It was found that the restriction ring elements caused more severe fiber breakage than the mixing elements. The milder brakeage occurred in the conveying elements. Comparison between the different machines was done using similar mixing conditions since it was found that the relative order of the machines in terms of fiber breakage could be changed by modifying the screw configuration. Overall, the results showed longest fiber length for the Co-Kneader.

Shon *et al.* (2005) investigated agglomerate breakage by compounding calcium carbonate into a polymer matrix. They did a comparison between the Co-Kneader, a continuous mixer, a co-rotating and counter-rotating twin screw extruder. By comparing intensive screw configurations in all the machines, they found that the Co-Kneader yielded the larger particle size.

Shon *et al.* (2008) studied the blending of immiscible polyamide 6 into polypropylene. They compared the same mixers as in their previous studies. The found that the order of the mixers according to the droplet size of the minor phase largely depended on the screw configuration and on the type of mixer. This was specially observed in the case of the Co-Kneader, where just by changing the screw configuration it produced a much finer morphology than the other mixers.

2.4 Flow Modeling

2.4.1 Flow, Pumping Characteristics and Filled Lengths

Booy & Kafka (1987) made the first attempt to model the flow inside a Co-Kneader. Their study concerned the flow of an isothermal Newtonian fluid between two flights with a single pin passing between them (**Figure 2–7**). For their analysis they used two methods: a Finite Element Method (FEM) program called POLYFLOW™, and an analytical approach using the Lubrication Method. They validated the results of the Lubrication Method with the results obtained with the FEM method. The calculations that they obtained were based on a Newtonian model fluid of $\mu = 1000$ Pa·s being processed in a 20 cm diameter Co-Kneader running at 60 rpm. They presented plots of the flow rate as a function of pin position, pressure distributions around the pin at a given position and shear rate along the tangential coordinate also in a particular pin position. They found that the pin passage between the flights caused splitting and reorientation of the flow. According to them this is what explains the good mixing capability of the kneader. At the narrow gaps located between the pin and the flights they found that the shear rates reached 400 s^{-1} at 60 rpm. These high shear mixing zones would give the kneader its capability in dispersive mixing, provided that all the fluid would pass through them. Concerning the analysis methods, they concluded that the differences between the results obtained with both methods were due to the coarseness of the FEM meshes and to imperfections in applying the Lubrication Method.

Brzoskowsky *et al.* (1989) sought also to model the isothermal flow of a Newtonian fluid in a section of the Co-Kneader. They performed their simulation using a modified Flow Analysis Network (FAN) method (Tadmor *et al.*, 1974). This method consists in splitting the flow field into rectangular cells thus forming a mesh. The continuity equation is then applied to each cell. The rheological properties of the fluid and the dimensions and operating conditions of the Co-Kneader were the same as those used by Booy & Kafka (1987). They presented pressure profiles along the flights for different pin positions. With curves of output vs. screw position they observed that the output changed in a sinusoidal way. The maximum output was found to be when the screw was at 240° and the minimum at 60°. These are the positions in which the axial component of the velocity has its maximum and minimum values. They also studied the effects

of the pins in the output and found that when the pins are between the flights the effects are negligible but when they are in the slices of flights their effect is important. They concluded that the effectiveness of the kneader as a distributive mixer was due to the different intensities of local flows. The general results obtained by these authors were almost the same as those of Booy & Kafka (1987).

Until this point, the two existing works that tried to understand the hydrodynamics of the Co-Kneader were carried out only taking into account a small section of the mixer (*i.e.* the elemental channel between two interrupted flights showed in **Figure 2–7**). Elemans & Meijer (1990) took a different approach and attempted to model the characteristics of the whole extruder. They investigated the effect of two important influences on the drag and pressure flow: the additional conveying action produced by the pins and the backflow through the flights slices. One important simplification in this work is that in their analysis they do not take into account the oscillatory motion of the Co-Kneader. The model they proposed for a Newtonian isothermal pressure and drag flow in an unrolled screw channel is

$$Q = (1-\alpha)Q_d + \varepsilon Q_{pin} + Q_p - Q_{LD} - Q_L \qquad (2.6)$$

This expression represents the overall flow that take into account the drag flow Q_d, the plug flow by pins Q_{pin}, the pressure flow Q_p, the leakage flow over the flights Q_L and the leakage flow through the interrupted flights Q_{LD}. There are two additional parameters: ε, an efficiency parameter of the pin that determines the amount of plug flow induced by it; and α, a geometrical factor given by the aspect ratio of the pins surface over the channel surface. The parameter ε was determined with the help of experimental data of output vs. pressure characteristics, filled lengths and pressure gradients. What the authors found in their work is that the pins have little influence in pumping and filled lengths, contrary to flight slices which have a significant effect on those characteristics.

Lyu & White (1995) first analyzed the effect of the oscillatory motion in the flow of the Co-Kneader. They made a momentum balance for a Newtonian fluid and they obtained the velocity profiles in the down channel direction

$$v_x(y,t) = U_x(t)\left(\frac{y}{H}\right) - \frac{H^2}{2\mu}\left(\frac{\partial p}{\partial x}\right)\left[\left(\frac{y}{H}\right) - \left(\frac{y}{H}\right)^2\right] \tag{2.7}$$

and in the cross channel direction

$$v_z(y,t) = U_z(t)\left(\frac{y}{H}\right) - \frac{H^2}{2\mu}\left(\frac{\partial p}{\partial z}\right)\left[\left(\frac{y}{H}\right) - \left(\frac{y}{H}\right)^2\right] \tag{2.8}$$

$U_x(t)$ and $U_z(t)$ were defined as

$$U_x(t) = \pi DN\cos\varphi + \frac{dS(t)}{dt}\sin\varphi \tag{2.9}$$

$$U_z(t) = -\pi DN\sin\varphi + \frac{dS(t)}{dt}\cos\varphi \tag{2.10}$$

where φ is the screw helix angle and $S(t)$ is the stroke of the oscillating screw defined as

$$S(t) = S_0\sin\omega t \tag{2.11}$$

S_o is the amplitude of the oscillation and the frequency ω is 2πN/60.

Taking the velocity profile of the down channel direction (**Equation 2.7**) they obtained the expression for the outflow which is given by

$$Q = \frac{1}{2}\frac{HWU_x(t)}{1+\frac{H^3W}{12kL}} \qquad (2.12)$$

where, k the die constant and L the length in the down channel direction. **Equation 2.12** demonstrates that the output at the die will oscillate as a result of the screw motion. That is why it is necessary to put a crosshead screw extruder or a gear pump at the end of the Co-Kneader. This development however, does not consider the presence of the pins. This analysis was later extended to Power-law fluids (Lyu & White, 1996) and to linear viscoelastic fluids (Lyu & White, 1997b). Using these analytical flow models, the authors calculated the velocity fields, flow rates and pressure profiles in a modular Co-Kneader including the discharge crosshead screw extruder. Their calculations began at the die of the crosshead screw extruder and then moved backwards to the Co-Kneader screw elements. In this fashion, they obtained dimensionless screw characteristic curves for the conveying, mixing and restriction ring elements. The Newtonian flow model (Lyu & White, 1995) showed that the conveying and mixing element were able to develop pressure but not the restriction ring element. Results with the Power-Law fluid (Lyu & White, 1996) indicated that the pumping capacity of all screw elements was less than for Newtonian fluids. In the same manner, the linear viscoelastic fluid flow model (Lyu & White, 1997b) showed that the deviation from the Newtonian behavior was more important for long relaxation times.

The FAN method was also used by Lyu & White (1996) to calculate Non-Newtonian flow fields in the mixing and conveying elements. The flow fields that they obtained excluded the pins in the barrel. The flow fields showed backward leakage through the flight slices and they showed that the backflow was greater for the mixing element than for the conveying element. They concluded that the more non-Newtonian the fluid is (*i.e.* lower power law index n) the more backward leakage there is.

Mehranpour *et al.* (2002a) used a Finite Volume Method (FVM) to numerically simulate the Newtonian velocity field in the conveying element. Their model accounted the oscillatory motion

of the screw but not the presence of pins. They found that the reciprocating action played a significant role in the mixing action of the Co-Kneader because it caused a periodical change in the flow field and shear rate distribution in the channel. In a following paper (Mehranpour *et al.*, 2003a) they extended the study to the mixing element. The results showed that the velocity changes during a period of reciprocating motion were greater for the transverse flow than for the down channel flow.

2.4.2 Residence Time Distributions

Mehranpour *et al.* (2002b) estimated the RTD using the flow model developed by Lyu & White (1995). They were able to obtain results for the mixing and conveying elements with a Newtonian fluid, taking into account the oscillatory motion but not the presence of pins. They found that the RTD in mixing elements was slightly narrower than in conveying elements. By using flow fields obtained previously (Mehranpour *et al.*, 2002a, 2003a) Mehranpour *et al* (2003b) predicted the RTD in the conveying and mixing screw elements using an elemental trajectory method by CFD. However, contrary to their analytical results, they found that the cumulative RTD for the mixing element was wider than that of the conveying element. As a final step, Mehranpour *et al.* (2004) were able to predict the RTD for different screw configurations by means of a method similar to additive rule named Cluster Model.

2.5 Summary

In this section, the previously detailed investigations are condensed. They are divided into two main categories, experimental studies and flow modeling studies. The summary of the experimental studies is represented in **Figure 2–8**. The classification is based on the topics that have been studied experimentally in the Co-Kneader. **Figure 2–9** shows the summary of the flow modeling studies. The first classification depends on whether it is an analytical or CFD model. Next, if the model considers the oscillation of the screw, the pins, or both features. Finally, in the case of CFD models, we highlight the method by which the problem was resolved.

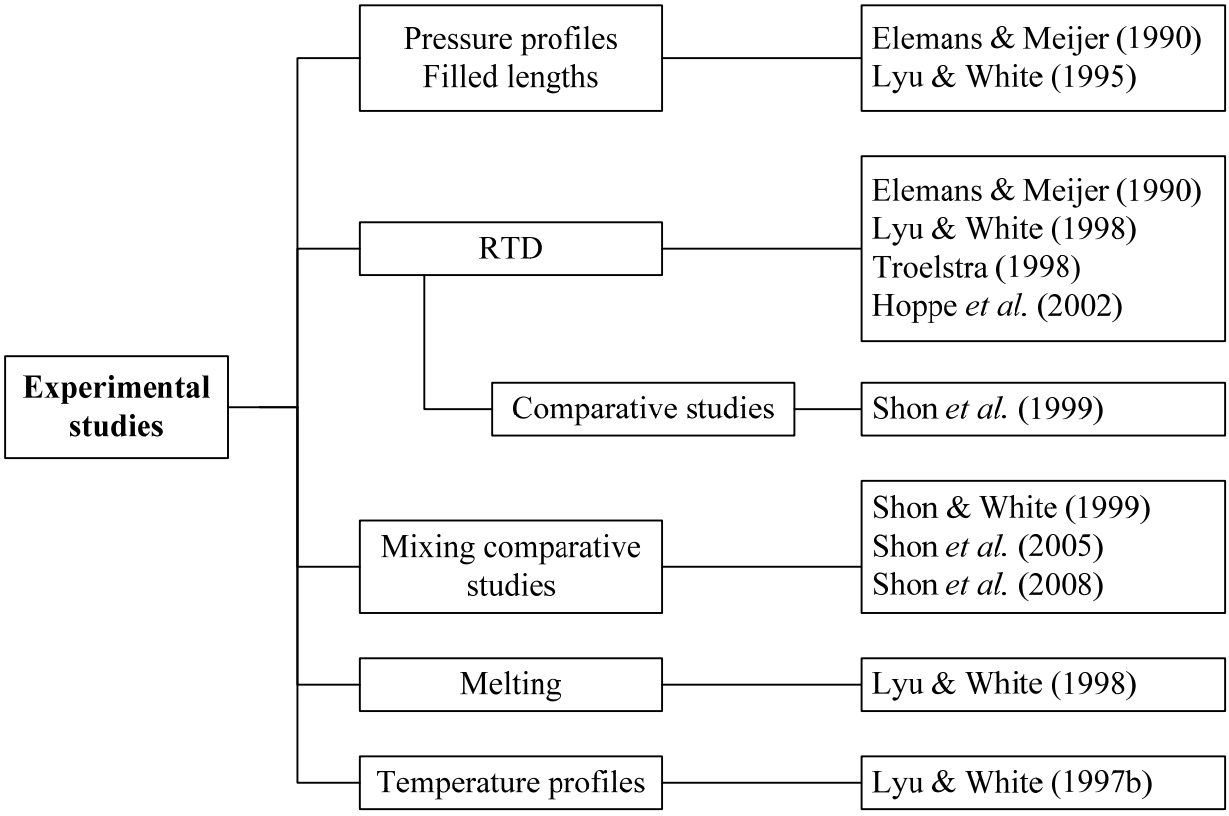

Figure 2–8. Summary of experimental studies.

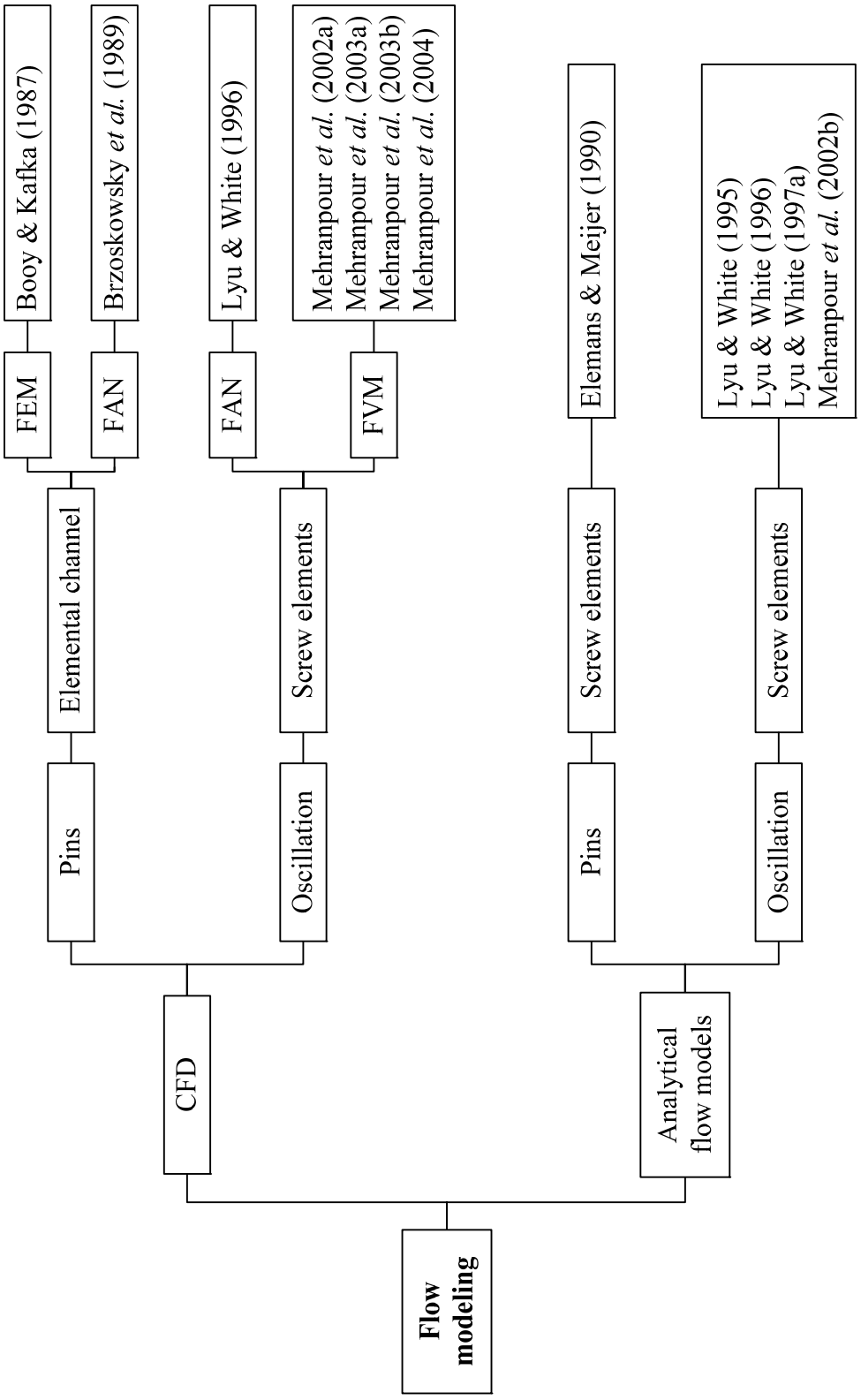

Figure 2–9. Summary of flow modeling studies.

2.6 Analysis of the Literature Review

The current knowledge about the Co-Kneader extruder is limited, and is concentrated on the studies of relatively few authors. The few available comparative studies have shown that in certain applications, the Co-Kneader has a better mixing performance compared to other equipment. Nevertheless, contrary to single and twin screw extruders, there is not enough information. Increasing the knowledge on the mixing and flow mechanisms of this mixer can widen the scope of applications in which it can be effectively used.

In this section the current state of knowledge is assessed. The areas where there is a lack of knowledge are also identified.

2.6.1 Experimental Characterization

The experimental studies available so far regarding the Co-Kneader have focused on general working parameters of the machine like pressure profiles and filled lengths. Flow characteristics like backmixing, which is an important aspect of the flow in the Co-kneader due to the number of slices in the screw flight, has been given little attention. Flow models have tried to determine the impact of operating conditions on the amount of backmixing by relating it with the pumping capacity of each type of screw element, mixing or conveying. However these models simplify the geometry by omitting the presence of the pins or they do not consider the oscillating motion of the screw. Experimental axial mixing determined by the analysis of RTD has only been examined once. It is clear that there is a lack of information regarding the axial mixing capacity of the mixer.

Direct flow visualization has been used as a tool to study flows inside mixing processing equipment. However, it creates many technical challenges when carried on with extrusion machinery working with real polymers. Small glass windows are usually installed on one side of the metal barrel. Therefore, axial and thermal expansion of the metal components must be accounted for and proper alignment and clearances become critical. Simplified mixers or

extruders inside transparent plastic barrels then become a good alternative for direct flow visualization. They are used at room temperature with model fluids and they usually give the chance to have a larger visualization area. Flow visualization setups of this kind have been used in polymer processing equipment. Yao et al. (1997) approximated the geometry of the helical channel of a single screw extruder by means of a transparent rectangular cavity with a moving top wall. Acrylic (PMMA) barrels have been used to study the mixing process in twin screw extruders using dyes (Bigio & Baim, 1991; Sanchez *et al.*, 1997) or colored particles (Ma *et al.*, 2003). More sophisticated flow visualization techniques, such as Particle Image Velocimetry, have required complete extruder models (barrel, shafts and screw elements) made out of acrylic (Jaffer *et al.*, 2000). Elemans & Meijer (1990) fitted a Co-Kneader in a Plexiglas barrel, however they only used it to directly measure the filled lengths. Even if the Co-Kneader is known to have a complex flow due to its operating principle (i.e. oscillation and rotation motion) there is no experimental flow visualization studies reported in the literature.

2.6.2 Numerical Simulation

Several flow models have been developed to represent the flow in the Co-Kneader. Different rheological behaviors have also been taken into account. Analytical flow models have considered the presence of the pins or the oscillation of the screw in geometries representing conveying or mixing screw elements. Computational Fluid Dynamics (CFD) models have simulated the passage of only one pin between two flights. Three dimensional geometries have also been investigated by CFD taking into account only the oscillation of the screw. The pins at the barrel together with the oscillatory motion of the screw are what distinguish the Co-Kneader from other extruders. However there are no modeling studies that take into account the interactions of both features.

The prediction of the characteristics of the flow like RTD or shear rate depends on the level of accuracy of the velocity field. In simple geometries, where analytical models of velocity profiles exits, the theoretical calculation of the RTD is straightforward. On the other hand, when more complex flows systems are encountered the modeling of the velocity profile, and consequently

the prediction of the RTD and other parameters, become more difficult. Simplifications of the system being studied have a direct impact on the accuracy of the predicted parameters.

Numerical modeling by CFD as an approach to study complex flow like the one inside the Co-Kneader, allows for the detailed observation of the three-dimensional flow at any time and at any location. By including into the model both the oscillating motion and the pins, a more accurate representation of the mixer could be achieved. The tracking of massless tracers allows calculating of RTD and other useful distributions for mixing analysis such as the trajectory length distribution (TLD) first introduced by Villermaux (1996).

2.6.3 Mixing Analysis in Screw Elements

Characterization of the different screw elements has mainly focused on the determination of their pumping capacities. This has been achieved by means of experiments or flow models. Flow models have explored the effect of rheological properties. Results on shear rate during the passage of one pin in a screw channel have been reported, however values of shear rate for the individual elements were only obtained without accounting for the pins. Also the existing RTD calculations for each type of element were obtained with no account of the pins.

The interchangeable modular screw elements of the Co-Kneader give the flexibility to change the screw configuration. It has been found that the screw profile has an impact on the distributive and dispersive capacity of the mixer. The impact can be of such an extent that it can make the Co-Kneader better or worse than other continuous mixers for a particular application. However, contrary to twin screw extruders, there are no general guidelines as to how to assemble a screw profile according to the application. More information and a more complete characterization of the screw elements in the Co-Kneader are thus needed.

CHAPTER 3
SPECIFIC OBJECTIVES

As mentioned in chapter 1, the general objective of this research is

> To develop a reliable description of the flow mechanisms and mixing in the Co-Kneader and to clarify how process variables impact the mixing capacity of the machine in order to facilitate the implementation of tailored screw profiles according to the application.

Based on the information already presented, the specific objectives of this thesis are:

1. To develop flow visualization techniques that will allow for the mixing mechanisms in the Co-Kneader to be evidenced and the effect of the operating conditions to be determined.

2. To assess the hydrodynamic characteristics of the Co-Kneader using a three dimensional numerical model that includes both the oscillating motion of the screw and the pins on the barrel.

3. To better characterize the hydrodynamics and mixing abilities of each type of screw element.

CHAPTER 4
OVERALL METHODOLOGICAL APPROACH

In this chapter a brief overview of the research strategy followed for the achievement of the specific objectives of the project is presented. Chapters 5 through 7 constitute the results sections of this thesis. Each of these chapters was conceived as a scientific publication, therefore each of them include the details of the corresponding methodology and techniques.

The research strategy followed in this thesis is summarized in **Figure 4–1**. It is divided in two main parts, experimental and numerical simulation.

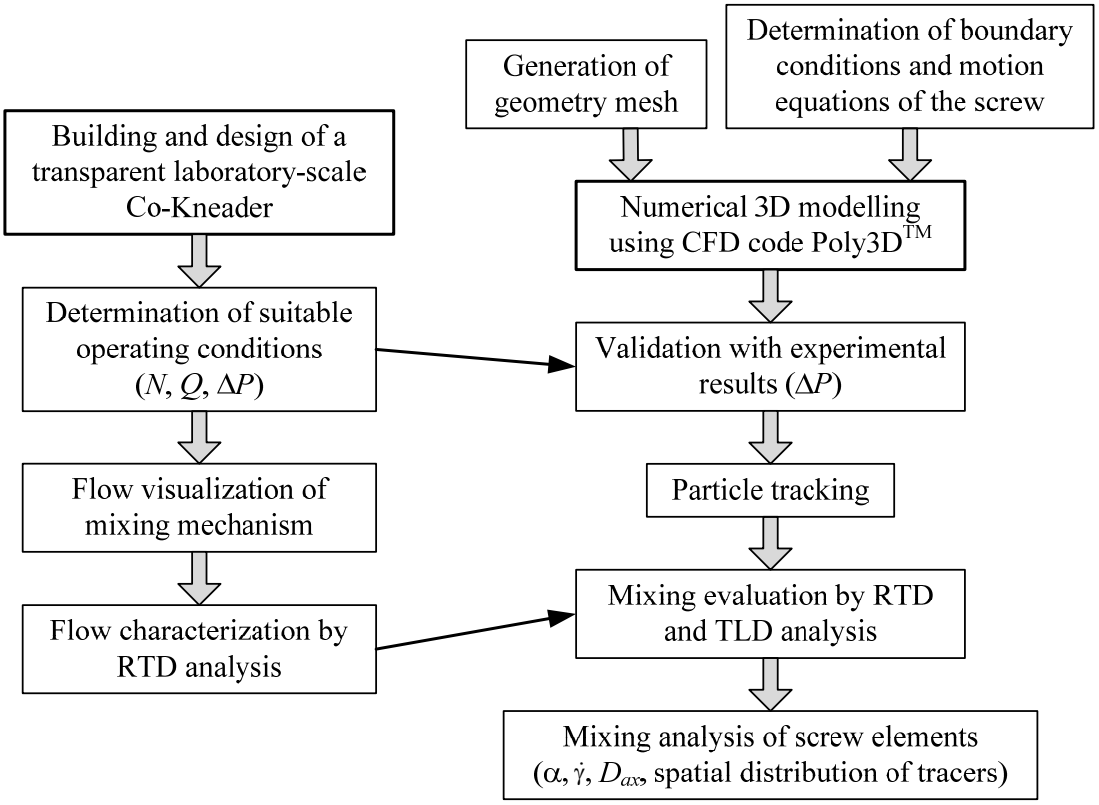

Figure 4–1. Research strategy.

The experimental part relies on the design and building of a fully transparent laboratory-scale Co-Kneader (**Figure 4–2**). Details about the dimensions and other characteristics of the setup can be found in Chapters 5 and 6. Design drawings and details on the screw profile and pin configuration can be found in Appendix 1. Suitable operating conditions were determined in which the screw could be operated fully filled. Then, flow visualization experiments of the mixing mechanism were performed as well as a flow characterization by RTD analysis. The results of this first step are presented in Chapter 5.

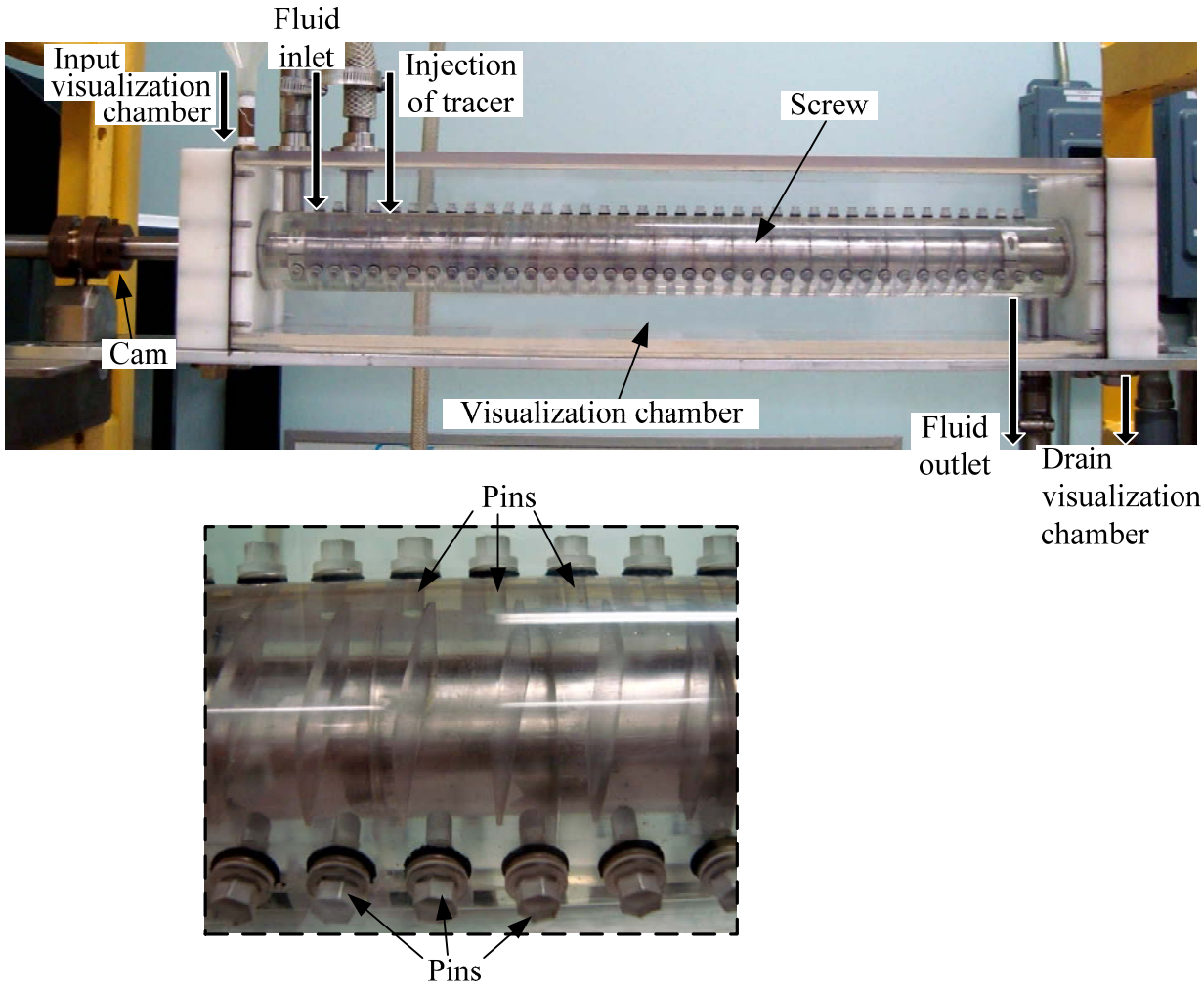

Figure 4–2. Experimental setup.

The numerical simulation part consisted in the 3D modelling of the Co-Kneader using a FEM-based CFD code (Poly3D™). It involved the generation of two 3D geometries, one of the barrel and the pins, and the other of the screw profile. The geometries were done following the dimensions and configuration of the experimental setup. Meshes based on these two geometries were then generated. The next step consisted in the determination of boundary conditions and motion equations for the moving parts of the geometry (*i.e.* the screw). The motion equations accounted for the rotational and reciprocating movements of the Co-Kneader. Details about the meshes, boundary conditions and motion equations are found in Chapter 6. The results of the flow simulations were then validated with experimental values of pressure. With a particle tracking technique, RTD and TLD were obtained. Results were validated with experimental RTD as well. Results obtained in this stage are detailed in Chapter 6.

The third and final step was based on the numerical model previously developed. It consisted in performing a mixing analysis of the individual screw elements. To this effect, results of extensional efficiency, shear rate and axial dispersion coefficients were obtained. Spatial distributions of tracers were also obtained. These results are presented in Chapter 7.

CHAPTER 5
EXPERIMENTAL FLOW VISUALIZATION AND RESIDENCE TIME DISTRIBUTIONS IN A CO-KNEADER

Magdalena Brito-Bazan, Louis Fradette, Philippe A. Tanguy

URPEI, Department of Chemical Engineering, École Polytechnique de Montréal P.O.Box 6079, Station Centre-Ville, Montreal, Que., Canada H3C 3A7

5.1 Presentation of the article

This article was submitted to the International Polymer Processing Journal.

This article tackles the first of the specific objectives which was to develop flow visualization techniques that will allow for the mixing mechanisms in the Co-Kneader to be evidenced and the effect of operating conditions to be determined.

The article presents for the first time experimental flow visualization results in a fully transparent laboratory Co-Kneader. Flow visualizations were performed by means of an acid-base discoloration method followed with an image analysis technique here for the first time applied to continuous systems. Residence times distributions analysis is also presented.

Keywords: Flow visualization, RTD, Co-Kneader, backmixing, Newtonian fluid

5.2 Abstract

Flow patterns and residence time distributions have been investigated in a transparent laboratory-scale Co-Kneader with a viscous fluid and different combinations of operating conditions. An image analysis technique, already successfully applied in stirred tanks, has been applied here for the first time in a continuous system. The flow visualization results are presented as mixing curves, which show quantitatively the evolution of the macromixing along the Co-Kneader. It has been found that the image analysis technique gives new insight into the mixing mechanism of the Co-Kneader and may be used as a simple experimental method to quantify the degree of backmixing. Residence time distributions have been used to obtain axial dispersion coefficients. A comparison of the cumulative distribution functions between different systems is also presented.

5.3 Introduction

Mixing is a very important and complex aspect of the majority of the polymer processing operations. End products often require blends of different base polymers, as well as regular incorporation of additives, fillers and reinforcing agents among others. Screw extruders in which polymer processing operations are carried out, act as continuous mixers. Among them, single and twin screw extruders are the most common. Sometimes however, the mixing is very inefficient (Rauwendaal, 2009). In order to improve the mixing action, design modifications are made to the screw and/or barrel. The Co-Kneader is a modified single screw extruder. It has an oscillatory screw with sliced flights fitted into a barrel that has stationary pins. The combination of the reciprocating movement and the presence of the pins results in a self-wiping action not found on others single screw extruders. The screw consists of interchangeable modular screw elements that are assembled into a shaft. This gives the flexibility to change the screw configuration depending on the application. The Co-kneader has been used in a wide variety of mixing applications, such as the manufacture of carbon electrode paste, rocket propellant fuel, food processing, and plastics compounds among others (Rauwendaal, 1991a).

Published studies about the Co-Kneader are scarce compared to other extrusion equipment like single screw and twin screw extruders. Studies focused on the application of the machine in compounding processes were the first to be available (Stade, 1977, 1978; Todd, 1987). Subsequent experimental studies investigated the influence of operating conditions on filled lengths and pressure generation (Elemans & Meijer, 1990) as well as temperature profiles and residence time distributions (RTD) (Lyu & White, 1995). More recently, efforts have been made to model the Co-Kneader using RTD for specific uses such as a polymerization reactor for acrylates (Troelstra *et al.*, 2002) and for manufacturing absorbent composite materials (Hoppe *et al.*, 2002). Numerical investigations have also been performed in order to study in more detail the complex flow of the Co-Kneader (Brzoskowski *et al.*, 1991; Lyu & White, 1996, 1997b; Mehranpour *et al.*, 2002a, 2003a).

An important flow characteristic in an extruder is backflow also known as backmixing. In single screw extruders, backmixing is a desirable feature since it promotes axial mixing, which is responsible for achieving the reduction of striation thickness (Rauwendaal, 2009). However, a large degree of backmixing can result in longer residence times and consequently increase the risk of material degradation. In conventional extruders, backmixing is due to pressure gradients in the channel and leakage flow through the clearances (Manas-Zloczower, 2009). Therefore, because of the number of slices in the screw flight of the Co-Kneader, backmixing becomes an important aspect of the characterization of this type of extruder. Flow models have tried to determine the impact of the operating conditions on the amount of backmixing by relating it with the pumping capacity of each different screw element (*i.e.* conveying or mixing element). However the models simplify the geometry by omitting the presence of pins (Lyu & White, 1995, 1996) or they do not consider the oscillating motion (Elemans & Meijer, 1990). The RTD in conventional extruders has a spreading effect superimposed on plug flow, which is caused by the backmixing (Manas-Zloczower, 2009). The extent of axial mixing can then be determined by the examination of the RTD. Lyu & White (1998) reported RTD results obtained with polystyrene and aluminum flakes as tracers. Their results showed that for a given screw speed, as the feed rate increased the average residence time decreased; also for a fixed feed rate, as the screw speed increased the RTD narrowed and tended to lose its long tail. Shon *et al.* (1999) compared the RTD of a Co-Kneader, a continuous mixer, an intermeshing co-rotating twin screw and a

counter-rotating twin screw extruders. Using polypropylene and aluminum flakes, they found that the Co-Kneader had the longest residence time and the broadest RTD, which according to the authors, could mean that the Co-Kneader had the best distributive mixing. More information is needed however, regarding the axial mixing capacity of the machine.

By direct visualization of the flow inside the Co-Kneader, the flow structure and therefore the backmixing could be studied in more detail. Yet, direct visualization of the mixing and fluid flows in extrusion machinery with real polymers creates many technical challenges. Proper alignment and clearances are critical when glass windows are installed on the side of a metal barrel. Axial and thermal expansion of the metal components must be accounted for as well, otherwise the window can crack or break (Manas-Zloczower, 2009). As a consequence these types of windows are usually small thus limiting the visualization area. To overcome these restrictions, simplified mixers or extruders inside transparent plastic barrels are used at room temperature with model fluids, which gives the possibility to visualize the complete flow behavior. Yao *et al*. (1997) approximated the geometry of the helical channel of a single screw extruder by means of a transparent rectangular cavity with a moving top wall. Acrylic (PMMA) barrels have been used to study the mixing process in twin screw extruders using dyes (Bigio & Baim, 1991; Carneiro *et al.*, 2002; Sanchez *et al.*, 1997) or colored particles (Ma *et al.*, 2003). More sophisticated flow visualization techniques, such as Particle Image Velocimetry, have required complete extruder models (barrel, shafts and screw elements) made out of acrylic (Jaffer *et al.*, 2000). Regarding the Co-Kneader, the only available visualization study is the work by Elemans & Meijer (1990). They fitted a Co-Kneader in a Plexiglas barrel and they measured filled lengths. Even if the Co-Kneader is known to have a complex flow due to its operating principle (*i.e.* oscillation and rotation motion) there is no experimental flow visualization studies reported in the literature.

In this work we report for the first time experimental results of flow visualization in a fully transparent Co-Kneader as well as residence time distributions. The objective is to gain a better understanding of the mixing mechanism in the Co-Kneader including the effect of operating

conditions on backmixing. An approach based on mixing curves is being applied for the first time to a continuous mixer.

5.4 Methods

5.4.1 Discoloration technique

A variety of flow visualization techniques have been used in stirred tanks over the years (Mavros, 2001). Among them, the single-indicator acid-base discoloration method is a practical non-intrusive global technique. It is based on following the color change of a solution containing an indicator, when an acid or alkaline solution generating a fast reaction is added. This technique has been applied to analyze flow patterns qualitatively and to determine mixing times in stirred vessels (Ascanio *et al.*, 2002).

Flow visualization experiments were performed in this work using the discoloration method. An advanced image analysis technique developed by Cabaret *et al*. (2007) was then used in order to analyze the results. This method has been used to successfully determine the macromixing time in several stirred tank studies and has demonstrated to be highly reproducible and robust (Bonnot *et al.*, 2007; Guntzburger *et al.*, 2009; Iranshahi *et al.*, 2007).

The image analysis technique consists in recording a video during the color change experiments. Images from the video are then sampled at a known rate. Next, the fluid area from each image is defined with imaging software and the rest is removed (*i.e.* the impeller or baffles). The resulting images are then analyzed individually using in-house analysis software coded in java. Using the Red-Green-Blue color model, the program determines the intensity of the green color for each pixel. An individual green threshold value is defined by comparing the first unmixed picture and the last fully mixed picture. By comparing its green value with the threshold a pixel can be considered mixed or unmixed. The curves resulting from this image analysis show the percentage over time of mixed pixels M (%), which is defined as

$$M(\%) = \frac{N_{\text{Mixed pixels}}}{N_{\text{Total pixels}}} \tag{5.1}$$

This analysis technique proved to give more information than the single mixing time in stirred tanks and it provided a picture of the mixing process over time (Cabaret *et al.*, 2007). To the best of our knowledge it has never been applied to a continuous system.

5.4.2 Residence Time Distributions

The analysis of residence time distributions (RTD) (Danckwerts, 1953) has proved to be a useful tool to understand the characteristics of the flow in extrusion equipment. It is based on the fact that depending on the geometry and hydrodynamics of the system, fluid elements spend different amounts of time to pass through the system. The distribution of these times of passage is called the residence time distribution of the fluid and is represented by the function *E(t)* (Levenspiel, 1999). Experimentally, the RTD function is the direct response to a tracer impulse. It is obtained by recording the concentration of tracer *C(t)* as a function of time and then normalizing this function by the total amount of tracer injected:

$$E(t) = \frac{C(t)}{\int_0^\infty C(t) \cdot dt} \tag{5.2}$$

The first moment of the *E(t)* curve is the mean residence time t_m and is defined by

$$t_m = \frac{\int_0^\infty t \cdot C(t) \cdot dt}{\int_0^\infty C(t) \cdot dt} \tag{5.3}$$

The second moment is known as the variance σ^2,

$$\sigma^2 = \int_0^\infty (t - t_m)^2 \cdot E(t) \cdot dt \qquad (5.4)$$

which gives a measure of the spread of the distribution around the mean.

5.5 Experimental procedure

5.5.1 Experimental setup

The experimental setup consisted of a transparent laboratory-scale modular Co-Kneader. The *L*/*D* of the Co-Kneader is 11 and the internal diameter of the barrel is 50.8 mm. The amplitude of the oscillation S_0 is 7.5 mm and for each complete turn the screw goes back and forth one time (**Figure 5–1**).

The barrel and the screw elements were specially manufactured from Plexiglas. The barrel has two inlets and an outlet; in one inlet the fluid is fed and in the other the tracer is injected. There are three rows of pins along the length of the barrel. Each pin is cylindrical, has a diameter of 4.2 mm and is 7.4 mm long. The fluid is pumped from a feeding tank to the inlet of the barrel by a progressive-cavity pump (PCM Pumps); nevertheless precautions were taken to avoid any effect on the flow inside the Co-Kneader. The flow delivered by the pump was monitored by an oval gear flow meter (Kobold Instruments) connected to a computer.

There are different types of screw elements available for this kind of extruder. In this study we used conveying elements (EZ) and mixing elements (KE), which are shown in **Figure 5–2**.

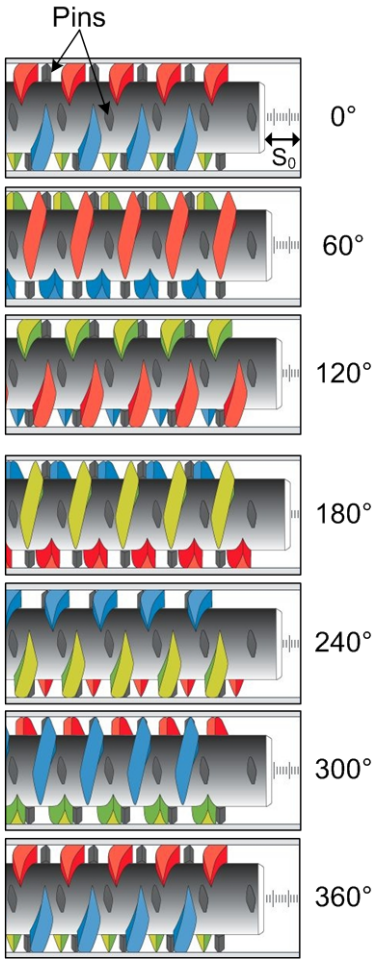

Figure 5–1. Screw motion of the Co-Kneader (Buss-Coperion brochure 2004)

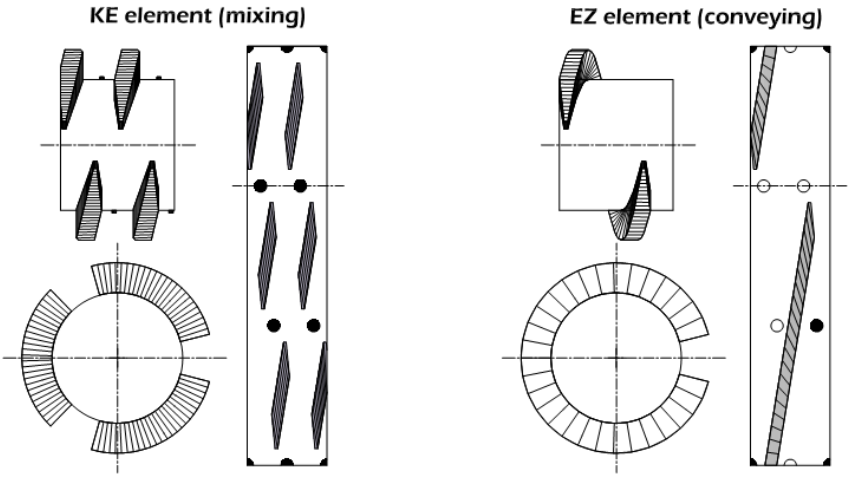

Figure 5–2. Different screw elements.

The EZ element has a single flight and one screw slice. The KE element has two flights and three screw slices. To each element corresponds a different pin configuration, therefore the distribution of the pins along the barrel depends on the screw profile. For the EZ element there is one pin in each of two rows and for the KE element there are two pins in each of the three rows. Detailed dimensions of the screw elements are summarized in **Table 5-1**. The screw configuration used in this work is shown in **Figure 5–3**. It comprises two conveying sections of as much as 5 elements each, and a mixing section of 8 elements.

Table 5-1. Geometrical configuration of the screw elements.

[Unit: mm]	KE	EZ
Inside diameter of barrel, D_b	50.80	50.80
Outside diameter of screw, D_o	50.20	50.20
Screw channel width, W	10.56	21.33
Screw channel depth, H	8.20	8.20
Length of one element, L_e	30	30
Flight angle, φ	9.37	9.37
Width of slice, s	8.53	8.53
Flight thickness, e	4.32	4.32
Number of flights	2	1
Number of slices	3	1

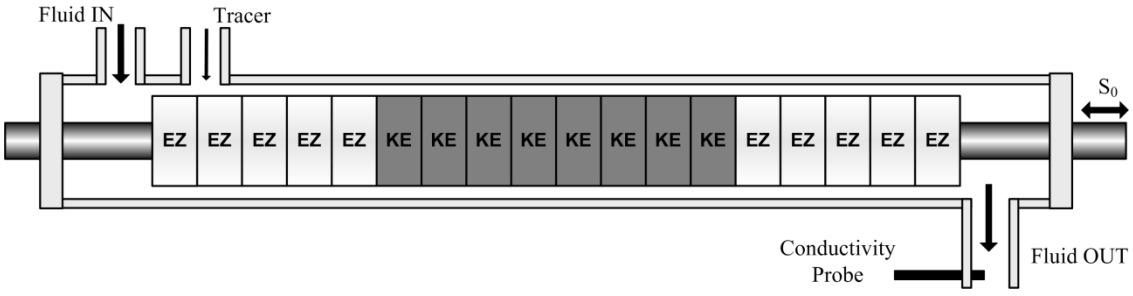

Figure 5–3. Studied screw profile

Each experiment was filmed with a digital CCD camera (Digital Handycam DCR-PC101, Sony). A rectangular water-filled chamber of 125 mm x 125 mm x 630 mm encased the barrel in order

to minimize optical distortions due to its curvature. White sheets of paper were used as light diffuser on the chamber in order to achieve homogenous illumination.

A homemade 2-pin conductivity probe was placed at the outlet of the Co-Kneader (**Figure 5–3**). The probe consists of stainless steel electrodes in a cylindrical casing of the same material which is sealed with Teflon caps. The electrodes are connected to an alternating current supply in order to prevent polarization or electrolysis. The measured output from the conductivity probe is collected on a computer using a data acquisition card.

5.5.2 Materials

An aqueous solution of corn syrup was used. The solution had a concentration in weight of 82% which corresponded to a Newtonian viscosity μ of 0.2 Pa·s and a density ρ of 1270 kg/m^3. A Bohlin Viscometer 88-BV with a Couette configuration was used to determine the rheological properties. Since the fluid had a low viscosity, the experimental setup was adjusted to avoid any flow induced by gravity.

Bromocresol purple was used as the indicator for the discoloration technique. The tracer solution injected into the Co-Kneader was prepared by adding 1.2% w/w of table salt (NaCl) and 1% v/v of 10N HCl solution to a given quantity of corn syrup/indicator solution.

5.5.3 Operating conditions

Each experiment was conducted having the Co-Kneader completely filled. Care was taken in order to eliminate all the bubbles in the fluid, since they cause interference with the image analysis technique. The tracer was injected into the second barrel inlet of the Co-Kneader (**Figure 5–3**) while the system was stopped; however, the low viscosity fluid quickly developed its velocity profile. By controlling the angular position of the screw we could ensure that the tracer did not leaked through the screw flight slices into the next screw channel. The camera, as well as

the computer, started to record each experiment moments before the system was initiated and it was stopped when the conductivity probe output returned to the baseline. Fifteen operating conditions (**Table 5-2**) were tested, with three repetitions for each condition. We kept the system running for 3 minutes after each repetition as well as after changing operating conditions, to ensure that no tracer was still in the system.

Table 5-2. Operating Conditions

Run no.	N (rpm)	Q (kg/h)
1	50	5.5
2	50	6.7
3	50	7.8
4	50	8.8
5	50	10.3
6	75	12.5
7	75	14.0
8	75	15.2
9	75	16.5
10	75	17.8
11	100	20.4
12	100	21.7
13	100	23.1
14	100	24.3
15	100	25.7

5.5.4 Discoloration technique

The first step of the discoloration technique is the incorporation of the indicator into the bulk glucose solution. The quantity of indicator in the fluid has a direct impact on the sharpness and intensity of the resulting color. A small quantity will yield pale colors, making the detection of the color change difficult. For the application of the technique in stirred tanks, Cabaret *et al.* (2007) recommended a concentration of 0.0043g of bromocresol purple per liter of solution. However, in our case this quantity was not enough to observe a bright and contrasting color; therefore the concentration of bromocresol purple had to be increased. In this work 0.016g of bromocresol purple was added per 1L of the corn syrup solution. The experiments followed the color change from purple (alkaline color) to yellow (acid color); therefore the corn syrup solution was set to purple by adding aqueous 10N NaOH solution.

The discoloration experiments were recorded showing the Co-kneader lengthwise in order to observe the color change evolution from the inlet to the exit. The injected tracer reacted and changed the bulk color gradually from purple to yellow as the mixing took place. The captured videos were then analyzed using the method proposed by Cabaret *et al*. (2007) to quantify the macromixing evolution along the Co-Kneader. Following the technique, one image per second was sampled from each video. With imaging software, the shaft was removed from each picture leaving two fluid areas, one above and one below (**Figure 5–4**). The upper fluid area was chosen as the fluid-only area to be analyzed since the lower part contains pins. The flights of the screw could not be removed from the images due to their complicated geometry; however, since the screw elements are transparent we do not expect them to greatly influence the results.

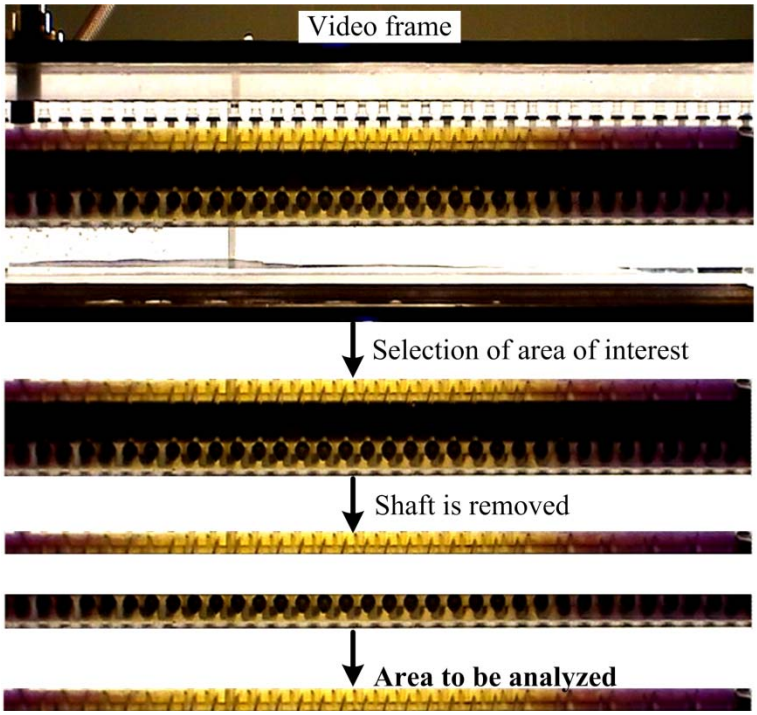

Figure 5–4. Example of video frame and area to be analyzed.

This image analysis technique is applied straightforward in stirred tanks as videos are usually recorded until a uniform yellow color is achieved. However, in a continuous system with a pulse

injection, this condition is never reached since the system will gradually return to its purple starting point. Therefore, a picture showing the fluid being completely yellow was used only as a reference.

5.5.5 Residence time distributions

The residence time distributions (RTD) were determined using a stimulus response technique. The salt in the tracer solution acts as the electrolyte that will produce a change in the conductivity of the system, given that the corn-syrup solution without tracer has a very low conductivity. The conductivity of the solution is found by measuring the amount of current obtained when a potential difference is applied to the electrodes in the conductivity probe. Since in a solution the current flows by ion transport, an increasing concentration of ions in the solution will result in higher conductivity values. The conductivity probe in the experimental setup monitored the local conductivity as a function of time. According to Brown *et al.* (2004) the data obtained by conductivity probes must be normalized to eliminate the effect of probe gain. The data is normalized between an initial zero value C_0 measured before the addition of tracer, and a typical stable value C_∞ measured after the test is complete. The normalized output is obtained by

$$C_i' = \frac{C_i - C_0}{C_\infty - C_0} \tag{5.5}$$

However, in our results the value of C_∞ - C_0 was very close to zero, which meant that our probe did not have any gain effect. Therefore the data was only shifted so that the baseline corresponded to a value of zero.

5.6 Results and discussion

5.6.1 Discoloration technique

Since this was the first time that mixing curves were obtained for a continuous mixer, the first step was to determine the acid concentration to be injected as the tracer into the system. Preliminary results showed that high acid concentrations caused all the fluid in the system to turn to yellow. On the other hand, the color change resulting from very small acid concentrations vanished in the bulk fluid. In both extreme cases, the discoloration experiments did not reveal any mixing pattern. A suitable acid concentration able to generate a sharp color change of only a portion of the fluid volume was thus looked for. In order to achieve this, four different concentrations of HCl were tested for the same operating condition and the mixing curves were obtained (**Figure 5–5**). It is important to note that even in a static system the tracer would eventually become mixed with the bulk fluid by means of molecular diffusivity. However, the time scale of this process is much larger than the time scale of the experiments, therefore in this case the molecular diffusivity of the tracer is negligible.

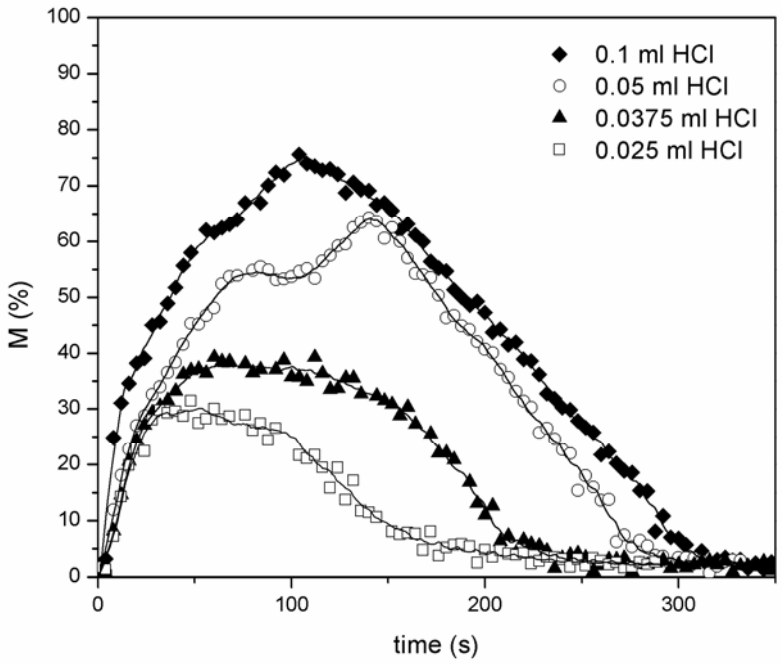

Figure 5–5. Mixing curve as a function of acid concentration, N = 50 rpm, Q = 10.3 kg/h.

As the concentration of acid is raised, the maximum value of *M* and the residence time increase. This was expected because as more acid is reacting, more fluid volume changes color; therefore it takes more time to leave the system. The shape of the curve however is different for each concentration. All the curves show two inflection points. In all cases, *M* increases from $t = 0$ s until the first point. Then, between the first and the second inflection point, the slope of the curve gradually increases as acid concentration increases. For the two lower concentrations, *M* starts to gradually decrease, while for the two higher concentrations a higher value of *M* is reached. Then, from the second inflection point on, *M* decreases more rapidly in all cases. This effect, which is more noticeable when 0.05 ml of HCl is injected, has to do with the different sections of the screw profile and it will be explained in more detail later. All the experiments were then carried out with a tracer having 0.05 ml of HCl.

The reproducibility of the image analysis technique is shown in (**Figure 5–6**). The mixing curves obtained after the image analysis present very small variations, which mean that the technique is as robust for continuous systems as for stirred tanks.

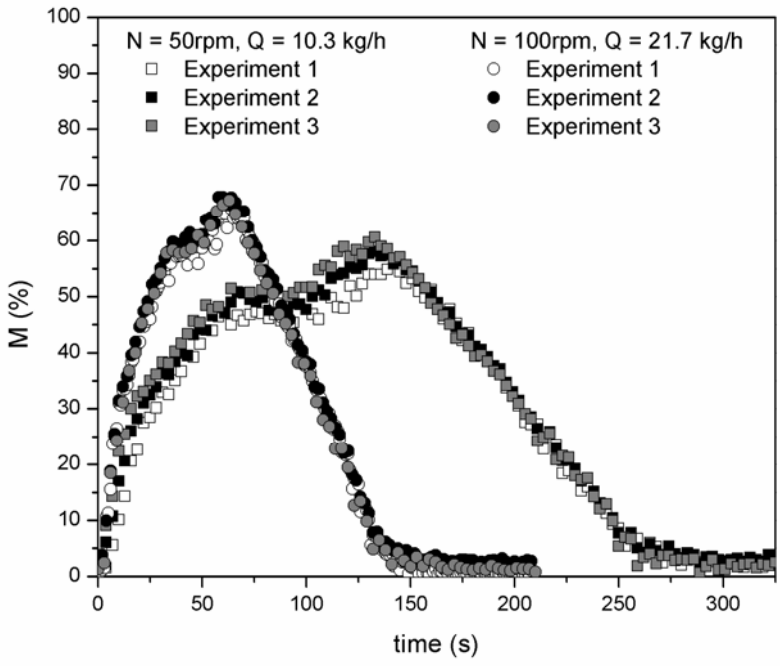

Figure 5–6. Mixing curve obtained for the reproducibility test, $N = 50$ rpm and $N = 100$ rpm.

Mixing curves obtained at N = 75 rpm for different flow rates are showed in **Figure 5–7**. For smaller flow rates the time spent inside the system increases. However, the general shape of the curve remains the same. A similar behavior was observed for the other two screw speeds.

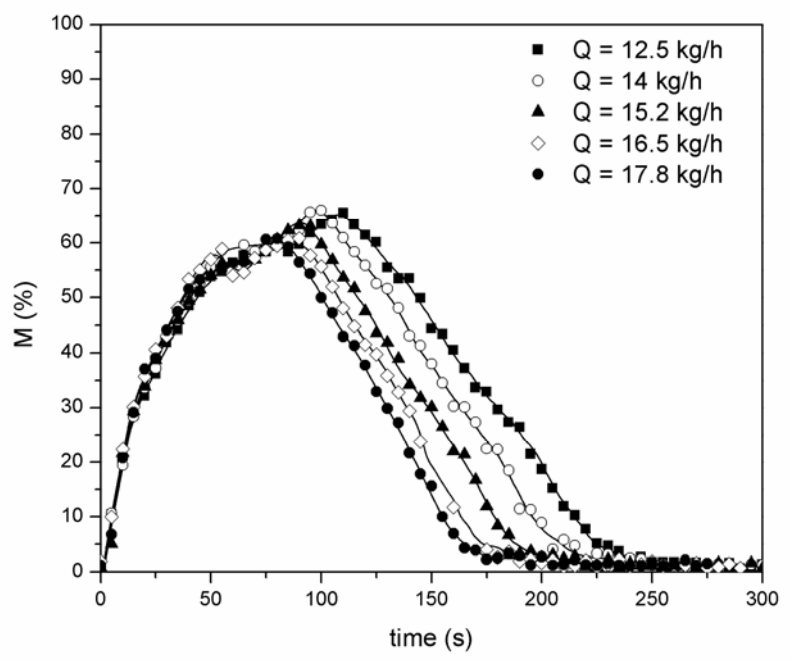

Figure 5–7. Effect of flow rate on the mixing curve at N = 75 rpm.

To be able to compare all operating conditions, the mixing curves were normalized by dividing the time by the theoretical mean residence time defined as V/Q, where V is the volume of the system, thus obtaining θ, a dimensionless time (**Figure 5–8**). The variation between the different conditions is not very significant. The maximum value of M is approximately the same for every curve, around 65% ±5%, which as mentioned earlier, depends on the quantity of acid being introduced into the system. Among the screw speeds, the difference in θ is only 0.1, which equals to a residence time 10% larger that the theoretical value obtained by V/Q. A slight tendency of the higher screw speeds towards this bigger value of θ is observed, which could mean a larger degree of backmixing.

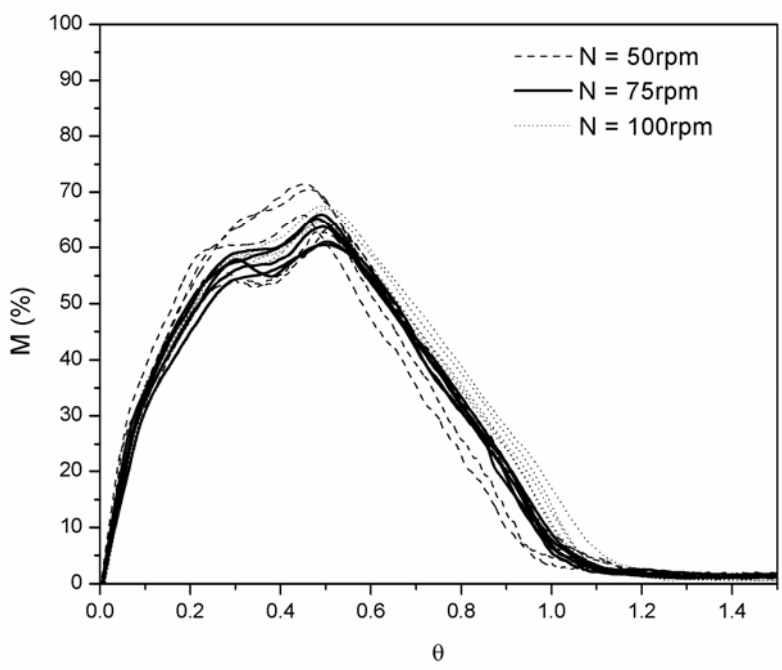

Figure 5–8. Normalized mixing curves, all conditions.

Figure 5–9 presents the mixing curve obtained at 50 rpm and 10.3 kg/h. As mentioned earlier, the curve shows three different regions, which are related to the different sections of the screw: two conveying sections with a mixing section in between. From the start of the experiment until $M \approx 55\%$ (**Figure 5–9a)** the extent of the mixed zone steadily increases. This corresponds to the mixed zone extending from the first conveying section to about two thirds into the mixing section. Then, as it goes forward into the mixing section (**Figure 5–9b**) M remains constant for a short time until it starts to increase again to reach a higher value of approximately 65%. This last point represents the moment when the mixed part of the fluid gets into the last conveying section (**Figure 5–9c**). Later on, the mixed region leaves the system gradually. It can be concluded that the different rates at which the mixed region expands (*i.e.* the slope m on the mixing curve) depend on the type of screw element. The value of the slope therefore gives an insight into the behavior of the flow. A slope of 0 indicates that the extent of the mixed zone remains constant trough time. If the slope changes from m_1 to m_2 and m_2 is smaller than m_1, then the mixed zone is expanding at a slower rate than previously in time, which may indicate the presence of backflow.

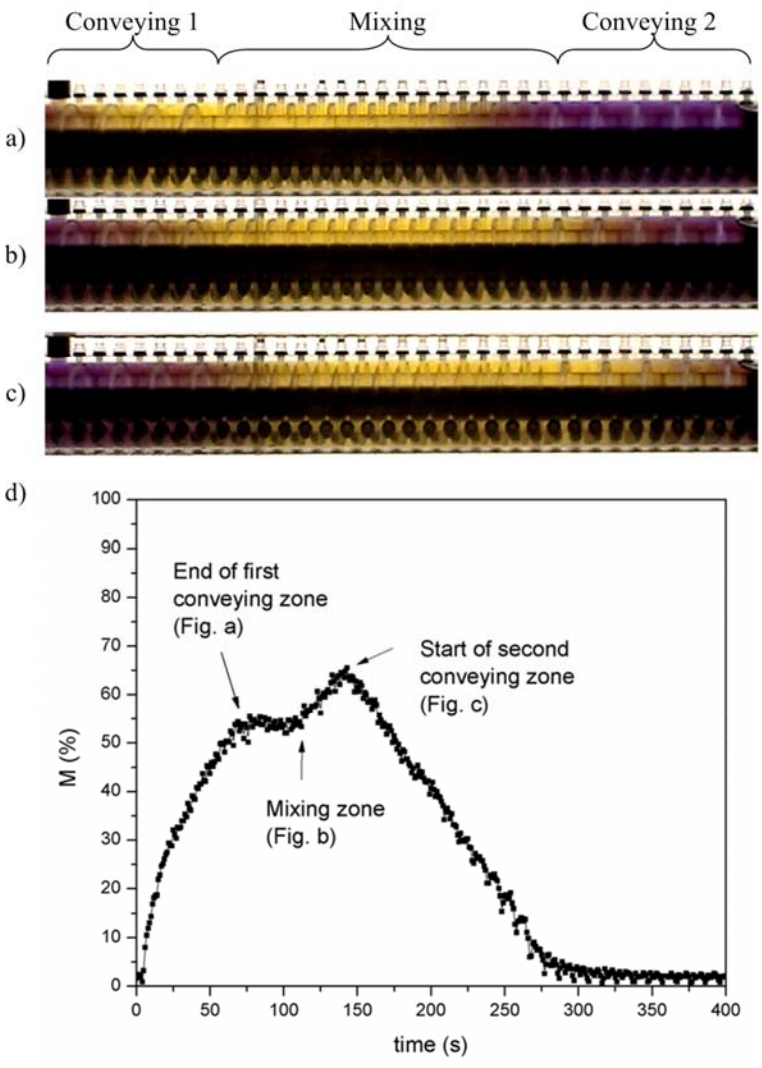

Figure 5–9. **a)** Discoloration area in the first conveying zone. **b)** Discoloration area in the mixing zone. **c)** Discoloration area in the second conveying zone. **d)** Mixing curve at N = 50 rpm and Q = 10.3 kg/h.

By performing a linear fitting in each region of the mixing curve as showed in **Figure 5–10**, we can obtain the value of the slope which can be expressed as an axial mixing rate m_r. This mixing rate can be defined as the increase in axial mixed area in time. **Figure 5–10** shows the value of the mixing rates obtained in each of the three regions of the mixing curve for all experimental conditions. We can clearly see the sharp change of the mixing rate depending on the screw section. It is interesting to see that the value of m_r2, which corresponds to the screw mixing zone, is not affected by either the screw speed or the flow rate. In this study we worked with a fixed

screw profile, however the effect of the number of screw elements on the mixing rate should be investigated.

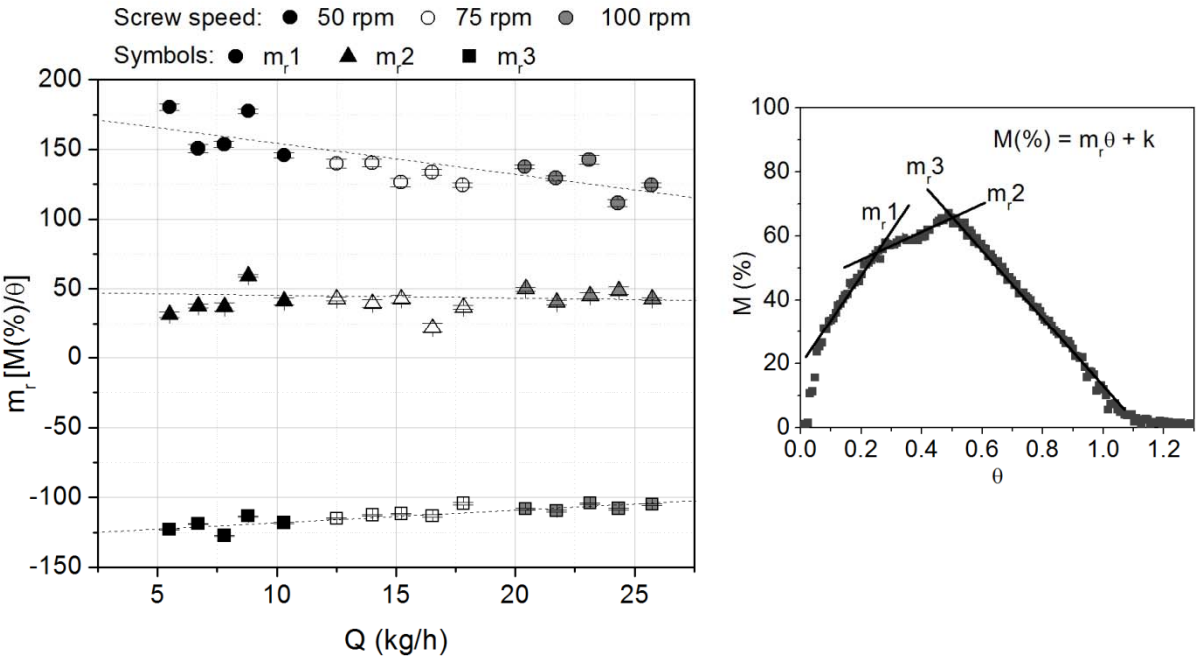

F**igure 5–10**. Mixing rates as a function of flow rates.

The results obtained by the discoloration technique together with the image analysis technique are preliminary The observed trends must be confirmed by exploring wider ranges of operating conditions as well as fluids with different rheological behaviors.

5.6.2 Residence time distributions

The reproducibility of the measurements obtained with the conductivity probe is demonstrated in **Figure 5–11**. The RTD curves for N = 75 rpm at different flow rates, are shown in **Figure 5–12**. For clarity of representation only the curves of three flow rates are plotted. It is observed that as the feed rates increase the residence times become shorter and the distributions become narrow. This behavior was observed for all operating conditions. Mean residence times were determined

by **Equation 5.3** and the results are presented in **Figure 5–13**. We can see that the flow rate has more impact on the mean residence time at lower screw speeds than at higher screw speeds.

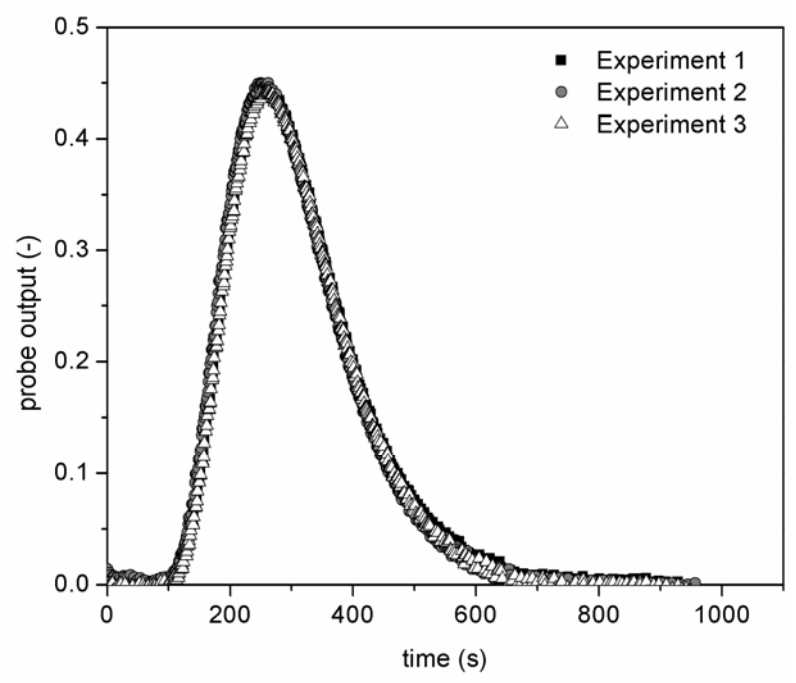

Figure 5–11. Probe output curve showing the reproducibility of the experiments, N = 50 rpm Q = 7.8 kg/h.

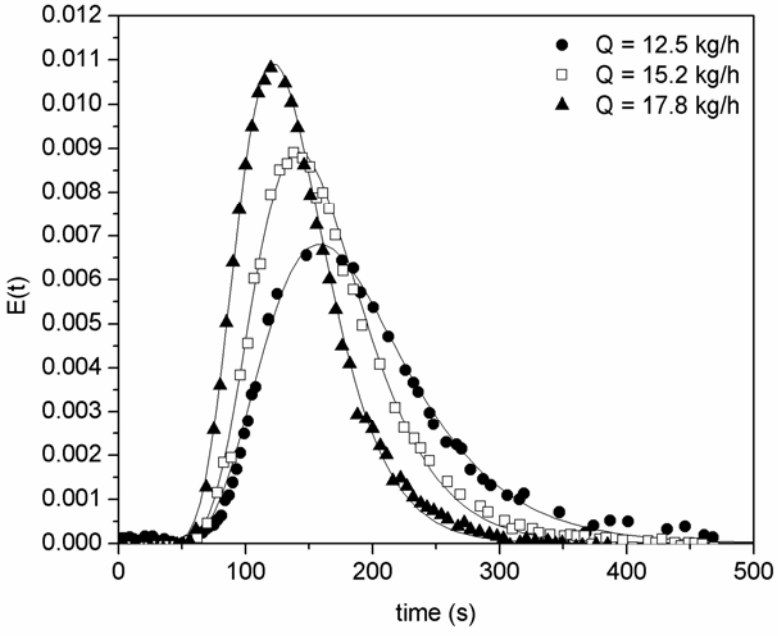

Figure 5–12. RTD curves for N = 75 rpm

As a reference, the mean residence times were compared with the theoretical values obtained from calculating *V*/*Q*. The experimental results are lower than the theoretical values by a relative error of ~12%. The difference can be attributed to experimental error and to the closed boundary condition assumption made when using **Equation 5.3**. The closed boundary assumption states that there should be no flow or diffusion or upflow eddies at the entrance and exit planes of the system (Levenspiel, 1999).

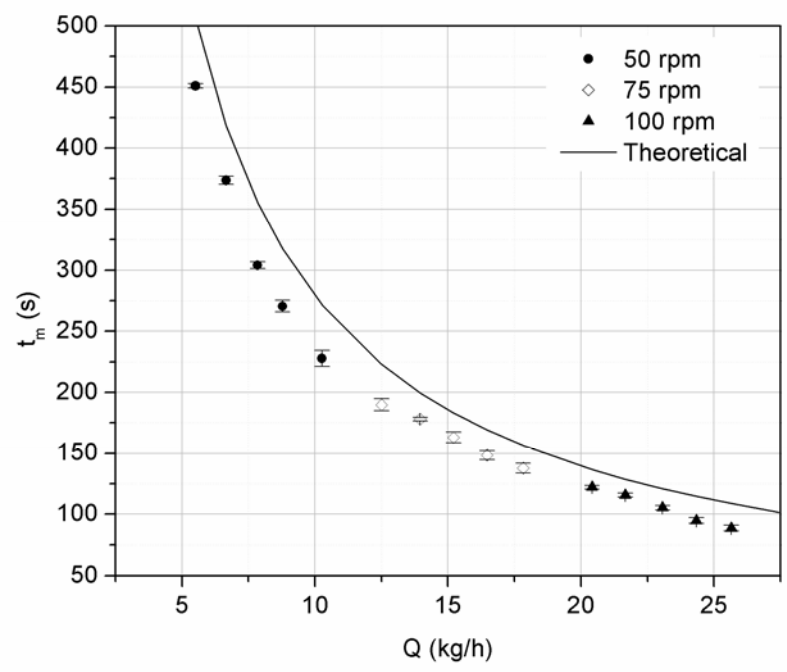

Figure 5–13. Average residence time as a function of flow rate for different screw speeds.

The spread σ^2 of the RTDs was also obtained (**Figure 5–14**). The value of σ^2 decreases as the flow increases for each fixed speed, which means that the distributions become narrower thus confirming the previous observation. As with the mean residence time results, it is observed that σ^2 decreases more rapidly at lower screw speeds. It should be reminded that the RTD results were obtained with the restriction of having to work with a fully filled system. Consequently, the effect of the screw speed on a fixed flow rate could not be studied. The RTD analysis results presented

in this work confirm the observations reported by Lyu & White (1998) regarding the relationship of the mean residence time and the variance with the operating conditions.

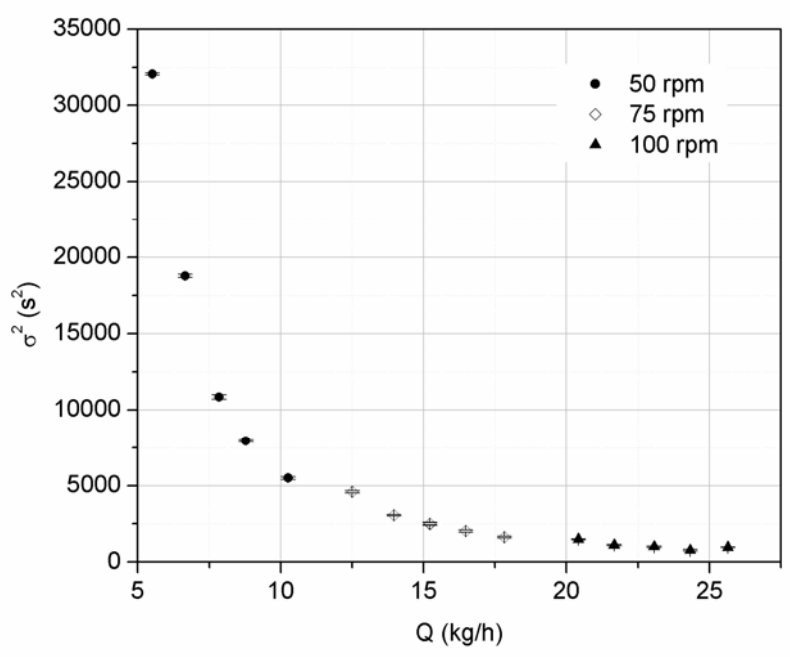

Figure 5–14. Variance of the RTD as a function of flow rate for different screw speeds.

We compared the RTD results obtained for the Co-Kneader to the axial dispersion model (Levenspiel, 1999). The normalized RTD curves presented in **Figure 5–15**, where $\theta = t/t_m$, show that the curves obtained experimentally are non-symmetrical and that they present a shift from the plug flow behavior (*i.e.* mean centered on $\theta = 1$). Therefore we used the axial dispersion model for a large deviation from plug flow and open-open boundary conditions:

$$E(\theta) = \frac{1}{2}\sqrt{\frac{Pe}{\pi\theta}}\exp^{\left[-\frac{Pe(1-\theta)^2}{4\theta}\right]} \qquad (5.6)$$

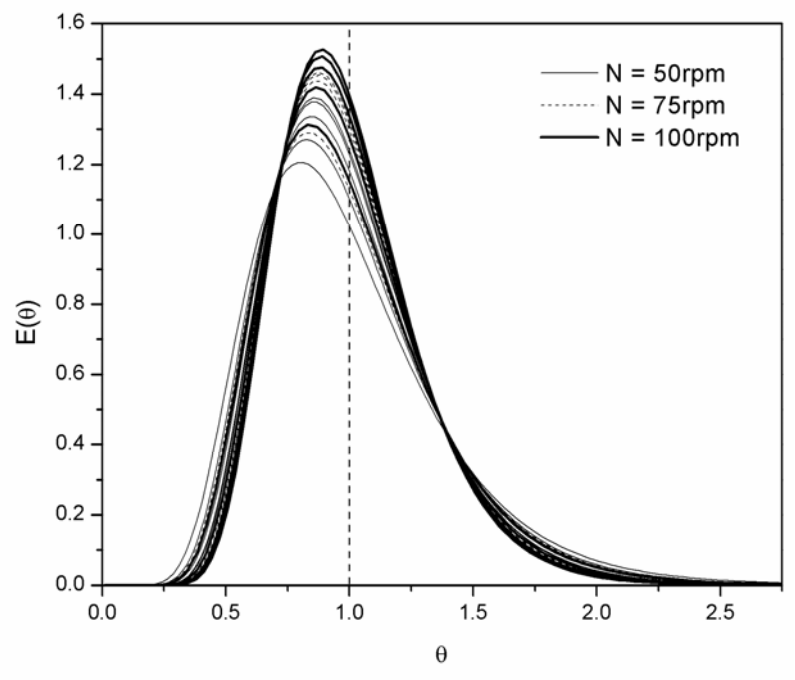

Figure 5–15. Dimensionless RTD, all conditions.

By fitting this model to the experimental results we can obtain the axial Peclet number *Pe* defined as

$$Pe = \frac{uL}{D_{ax}} \tag{5.7}$$

where u is the mean axial velocity of the flow, L the axial length and D_{ax} the axial dispersion coefficient. At *Pe* higher than 100, this model approximates plug flow behavior. On the other hand, a *Pe* approaching 0 indicates fully mixed flow (Nauman, 2008).

Figure 5–16 shows the fitting of the experimental RTD to the axial dispersion model. The number on each curve corresponds to the run number associated to each operating condition as listed in **Table 5-2**. For each screw speed, the lowest and the highest studied flow rates are presented. We can observe that the shape of the curve is closely represented by the model.

However, the experimental results are more shifted towards small values of θ. It is also observed that the ability of the model to fit the experimental results does not change noticeably according to the operating conditions. This fact is confirmed by comparing the values of the adjusted R^2 from each fitting (**Table 5-3**). The *Pe* values obtained from the model fit are presented in **Table 5-3**.

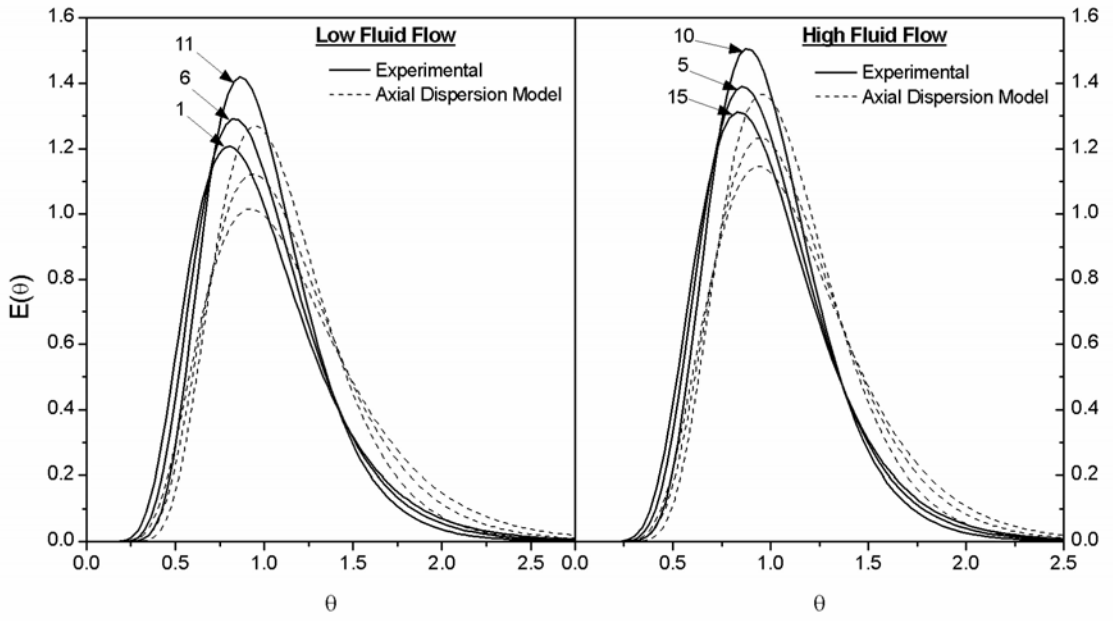

Figure 5–16. Fitting of experimental results with the axial dispersion model.

From the obtained *Pe* numbers the axial dispersion coefficients were calculated (**Equation 5.7**). Even if the axial dispersion model was not an exact fit, the value of an estimated D_{ax} can yield information on the spreading process. **Figure 5–17** shows the influence of the flow rate on D_{ax}. An increase in flow rate results in an increase of D_{ax}. Since our system is fully filled, the flow rate directly affects the amount of backmixing. However it has been found that on partially filled systems the variation of flow rate results in a variation of the degree of fill without significantly impacting the value of D_{ax} (Troelstra, 1998). The effect of the screw speed is presented in **Figure 5–18**. As the screw speed increases the value of D_{ax} increases following an approximated linear dependency. Troelstra (1998) reported this linear dependency and it was attributed to the direct relationship between the number of pin passages and the screw speed. With every passage of the

pin through the slices in the screw flight the material is pushed backwards and the axial mixing is induced.

Table 5-3. Values of *Pe* and adjusted R^2 obtained from the axial dispersion model.

Run no	*N* (rpm)	*Q* (kg/h)	*Pe*	Fit adj. R^2
1	50	5.5	12.47	0.902
2	50	6.7	14.58	0.908
3	50	7.8	16.80	0.927
4	50	8.8	18.23	0.935
5	50	10.3	18.65	0.940
6	75	12.5	15.31	0.909
7	75	14.0	20.45	0.933
8	75	15.2	21.00	0.935
9	75	16.5	21.33	0.935
10	75	17.8	22.96	0.939
11	100	20.4	19.74	0.931
12	100	21.7	23.78	0.941
13	100	23.1	21.84	0.936
14	100	24.3	23.00	0.943
15	100	25.7	15.99	0.918

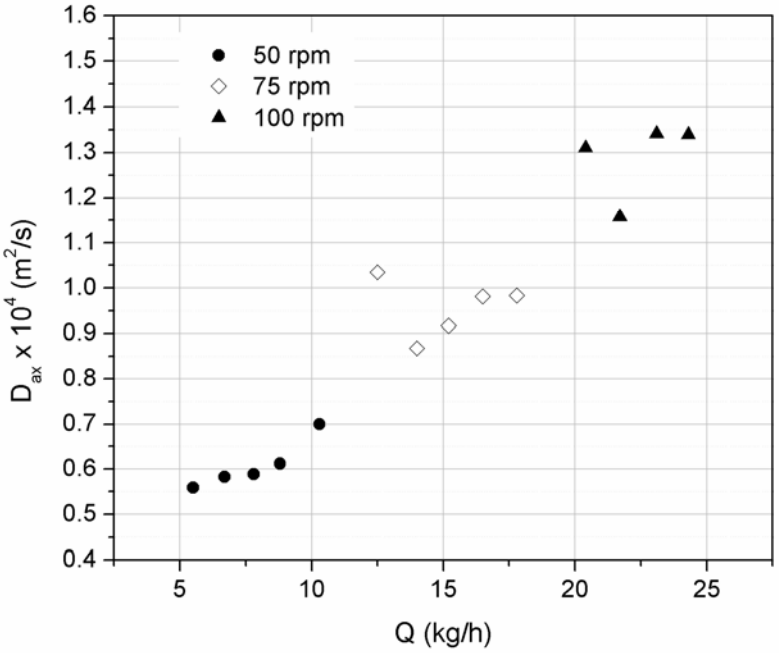

Figure 5–17. Axial dispersion coefficient as a function of flow rate at different screw speeds.

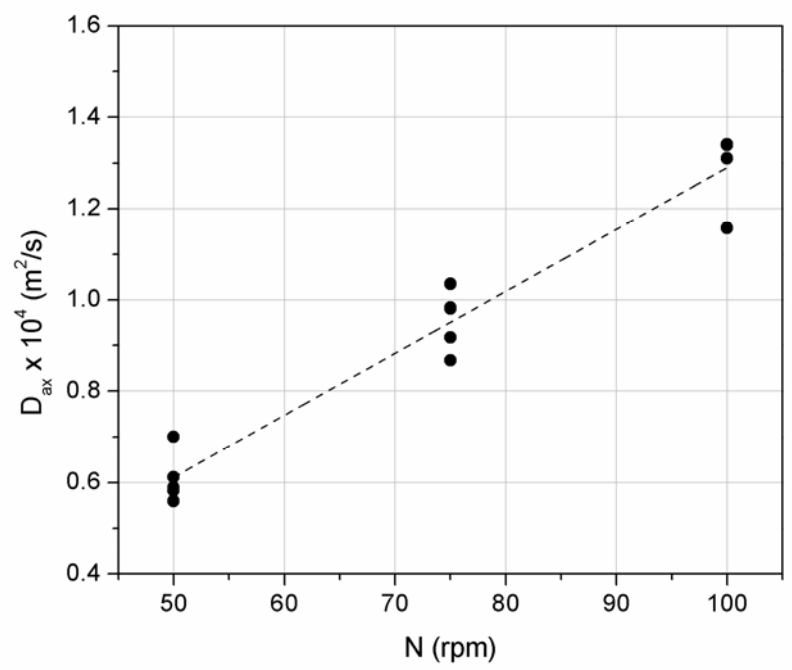

Figure 5–18. Axial dispersion coefficient as a function of screw speed. Flow rate ranges from 5.5 kg/h to 24.7 kg/h.

A comparison between the Co-Kneader and other systems was performed (**Figure 5–19**). The dimensionless cumulative distribution function $F(\theta)$ at two screw speeds was obtained from the experimental RTD curves of the Co-Kneader by

$$F(\theta) = \int_0^{\theta} E(\theta)dt \tag{5.8}$$

The $F(\theta)$ curve for a single screw extruder was calculated following the RTD model developed by Pinto & Tadmor (1970):

$$F(t) = F(\xi) = 0.5\left(3\xi^2 - 1 + (\xi - 1)\sqrt{1 + 2\xi - 3\xi^2}\right) \tag{5.9}$$

where ξ is the dimensionless normal coordinate defined as

$$\xi = 2\frac{y}{H} \tag{5.10}$$

The dimensionless time θ can be expressed as a function of ξ

$$\theta = \frac{3\xi - 1 + 3\sqrt{1 + 2\xi - 3\xi^2}}{6\xi\left(1 - \xi + \sqrt{1 + 2\xi - 3\xi^2}\right)} \tag{5.11}$$

This model was derived for a Newtonian fluid using the flat plate approximation and considering both down- and cross-channel velocity components. Three dimensional models of single screws based on computer simulations have proven to yield narrower RTD curves (Joo & Kwon, 1993).

The theoretical $F(\theta)$ curve for an empty tube was obtained from

$$F(\theta) = \frac{1}{4}\frac{1}{\theta^2} \qquad \theta > 0.5 \tag{5.12}$$

Finally, the curves for the Kenics (Chemineer) and the SMX (Sulzer) static mixers were modeled by the axial dispersion model (**Equation 5.6**) using a *Pe* of 80 and 110 respectively as suggested by the manufacturers.

The cumulative RTD curves of the single screw and the empty tube show that the residence times are not uniformly distributed around the mean, which leads to an uneven mixing history. The Co-Kneader and the static mixers on the contrary show a more even and narrow distribution. Both systems exhibit axial dispersion as well, which is not found on either the single screw or the empty tube. It is clear that the combination of the oscillating motion and the pins in the barrel greatly improves the mixing performance of a single screw by promoting axial mixing. It is also

observed that the distribution of the static mixers is narrower compared to that of the Co-Kneader and has a shorter tail.

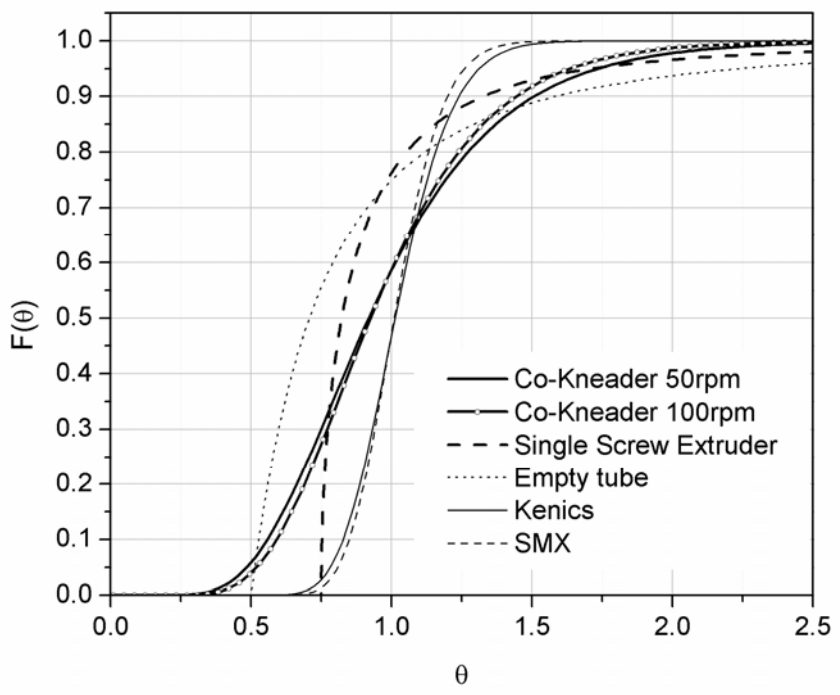

Figure 5–19. Comparison of RTD between different systems.

5.7 Conclusions

Flow visualization experiments were performed in a fully transparent laboratory-scale Co-Kneader. An image analysis technique usually used in stirred tanks was applied for the first time in a continuous mixer. The mixing curves resulting from the image analysis gave a different insight into the mixing mechanisms of the Co-Kneader. This technique may prove useful towards the evaluation of the degree of backmixing. However, experiments should be done in well known geometries (*e.g.* a single screw extruder in which the backmixing is known to be minimal) in order to have a point of reference and confirm these results. Different Co-Kneader screw profiles should also be investigated.

Results of mean residences times and variance from the RTD analysis confirmed previous work. The axial dispersion model allowed for an estimation of the axial dispersion coefficient. In a fully filled system, the dispersion coefficient increases with the flow rate and the screw speed. Contrary to the single screw extruder, the pins and the slices in the screw of the Co-Kneader generate residence times evenly distributed around the mean residence time. Compared to a static mixer the Co-Kneader has a broader residence time distribution.

5.8 Acknowledgements

The financial support of the National Science and Engineering Research Council of Canada (NSERC) and of TOTAL is greatly acknowledged. Thanks are also directed to CONACYT (Mexico) for the financial support of M. Brito-Bazan.

5.9 Notation

θ	Dimensionless time	Dimensionless
μ	Newtonian viscosity	Pa s
ρ	Density	kg/m^3
σ^2	Variance	s^2
ξ	Dimensionless normal coordinate	Dimensionless
φ	Flight angle	°
C_i	Output from conductivity prove	Dimensionless
C_0	Initial zero value from conductivity probe	Dimensionless
C_∞	Final stable value from conductivity probe	Dimensionless
D	Diameter	m

D_{ax}	Axial dispersion coefficient	m^2/s
D_b	Inside diameter of barrel	mm
D_o	Outside diameter of screw	mm
e	Flight thickness	mm
H	Screw channel depth	mm
N	Screw speed	rpm
L	Axial length	m
L_e	Length of screw element	mm
M	Mixed pixels	%
m	Slope on mixing curve	Dimensionless
m_r	Mixing rate	Dimensionless
Pe	Peclet number	Dimensionless
Q	Flow rate	kg/h
S_0	Amplitude of screw stroke	mm
s	Width of screw slice	mm
t	Time	s
t_m	Mean residence time	s
u	Mean axial velocity	m/s
V	Volume	m^3
W	Screw channel width	mm

5.10 References

Ascanio, G., Brito-Bazan, M., Brito-De La Fuente, E., Carreau, P. J., & Tanguy, P. A. (2002). Unconventional configuration studies to improve mixing times in stirred tanks. *Canadian Journal of Chemical Engineering, 80*(4), 558-565.

Bigio, D., & Baim, W. (1991). Study of the mixing abilities of the NITSE using a Newtonian fluid. *SPE ANTEC Tech. Papers*, 146-148.

Bonnot, S., Cabaret, F., Fradette, L., & Tanguy, P. A. (2007). Characterization of mixing patterns in a coaxial mixer. *Chemical Engineering Research and Design, 85*(8 A), 1129-1135.

Brown, D. A. R., Jones, P. N., & Middleton, J. C. (2004). Experimental Methods. In E. L. Paul, V. A. Atiemo-Obeng & S. M. Kresta (Eds.), *Handbook of Industrial Mixing: Science and Practice* (pp. 145-256). Hoboken, N.J.: John Wiley & Sons.

Brzoskowski, R., Kumazawa, T., & White, J. L. (1991). A Model of Flow in the Mixing Section of the List Kokneader. *International Polymer Processing, 6*(2), 136-142.

Cabaret, F., Bonnot, S., Fradette, L., & Tanguy, P. A. (2007). Mixing time analysis using colorimetric methods and image processing. *Industrial and Engineering Chemistry Research, 46*(14), 5032-5042.

Carneiro, O. S., Poulesquen, A., Covas, J. A., & Vergnes, B. (2002). Visualisation and analysis of the flow along the kneading block of a twin-screw extruder. *International Polymer Processing, 17*(4), 301-308.

Danckwerts, P. V. (1953). Continuous-flow systems. Distribution of residence times. *Chemical Engineering Science, 2*(1), 1-13.

Elemans, P. H. M., & Meijer, H. E. H. (1990). On the modeling of continuous mixers. Part II. The cokneader. *Polymer Engineering & Science, 30*(15), 893-904.

Guntzburger, Y., Fradette, L., Farhat, M., Heniche, M., Tanguy, P. A., & Takenaka, K. (2009). Effect of the geometry on the performance of the Maxblend impeller with viscous Newtonian fluids. *Asia-Pacific Journal of Chemical Engineering, 4*(5), 528-536.

Hoppe, S., Detrez, C., & Pla, F. (2002). Modeling of a cokneader for the manufacturing of composite materials having absorbent properties at ultra-high-frequency waves. Part 1: Modeling of flow from residence time distribution investigations. *Polymer Engineering & Science, 42*(4), 771-780.

Iranshahi, A., Devals, C., Heniche, M., Fradette, L., Tanguy, P. A., & Takenaka, K. (2007). Hydrodynamic characterization of the Maxblend impeller. *Chemical Engineering Science, 62*(14), 3641-3653.

Jaffer, S. A., Bravo, V. L., Wood, P. E., & Hrymak, A. N. (2000). Experimental validation of numerical simulations of the kneading disc section in a twin screw extruder. *Polymer Engineering & Science, 40*(4), 892-901.

Joo, J. W., & Kwon, T. H. (1993). Analysis of residence time distribution in the extrusion process including the effect of 3-d circulatory flow. *Polymer Engineering & Science, 33*(15), 959-970.

Levenspiel, O. (1999). *Chemical reaction engineering* (3rd ed.). New York: Wiley.

Lyu, M.-Y., & White, J. L. (1995). Models of Flow and Experimental Studies on a Modular List/Buss Kokneter. *International Polymer Processing, 10*(4), 305-313.

Lyu, M.-Y., & White, J. L. (1996). Modelling of a Viscous Non-Newtonian Polymer Melt in a List/Buss Kneader and Comparison to Experiment. *International Polymer Processing, 11*(3), 208-221.

Lyu, M.-Y., & White, J. L. (1997). Simulation of linear viscoelastic flow behavior in the Buss Kneader. *Polymer Engineering & Science, 37*(3), 623-635.

Lyu, M.-Y., & White, J. L. (1998). Residence time distributions and basic studies of flow and melting in a modular Buss Kneader. *Polymer Engineering & Science, 38*(9), 1366-1377.

Ma, X., Geng, X., & Zhu, L. (2003). Study on the characteristic of axial circular flow field in co-rotating twin screw extrusion. *SPE ANTEC Tech. Papers*, 142-146.

Manas-Zloczower, I. (2009). Continuous process visualization: visual observation, on-line monitoring, model-fluid extrusion and simulation. In I. Manas-Zloczower (Ed.), *Mixing and compounding of polymers: theory and practice* (2nd ed., pp. 473-576). Munich: Hanser.

Mavros, P. (2001). Flow visualization in stirred vessels - A review of experimental techniques. *Chemical Engineering Research & Design, 79*(A2), 113-127.

Mehranpour, M., Nazokdast, H., & Dabir, B. (2002). Computational study of the velocity field in the conveying element of a Ko-Kneader with CFD method. *International Polymer Processing, 17*(2), 108-114.

Mehranpour, M., Nazokdast, H., & Dabir, B. (2003). Computational study of velocity field in the KE element of a modular Ko-Kneader with CFD method. *International Polymer Processing, 18*(4), 330-337.

Nauman, E. B. (2008). Residence Time Theory. *Industrial & Engineering Chemistry Research, 47*(10), 3752-3766.

Pinto, G., & Tadmor, Z. (1970). Mixing and Residence Time Distribution in Melt Screw Extruders. *Polymer Engineering & Science, 10*(5), 279-288.

Rauwendaal, C. (1991). Mixing in single-screw extruders. In C. Rauwendaal (Ed.), *Mixing in polymer processing* (pp. 129-239). New York: Marcel Dekker.

Rauwendaal, C. (2009). Mixing in Single-Screw Extruders. In I. Manas-Zloczower (Ed.), *Mixing and compounding of polymers: theory and practice* (2nd ed., pp. 853-945). Munich: Hanser.

Sanchez, R., Bigio, D. I., & Karnik, S. (1997). Mixing of a low molecular weight additive in a co-rotating twin screw extruder: Visualization of the flow path. *SPE ANTEC Tech. Papers*, 3724-3729.

Shon, K., Chang, D., & White, J. L. (1999). A comparative study of residence time distributions in a kneader, continuous mixer, and modular intermeshing co-rotating and counter-rotating twin screw extruders. *International Polymer Processing, 14*(1), 44-50.

Stade, K. (1977). Techniques for Compounding Glass Fiber-Reinforced Thermoplastics. *Polymer Engineering & Science, 17*(1), 50-57.

Stade, K. (1978). Production of Glass Fiber-Reinforced Poly(Butylene Terephthalate) on a Continuous Kneader. *Polymer Engineering & Science, 18*(2), 107-113.

Todd, D. B. (1987). Mixing Mechanisms for Polyoxymethylene. *SPE ANTEC Tech. Papers*, 128-132.

Troelstra, E. J. (1998). *The Buss Kneader as Polymerization Reactor for Acrylates.* PhD, University of Groningen, The Netherlands.

Troelstra, E. J., Van Lune, J., Van Dierendonck, L. L., & Janssen, L. P. B. M. (2002). Modeling of a Buss-Kneader as a polymerization reactor for acrylates. Part I: Model validation. *Polymer Engineering & Science, 42*(1), 230-239.

Yao, W. G., Takahashi, K., Koyama, K., & Dai, G. C. (1997). Design of a new type of pin mixing section for a screw extruder based on analysis of flow and distributive mixing performance. *Chemical Engineering Science, 52*(1), 13-21.

CHAPTER 6
NUMERICAL FLOW SIMULATION OF A CO-KNEADER USING 3D FINITE ELEMENT METHOD

Magdalena Brito-Bazan, Mourad Heniche, Louis Fradette, Philippe A. Tanguy

URPEI, CREPEC, Department of Chemical Engineering, École Polytechnique de Montréal

P.O.Box 6079, Station Centre-Ville, Montreal, Que., Canada H3C 3A7

6.1 Presentation of the article

This article was submitted to the Polymer Engineering & Science Journal.

This article aims the second specific objective which was to assess the hydrodynamic characteristics of the Co-Kneader using a three dimensional numerical model that includes both the oscillating motion of the screw and the pins on the barrel.

This article presents for the first time results obtained with a numerical flow model that takes into account both the oscillation of the screw and the pins in the barrel of the Co-Kneader. Results of pressure profiles and RTD are validated with experimental data. A trajectory length distribution (TLD) analysis is performed here for the first time in a continuous system.

Keywords: Co-Kneader, CFD, flow fields, finite element method, RTD, TLD.

6.2 Abstract

The 3D flow inside a Co-Kneader has been predicted taking into account the presence of pins as well as the influence of screw oscillation. The studied screw geometry included conveying and mixing screw elements. Calculations were made using a MINI-based fictitious domain finite element method. Numerical results were first validated by means of experimental pressure vs. flow rate characteristic curves. The results were found to be in good agreement with the experimental results. To characterize the mixing ability of the Co-Kneader, RTD analysis as well as the recently introduced TLD analysis were performed. RTD results were further validated with experimental results, showing good agreement. TLD analysis shows that the mixing element yields axial mixing whereas the conveying element causes down-channel mixing. Predictions of pressure profiles and velocity fields are presented as well as RTD and TLD curves.

6.3 Introduction

Single screw extruders are a very common type of extruders in polymer processing. Because they are not very good mixers as such, different devices or adaptations are made to the screw and/or barrel to enhance the mixing action. The Co-Kneader is an example of such modifications. It is a single screw extruder that combines the usual rotational motion with a reciprocating action. The screw is made of interchangeable screw elements that have interrupted flights. In addition, three rows of stationary pins are placed along the barrel. The combination of the rotational and reciprocating motions of the screw causes the pins to move (relative to the screw) in a sinusoidal way through the flight clearances of the screw, which results in a self-wiping action. Applications of the Co-Kneader include the manufacture of carbon electrode paste, rocket propellant fuel, food processing, and plastics compounds among others (Rauwendaal, 1991a).

Work aimed at understanding the flow inside the Co-Kneader began with Booy & Kafka (1987) and Brzoskowsky *et al.* (1989). Both works modelled the flow of a Newtonian fluid between two flights with a single pin passing between them. These investigations were carried out using the

finite element method program POLYFLOW™ and a modified Flow Analysis Network (FAN) method respectively. The first experimental effort to understand the working principle of the extruder was performed by Elemans & Meijer (1990). They worked with a Co-Kneader fitted into a transparent barrel and the results obtained were used to validate a simplified model which only considered the rotational motion of the screw. Lyu & White, in a series of reports (1995, 1996, 1997a, 1997b, 1997c, 2000) developed a mathematical flow model that accounted for the oscillation of the screw, as well as non-Newtonian and non-isothermal aspects. They analysed the local and global characteristics of a Co-Kneader using the FAN method; however, they excluded the presence of the pins at the barrel. More recently, Mehranpour *et al.* (2002a, 2002b, 2003a, 2003b, 2004) used the model developed by Lyu & White to estimate residence time distributions (RTD) for conveying and mixing screw elements separately. They used 3D Finite Volume Method (FVM) for the flow fields and a Cluster Model for the RTD. Since they used Lyu & White's model, they neither took into consideration the presence of the pins. The oscillatory motion and the pins at the barrel are what distinguish the Co-Kneader from other extruders. However there are not modeling studies that take into account the interaction of both features.

The residence time distribution (RTD) is a common tool to describe continuous flow systems. In polymer processing, the RTD is used when analyzing the probability of polymer thermal, mechanical or chemical degradation (Rauwendaal, 1994). The mixing process in the extruder can also be examined with the RTD. In reactive extrusion, the chemical reaction depends on the time-temperature history of the polymer. Moreover, when in operation, the time needed to purge a system or to switch materials is also given by this distribution (Tadmor & Gogos, 1979). Therefore, RTD functions have an important role in the design, operation, and selection of extruders. In simple geometries (*e.g.* a pipe) the theoretical calculation of the RTD is straightforward since analytical models of velocity profiles exist. In single screw extruders, simplifying assumptions help to determine reasonably well velocity profiles (Rauwendaal, 1994). On the other hand, when more complex flow systems are encountered the modeling of the velocity profile, and consequently the prediction of the RTD, become more difficult. Simplifications of the system being studied will then have a direct impact on the accuracy of predicted RTD.

A different distribution function for mixing analysis in flow systems was introduced by Villermaux (1996). The trajectory length distribution (TLD) is based on the distance covered by fluid elements. In the same manner that the RTD is constructed from the different times spent by fluid elements inside the system, the TLD is defined by the different distances covered by the same fluid elements. It was demonstrated that for a given RTD there is a great variety of TLD that may be encountered, thus concluding that the TLD yields a different aspect of mixing from that shown by the RTD (Villermaux, 1996). It is not easy to experimentally obtain the trajectory length of a particle. To this effect, methods like radioactive particle tracking (Kiared *et al.*, 1997) or positron emission particle tracking (Fangary *et al.*, 2000) have been used. The TLD approach has already been applied in the study of a three-phase fluidized bed (Kiared *et al.*, 1997) and in stirred vessels (Campolo *et al.*, 2003; Fangary *et al.*, 2000). However, to the knowledge of the authors, it has never been applied to an extruder.

Computational Fluid Dynamics (CFD) is an alternative approach to study complex flows, like the one inside the Co-kneader. Numerical modeling by CFD allows for the detailed observation of the three dimensional flow at any time and at any location. Additionally, RTD and TLD can be simultaneously obtained by tracking massless tracers in the flow field. The prediction of residence times from CFD calculations has been extensively reported for continuous mixers such as twin screw extruders (Bravo *et al.*, 2004; Ishikawa *et al.*, 2002), single screw extruders with mixing sections (Yao *et al.*, 2001) and static mixers (Fradette, 1999; Heniche *et al.*, 2005). Trajectory lengths from CFD have only been reported for static mixers (Fradette, 1999) and for a stirred tank (Campolo *et al.*, 2003).

The objective of this work is to assess the hydrodynamic characteristics of the Co-Kneader using computer simulations. The challenge is to include in the numerical model both the oscillating motion and the pins on the barrel. To achieve this, a 3D fictitious domain finite element method is used in order to account for the moving parts. A mixing analysis using particle tracking results is performed as well. The results presented include pressure profiles, velocity profiles, RTD and TLD. The results are validated with experiments.

6.4 Methodology

6.4.1 Experimental Methodology and Setup

Experimental results were obtained with a laboratory-scale modular Co-Kneader. The internal diameter of the barrel D_b is 50.8 mm and the L/D_b ratio is 11. The amplitude of the oscillation S_0 is 7.5 mm and for each complete turn the screw goes back and forth one time. There are three rows of pins along the length of the barrel. Each pin is cylindrical, has a diameter of 4.2 mm and is 7.4 mm long.

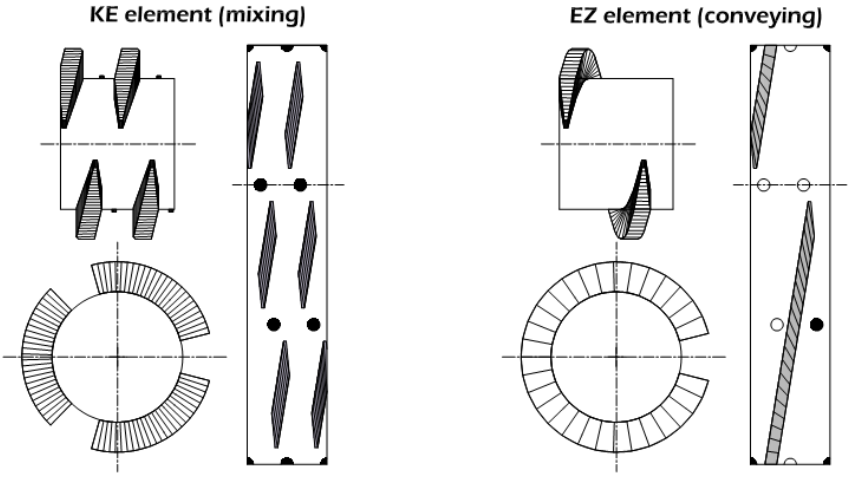

Figure 6–1. Screw elements.

Two different types of screw elements were used, conveying elements (EZ) and mixing elements (KE) (**Figure 6–1**). The EZ element has a single flight and one screw slice. The KE element has two flights and three screw slices. There is a different pin configuration for each element. The EZ element has one pin in each of two rows and the KE element has two pins in each of the three rows. Detailed dimensions of the screw elements are summarized in **Table 6-1**. The screw configuration used in this work is shown in **Figure 6–2**. It comprises two conveying sections of 5 elements each, and a mixing section of 8 elements. The pressure build up along the screw was measured using open tube manometers placed near the inlet and at the exit of the system (**Figure**

6–2). RTD results were obtained by means of a conductivity probe placed at the outlet of the system (**Figure 6–2**).

Table 6-1. Geometrical configuration of the screw elements.

[Unit: mm]	KE	EZ
Inside diameter of barrel, D_b	50.80	50.80
Outside diameter of screw, D_s	50.20	50.20
Screw channel width, W	10.56	21.33
Screw channel depth, H	8.20	8.20
Length of one element, L_e	30	30
Flight angle, φ	9.37	9.37
Width of slice, s	8.53	8.53
Flight thickness, e	4.32	4.32
Number of flights	2	1
Number of slices	3	1

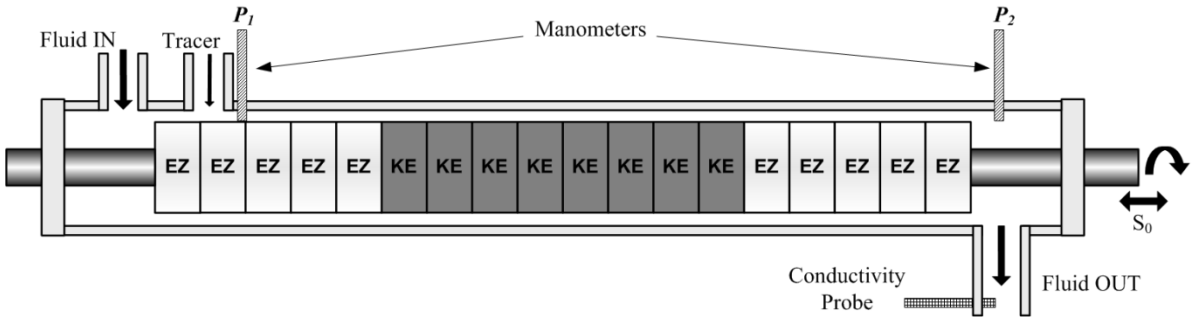

Figure 6–2. Studied screw profile, location of the manometers and of the conductivity probe.

An aqueous solution of corn syrup was used. The solution had a concentration in weight of 82% which corresponded to a Newtonian viscosity of 0.2 Pa·s and a density of 1270 kg/m^3. Since the fluid had a low viscosity, the setup was adjusted to avoid any flow induced by gravity. The tracer used for the residence time measurements was prepared by adding 1.2 %w/w of table salt (NaCl) to a given quantity of corn syrup solution. The operating conditions used for the experiments are listed in **Table 6-2**.

Table 6-2. Experimental operating conditions.

Run no.	N (rpm)	Q (kg/h)
1	50	5.5
2	50	6.7
3	50	7.8
4	50	8.8
5	50	10.3
6	75	12.5
7	75	14.0
8	75	15.2
9	75	16.5
10	75	17.8
11	100	20.4
12	100	21.7
13	100	23.1
14	100	24.3
15	100	25.7

6.4.2 Numerical Methodology

The numerical prediction of the unsteady three-dimensional flow field in the Co-Kneader was obtained by solving the incompressible Navier-Stokes equations with a finite element method.

$$\rho\left(\frac{\partial \mathbf{v}}{\partial t} + \mathbf{v}\cdot\nabla\mathbf{v}\right) + \nabla p + \nabla\cdot\tau = f \tag{6.1}$$

$$\nabla\cdot\mathbf{v} = 0 \tag{6.2}$$

The 5-node P1+-P1 (MINI) tetrahedral element was used to approximate the velocity and the pressure (Arnold *et al.*, 1984). Due to the complex movement of the Co-Kneader screw and aiming at simplifying the boundary conditions, an Eulerian frame of reference was used. In order to do so, a fictitious domain method known as virtual finite element method (VFEM) was employed. Within the VFEM framework, a unique mesh is required during the computations and the screw is represented by a set of moving control points that act like kinematic constraints (Bertrand *et al.*, 1997; Glowinski *et al.*, 1994). It has been showed that the MINI-based VFEM is

a suitable strategy for simulating complex mixing systems since the accuracy obtained is comparable with that given by other more costly elements (Coesnon *et al.*, 2008). A portion of the surface grid used to generate the control points that represent the screw (virtual object) is shown in **Figure 6–3b**. The complete screw profile (**Figure 6–2**) was constituted by approximately 135 000 control points.

The geometry which represented the fluid field consisted of a 3D cylindrical mesh with an annulus section, in which the shape of the pins was subtracted. Additionally, the inlet and outlet of the system was accounted for by two short pipe sections placed perpendicularly on each end of the main part and facing opposite directions. The model geometry had the same dimensions as the experimental setup. The final 3D unstructured mesh required about 1 million elements (**Figure 6–3a**), yielding a system of nearly half a million equations.

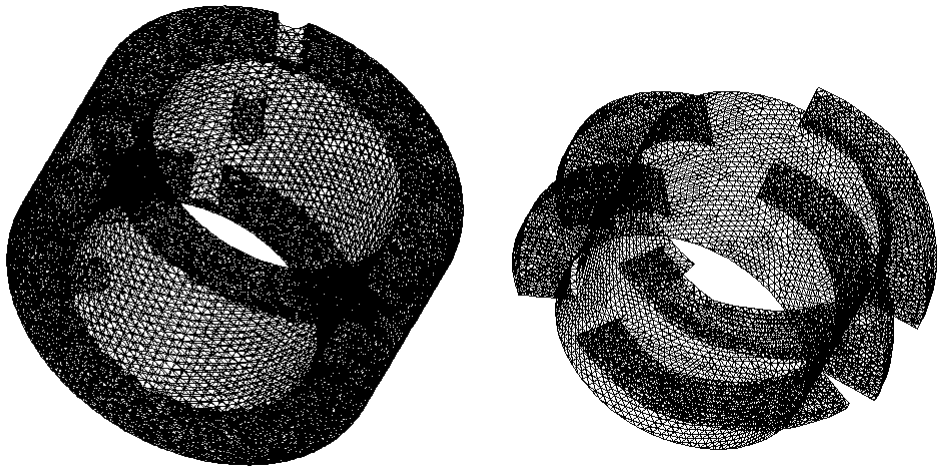

Figure 6–3. Section of the finite element meshing of the Co-kneader. **a)** 3D mesh of the barrel and pins, **b)** surface grid of the screw elements.

Cartesian coordinates (*x, y, z*) were used as reference frame in the numerical model. The screw is oriented along the *z*-axis, the barrel cross-section is defined in the *x*-*y* plane, and the inlet and outlet cross-sections are defined in the *x*-*z* plane. The set of boundary conditions employed were the following:

- Laminar velocity profile in the axial direction at the fluid inlet: $v_x = v_z = 0$ and v_y given by **Equation 6.3** in cylindrical coordinates (r, θ, y), where Q is the mass flow rate and $R=\sqrt{(x^2+z^2)}$ is the radius of the inlet pipe.

$$v_y = \frac{2Q}{\rho\pi R^2}\left[1-\left(\frac{r}{R}\right)^2\right] \tag{6.3}$$

- At the exit $V_x = V_z = 0$
- No slip condition at the barrel wall: $\mathbf{v} = 0$
- Imposed velocity on the control points is given by **Equation 6.4** and **Equation 6.5**, where S_0 is the amplitude of the oscillation and the frequency ω is $2\pi N/60$.

$$v = \pi DN + \frac{dS(t)}{dt} \tag{6.4}$$

$$S(t) = \frac{S_0}{2}\sin\omega t \tag{6.5}$$

The fluid properties of the corn syrup solution used in the experimental study were used for the simulation work as well. Calculations were done at each 3° of screw rotation, which corresponds to 120 time steps to complete a single screw turn and its corresponding back and forth cycle. It was observed that the solutions were already periodic after the first screw turn. All simulations were run on an IBM P690 cluster and each required approximately 70 hours of CPU time. The problem was resolved using a Newton-Raphson iterative scheme available in the commercial 3D finite element software POLY3D™ (Rheosoft, Inc.). Both the 3D and the surface mesh were generated on I-DEAS (EDS) software, and post-processing visualization was done with Ensight (CEI).

6.5 Results and discussion

6.5.1 Pressure profiles

In order to validate the simulations, numerical results are compared with experimental values in the form of flow rate versus pressure characteristic curves (**Figure 6–4**). The pressure gradient ΔP is P_2-P_1, where P_1 is the pressure near the inlet of the system, and P_2 the pressure at the exit (**Figure 6–2**). The numerical results of P_1 and P_2 are averaged values of all the time steps, at the same position as the location of the manometers. The relative error calculated between the experimental and the numerical results in all cases is less than 8%. However, the difference between experimental and numerical results tends to increase slightly as the speed increases.

Figure 6–5 shows the calculated pressure profiles along the length of the Co-Kneader for different operating conditions. The different pumping capacities of the two types of screw elements are clearly evidenced. Both conveying zones (EZ screw elements) develop most of the pressure whereas in the mixing zone (KE screw elements) the pressure remains almost constant. The difference in pumping capacities of the screw elements is a result of their geometry; the mixing element has two more screw slices than the conveying element, therefore it generates less pressure.

Figure 6–6 shows lengthwise calculated pressure distributions in the Co-Kneader. The cylindrical surface is placed at mid-channel distance from the screw root. In **Figure 6–6a** the pressure distribution along the complete length of the extruder shows that the pressure gradient is developed axially, whereas in standard single screw extruders (no interrupted flights) the pressure gradient follows the down channel direction. **Figure 6–6b** is a close up to the mixing section in which the color scale has been modified in order to represent more clearly the differences in pressure values around the pin section. Following the down channel direction, the pressure in front of the pins is generally higher that behind the pins.

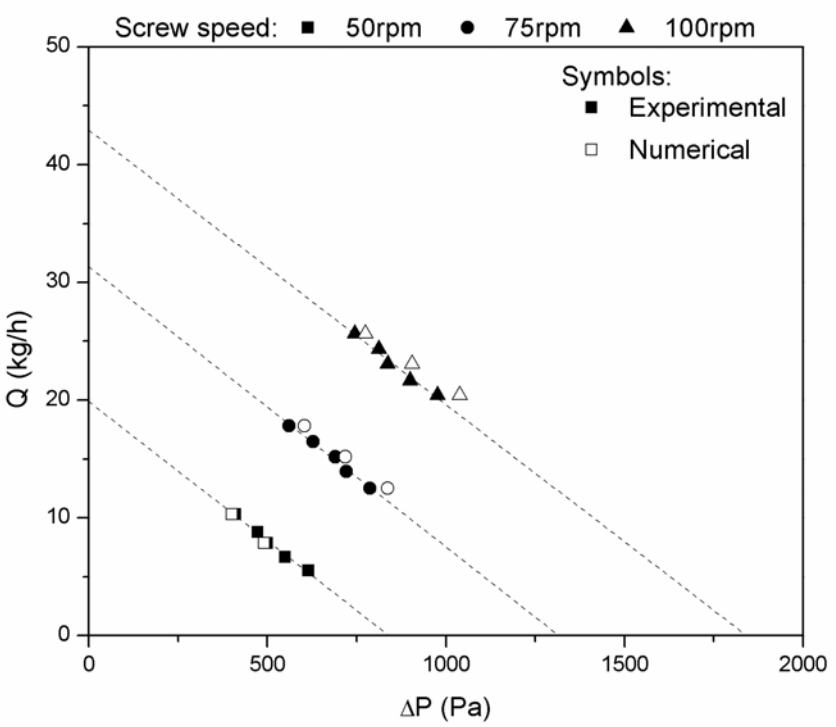

Figure 6–4. Experimental and numerical characteristic curves.

6.5.2 Velocity fields

Figure 6–7 shows velocity magnitude distributions for N = 50 rpm and Q = 10.3 kg/hr in a segment of the mixing section. The local effect of the pin can be observed by comparing different screw positions. The flow is split and recombined from one channel to another when a pin is located between the slices of the screw (**Figure 6–7a**), thus promoting backflow and distributive mixing. However, when there is no pin between the slices (**Figure 6–7b**) the flow simply continues down channel. In the same way, the regular down channel flow between the screw flights (**Figure 6–7d**) is disrupted when there is a pin in the channel (**Figure 6–7c**). The leakage flow associated with the screw slices is affected by the pins as well. In **Figure 6–7a**, the flow appears to accelerate more between adjacent pins than it does when there are no pins (**Figure 6–7b**).

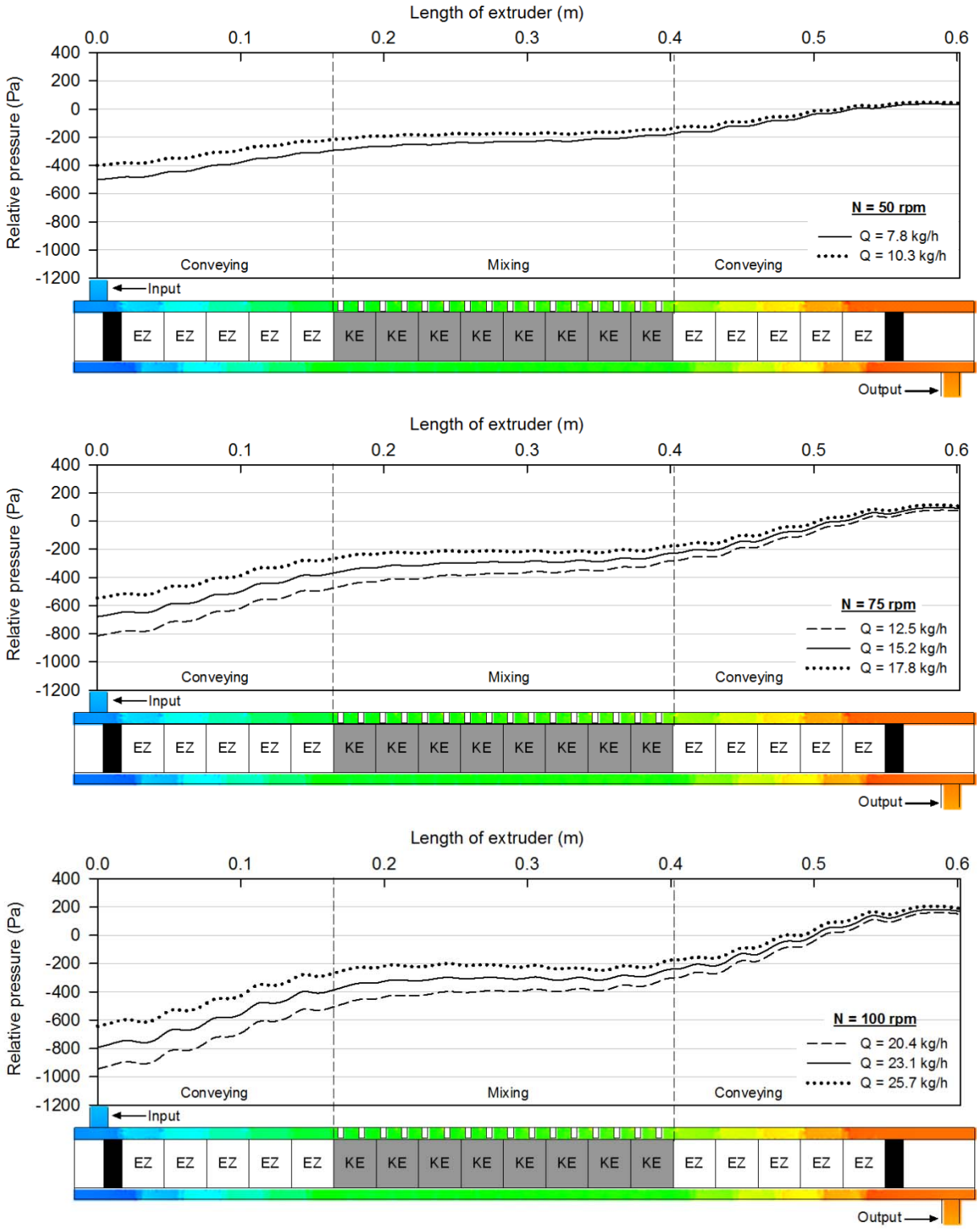

Figure 6–5. Calculated pressure profiles along the extruder at different screw speeds.

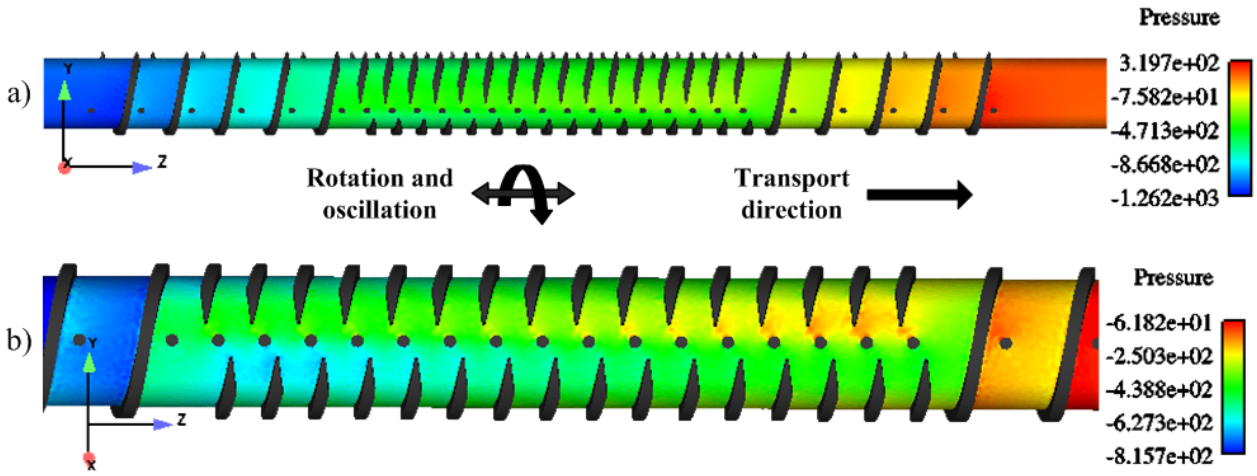

Figure 6–6. Pressure distribution in Co-Kneader at 100 rpm; **a)** complete screw, **b)** close up of mixing section. Pressure values in Pa.

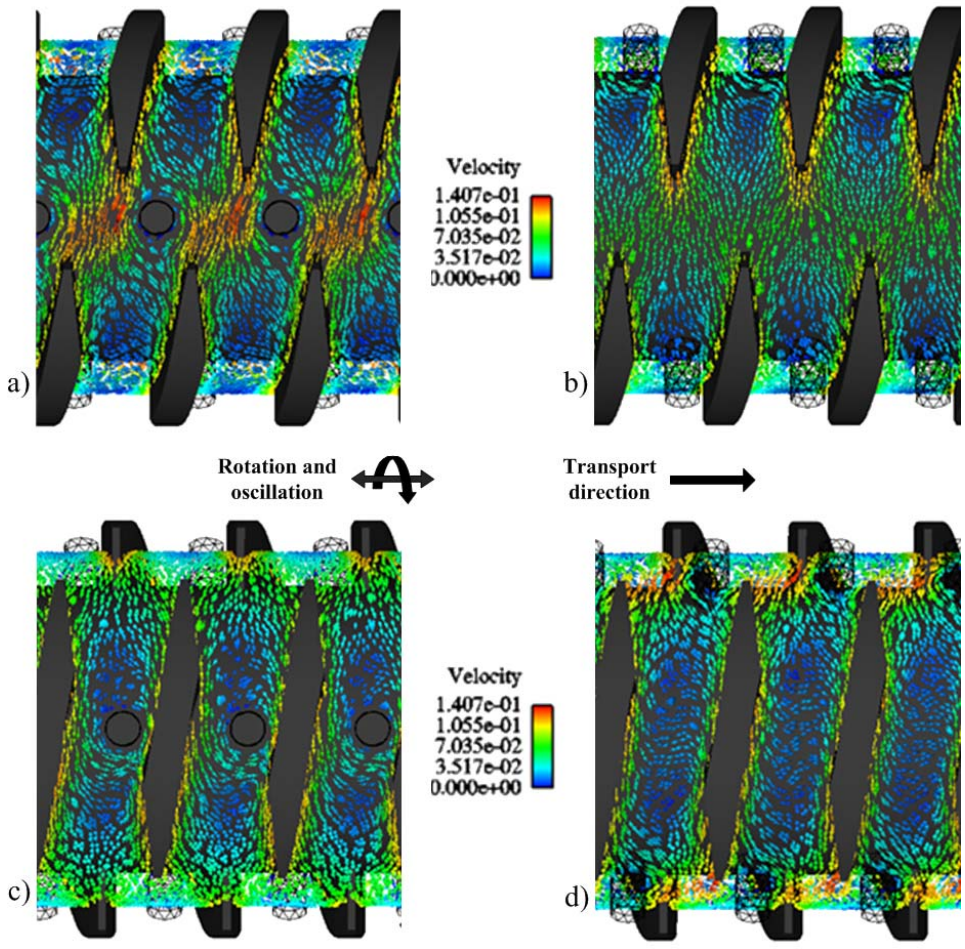

Figure 6–7. Calculated velocity field (magnitude) in the mixing section of the Co-Kneader at N = 50 rpm and Q = 10.3 kg/hr.

6.5.3 Particle tracking

The RTD and TLD results presented in this work were obtained by the particle tracking technique, where the motion of massless particles is dominated only by the flow field. The path followed by a particle is obtained by the following equation

$$\mathbf{v}(\mathbf{x}) = \frac{d\mathbf{x}}{dt} \tag{6.6}$$

where $\mathbf{v}(\mathbf{x})$ is the velocity vector, $\mathbf{x}$ is the vector position and t is the time. To solve the problem, we used the element-by-element approach coupled with a predictor-corrector shooting scheme proposed by Heniche & Tanguy (2006). This method, which has been successfully apply to the complex geometries of static mixers (Heniche *et al.*, 2005), does not require the use of any time steps. Nevertheless, the accuracy of computed trajectories depends on the number of shootings. The trajectories used for the RTD and TLD analyses were obtained using 300 shootings per element. A problem in particle tracking techniques is the loss of particles due to zero velocity regions (no-slip boundary condition) or because the particles exit the computational domain (round-off errors on computed coordinates). To minimize the particle loss due to zero velocity near the walls, the injected particles were positioned leaving a small gap from the wall. All subsequent analyses were then performed based on the number of particles arriving at the exit plane. The injection of particles was done following the screw cross section plane *x*-*y*. In preliminary results it was found that out of a large number of tracers initially injected at the start of the screw (location 1 in **Figure 6–8**) only a very small number, if any, reached the exit plane. To tackle this problem without largely increasing the number of particles paths to calculate, the screw was divided in three main sections as shown in **Figure 6–8**. Every particle path was then calculated from the injection plane until the end of each section.

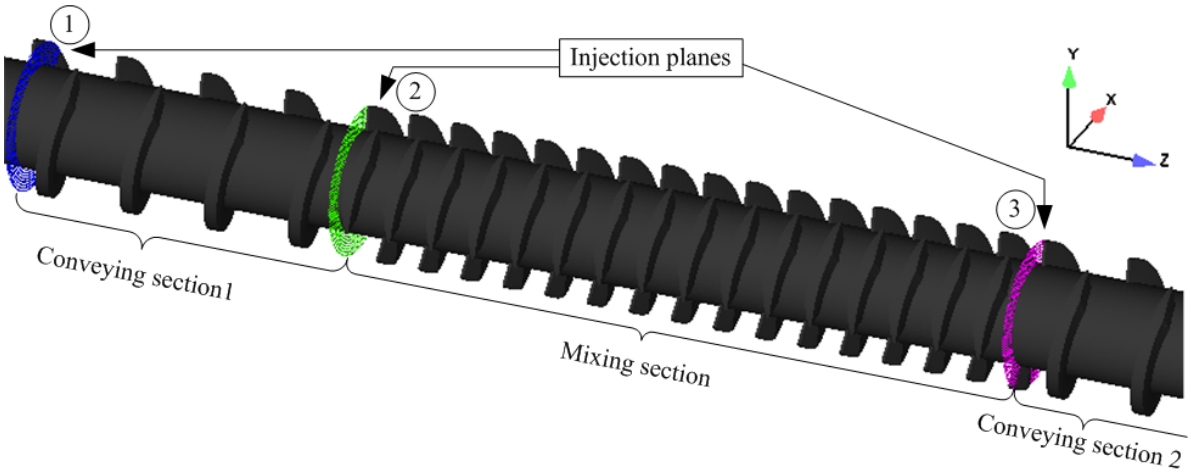

Figure 6–8. Location of the injection planes.

6.5.3.1 Residence Time Distributions

Residence time analysis is a very common tool for understanding flow systems. It is based on the fact that depending on the geometry and hydrodynamics of the system, fluid elements spend different amounts of time to pass through the system. The distribution of these times of passage is called the exit age distribution *E*, or the residence time distribution of the fluid (Levenspiel, 1999). Experimentally, this function *E(t)* is the direct response to a tracer impulse and it is obtained by normalizing the output concentration by the total amount of tracer injected.

The mean residence time t_m is the first moment of the $E(t)$ distribution and is defined by

$$t_m = \sum_0^\infty t \cdot E(t)\Delta t \qquad (6.7)$$

The second moment, which gives a measure of the spread of the distribution around the mean, is known as the variance σ^2,

$$\sigma^2 = \sum_0^\infty (t - t_m)^2 \cdot E(t) \cdot \Delta t \qquad (6.8)$$

From the material balance of the system, a theoretical mean residence time can be calculated as

$$t_m = \frac{V}{Q} \tag{6.9}$$

A cumulative distribution function $F(t)$ can be defined such as

$$F = \int_0^t E dt \tag{6.10}$$

Numerical RTD was obtained by determining the time (t_i) taken by each of the massless tracer particles to get from the injection point to the exit plane. According to Nauman & Buffham (1983), a fraction of the volumetric flow rate ΔQ_i has to be associated to each particle. This fraction can be approximated by

$$\Delta Q_i = V(r_i) \cdot \Delta A_i \tag{6.11}$$

where $V(r_i)$ is the velocity at the point of entry which varies according to the position $r_i(x,y)$, and ΔA_i is a small area element determined by

$$\Delta A_i = \frac{A}{N_{particles}} \tag{6.12}$$

where A is the injection plane area and $N_{particles}$ is the number of particles that reached the exit plane. Paired values of ΔQ_i and t_i can then be used to construct a histogram, which once normalized will become the $E(t)$ function defined as the fraction of the volumetric flow which has a residence time between t and $t+dt$. Analysing the data in this manner means that the residence

time histogram is being weighted according to ΔQ and not ΔA. Weighting by ΔA results in a distribution with respect to resident fluid, not flowing fluid (Nauman, 1991).

The number or size of intervals, also called bins, is an important and often subjectively selected parameter when constructing a histogram. The choice of bin width has a direct effect on the visual representation of the resulting histogram. A very small bin width (*i.e.* too many bins) results in a very irregular histogram where the noise in the data is not sufficiently averaged out and the underlying distribution of the data is hard to discern. On the other hand, a very large bin width (*i.e.* too few bins) results in an over-smoothed distribution with little detail. The choice of bin width is then critical in RTD analysis since the shape of the distribution helps diagnose faulty flows like channelling, internal recirculation or stagnant fluid. To help in the determination of an appropriate bin width there are guidelines or rules. Some of them only take into account the number of data points (Square-Root Rule) or the data range (Sturges Rule), others consider some characteristic of the distribution like the standard deviation (Scott's Rule) or the interquartile range (Freedman & Diaconis, 1981), and others more elaborated formulas seek to minimize the mean integrated squared error (Shimazaki & Shinomoto, 2007; Wand, 1997). The results presented here are based on histograms constructed with the bin width obtained from the Freedman-Diaconis Rule (1981) which is defined as

$$h = 2\frac{IQR(x)}{n^{1/3}} \tag{6.13}$$

where h is the bin width, n is the number of data points and IQR is the interquartile range of the data which is equal to the difference between the third and first quartiles. The IQR is a better choice over the standard deviation as a measure of the statistical dispersion of the data since it is less sensitive to outliers. Additionally, for the purpose of comparison, the bin width was also calculated following the Shimazaki-Shinomoto optimization method (Shimazaki & Shinomoto, 2007). The resulting bin size was of the same value as the one obtained by the Freedman-Diaconis Rule.

Approximately 1000 particles were injected in each of the planes shown in **Figure 6–8**. In the mixing zone only between 11% and 31% of the particles injected reached the exit plane. The amount of particles recovered increased with higher screw speeds and higher flow rates. In the first conveying zone the fraction of particles recovered at the exit plane was approximately 70% and in the second conveying zone approximately 60%. **Figure 6–9** shows the start location of the particles recovered at the exit plane of each zone for two extreme operating conditions: low screw speed-low flow rate, and high screw speed-high flow rate.

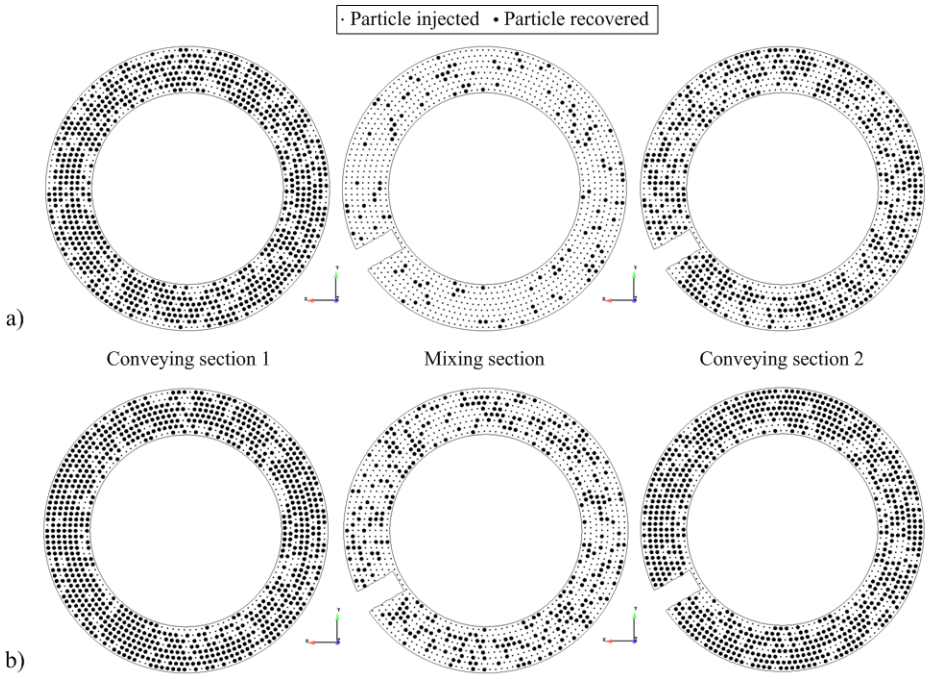

Figure 6–9. Start positions of the particles injected and of the particles recovered at the exit plane in each of the three injection planes: **a)** N = 50 rpm, Q = 5.5 kg/hr; **b)** N = 100 rpm, Q = 25.7 kg/h.

It is shown that the lost particles are not only located near the walls, where the velocity is zero. Therefore the loss of particles must be attributed to the complex geometry in which the round-off errors have a more significant impact. In order to determine the impact of the amount of particles that reached the exit plane on the value of the mean residence time, two additional computations were performed for the operating condition of low screw speed-low flow rate. The results are presented in **Table 6-3**. As we can see the fraction of particles recovered does not increase

significantly when more particles are injected. In the same manner, the relative error between the calculated mean time and the theoretical value only changes 2%. The required CPU time however, increases linearly with the number of particles.

Table 6-3. Effect of the number of particles on the mean residence time. N = 50 rpm, Q = 7.8kg/h

Injected particles	Recovered particles	Recovered Fraction (%)	CPU time (h)	Numerical t_m (s)	Theoretical t_m (s)	Relative error (%)
1049	118	11.25	58	126.60	151.44	16.40
2476	337	13.61	136	125.06	151.44	17.42
5107	662	12.98	266	123.26	151.44	18.61

In order to assemble the RTD curve of the whole screw the individual curves obtained for the different sections where combined by means of a convolution operation, which is based on a statistically independent hypothesis (Levenspiel, 1999). Therefore, the $E(t)$ function of the whole screw can be expressed as

$$E(t) = E_{EZ-1}(t) * E_{KE}(t) * E_{EZ-2}(t) \qquad (6.14)$$

where $E_{EZ-1}(t)$ and $E_{EZ-2}(t)$ are the RTD functions of the first and second conveying sections respectively, and $E_{KE}(t)$ is the RTD function of the mixing section. Since the time interval (bin size) for each E(t) curve is different, a non-linear regression analysis was performed to fit the data and obtain continuous functions. **Figure 6–10** shows the $E(t)$ curves for each screw section and the resulting convoluted curve for one operating condition.

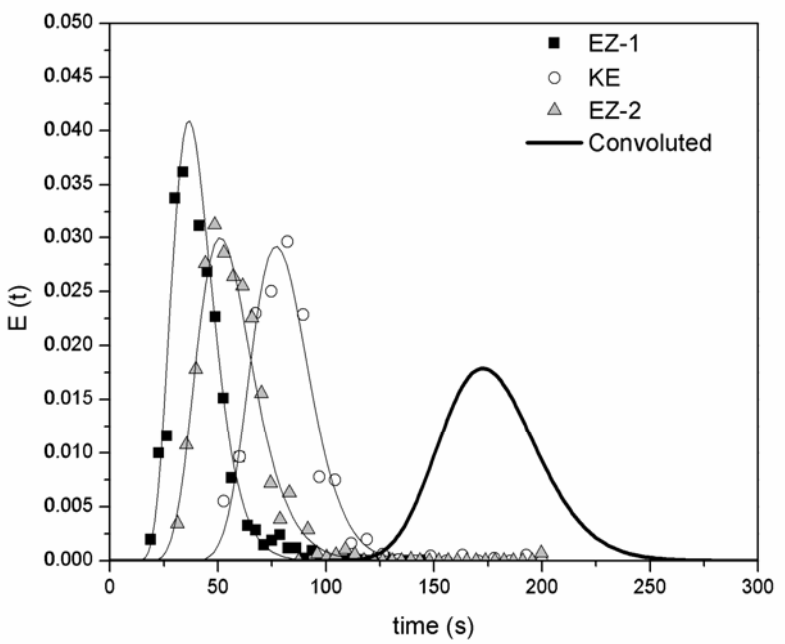

Figure 6–10. Individual and convoluted $E(t)$ curves for N = 75 rpm, Q = 12.5 kg/h.

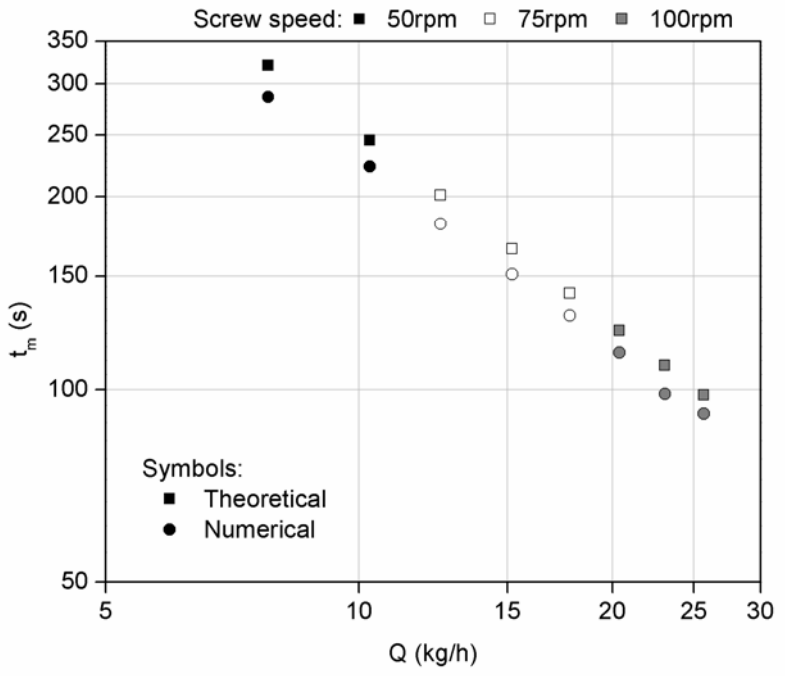

Figure 6–11. Numerical and theoretical mean residence time.

The numerical and theoretical mean residence times of the whole system are presented in **Figure 6–11**. For clarity of presentation the graph is presented in logarithmic scale. The difference between the numerical and the theoretical values is higher for low screw speeds and low flow rates. When all operating conditions are compared, it is found that the higher relative error between numerical and theoretical values is 11% and the smallest is 6%. A smaller number of data bins in the histogram can diminish this difference; however the shape of the RTD is directly affected and detail is lost. It is confirmed that, as reported by other experimental studies (Lyu & White, 1998), the flow rate has a greater effect on the mean residence time than the screw speed.

Due to the configuration of the experimental setup (**Figure 6–2**), the volume occupied by the fluid in the experiments differs from the volume considered by the particle tracking analysis. To be able to compare the results, the residence time corresponding to the volume difference was calculated with **Equation 6.9** and then added to the previously obtained numerical value. **Table 6-4** shows the adjusted numerical results, the experimental results and their standard error, as well as the relative error between numerical and experimental values. In all cases the numerical mean times are higher compared with the experimental results; however, the relative error is less than approximately 13%.

Table 6-4. Numerical and experimental mean residence time.

Run No.	N (rpm)	Q (kg/h)	Numerical	Experimental		Relative error
			t_m adj. (s)	t_m (s)	SE	δ (%)
1	50	7.8	333.9	309.7	0.9	7.83
2	50	10.3	259.5	241.1	2.2	7.64
3	75	12.5	211.0	189.8	1.6	11.19
4	75	15.2	175.6	162.1	1.4	8.35
5	75	17.8	151.1	137.9	1.3	9.60
6	100	20.4	132.5	122.1	0.5	8.50
7	100	23.1	114.7	108.9	0.6	5.32
8	100	25.7	106.2	94.7	0.8	12.16

Table 6-5 presents the numerical and experimental results of σ^2 as well as the relative error between the two values. As can be seen, the error for all cases is very high and it does not depend on the operating conditions.

Table 6-5. Numerical and experimental variance.

Run No.	N (rpm)	Q (kg/h)	Numerical	Experimental		Relative error
			σ^2	σ^2	SE	δ (%)
1	50	7.8	1501.1	11139.4	47.9	86.52
2	50	10.3	705.3	5325.9	28.9	86.76
3	75	12.5	520.9	4595.0	24.2	88.66
4	75	15.2	296.4	2497.3	29.1	88.13
5	75	17.8	148.9	1634.7	18.6	90.89
6	100	20.4	231.6	1490.3	10.0	84.46
7	100	23.1	155.2	1082.1	13.3	85.66
8	100	25.7	102.1	771.7	19.7	86.78

Figure 6–12, **Figure 6–13** and **Figure 6–14** show the numerical and experimental cumulative distribution function for each of the studied screw speeds respectively, expressed in terms of the dimensionless time θ

$$\theta = \frac{t}{t_m} \tag{6.15}$$

We can see that for every operating condition the numerical curves behave more like a plug flow than the experimental curves. However, the overall shape of the curves is the same. The difference between the numerical and the experimental σ^2 values can be attributed to the fact that the region in which the measurements were taken is not the same in each case and are hydrodynamically drastically different. The experimental readings were taken in the center of the outlet pipe (**Figure 6–2**) whereas the numerical results are calculated from the annular cross-section exit planes defined on the extruder (**Figure 6–9**). Another factor contributing to the difference is the simplifying assumption of statistically independent regions made in order to

perform the convolution operation. This condition is very difficult to obtain due to the oscillating nature of the Co-Kneader and the slices in the screw.

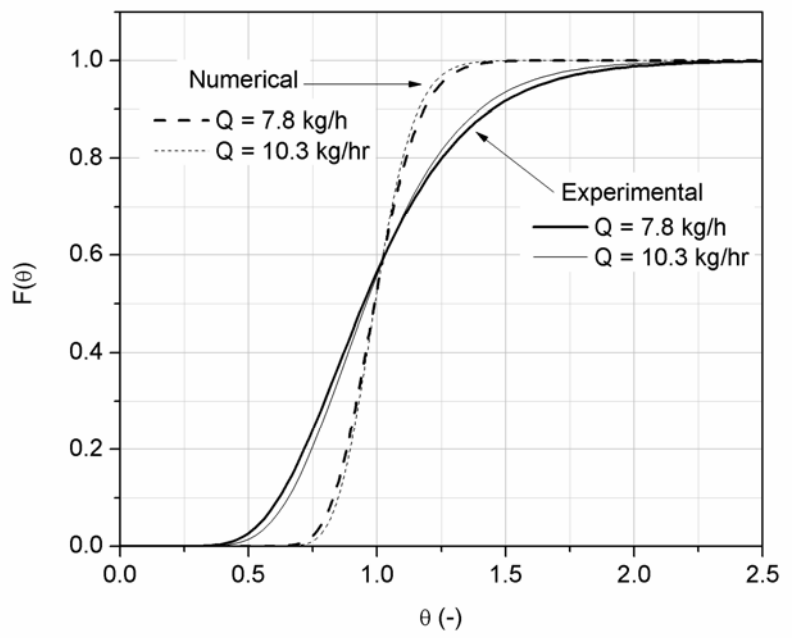

Figure 6–12. Cumulative distribution function for $N = 50$ rpm.

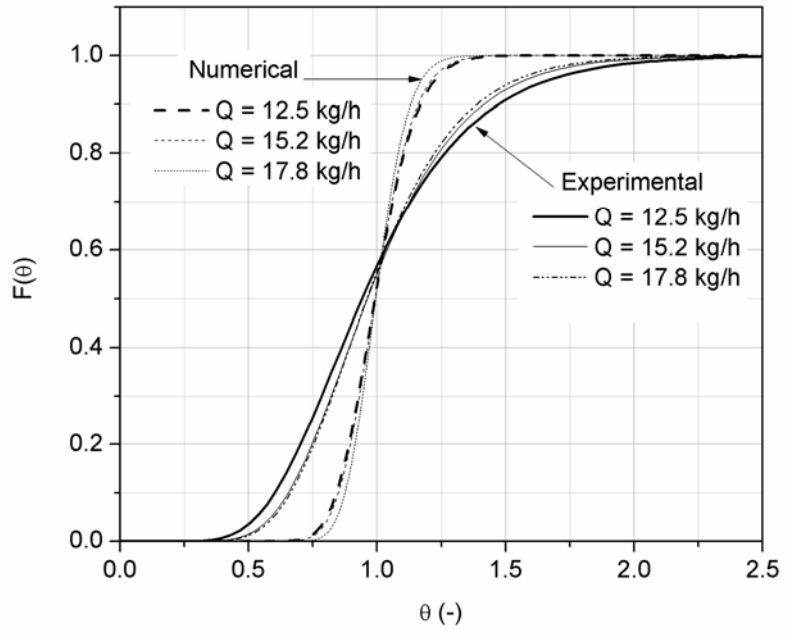

Figure 6–13.Cumulative distribution function for $N = 75$ rpm.

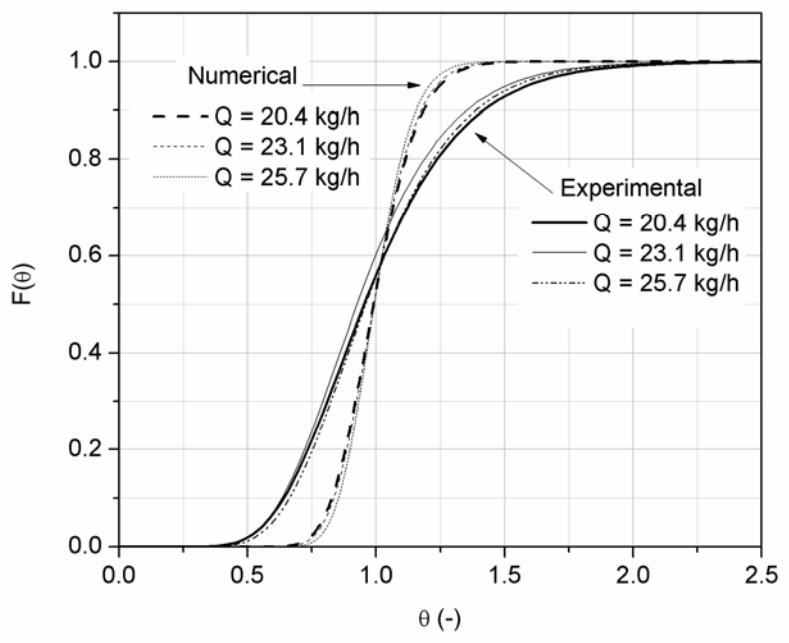

Figure 6–14. Cumulative distribution function for N = 100 rpm.

6.5.3.2 Trajectory Length Distributions

As previously mentioned, the trajectory length for each particle was obtained simultaneously with the residence time. As with the RTD, a normalized trajectory length distribution E(l) is defined such that E(l)dl represents the fraction of fluid particles in the exit plane following trajectories whose lengths are comprised between l and l + dl. Following the formerly detailed procedure to analyse the RTD results, each trajectory length was weighted by ΔQ (**Equation 6.11**) and the bin size for the histogram was calculated by **Equation 6.13**. In the same manner, the TLD curve of the whole screw was obtained by convoluting the individual TLD curves obtained for each section by means of **Equation 6.14** and by replacing t with l. **Figure 6–15** shows the individual TLD curves as well as the resulting convoluted curve for one operating condition.

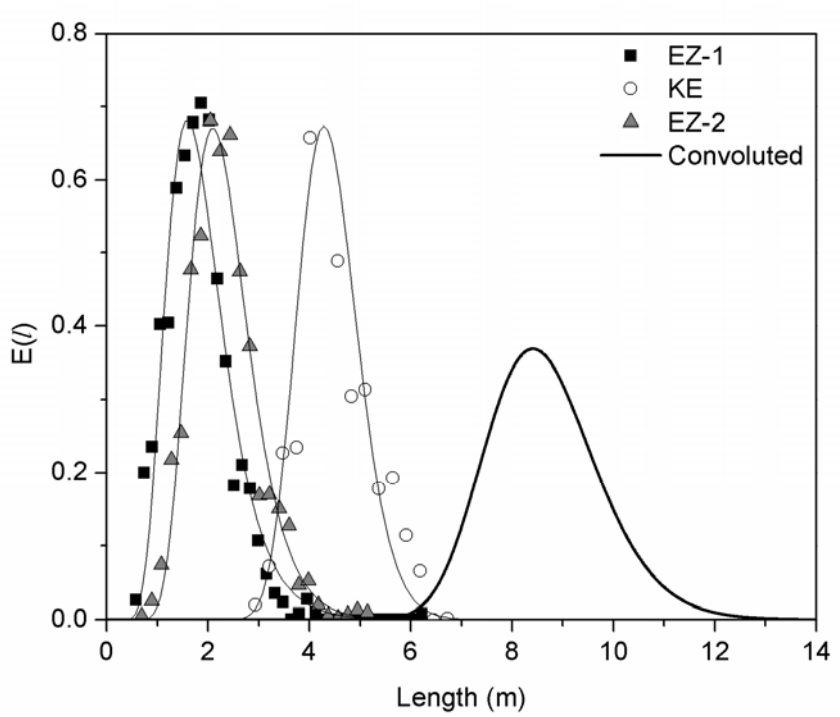

Figure 6–15. Individual and convoluted $E(l)$ curves for N = 100 rpm, Q = 25.7 kg/h

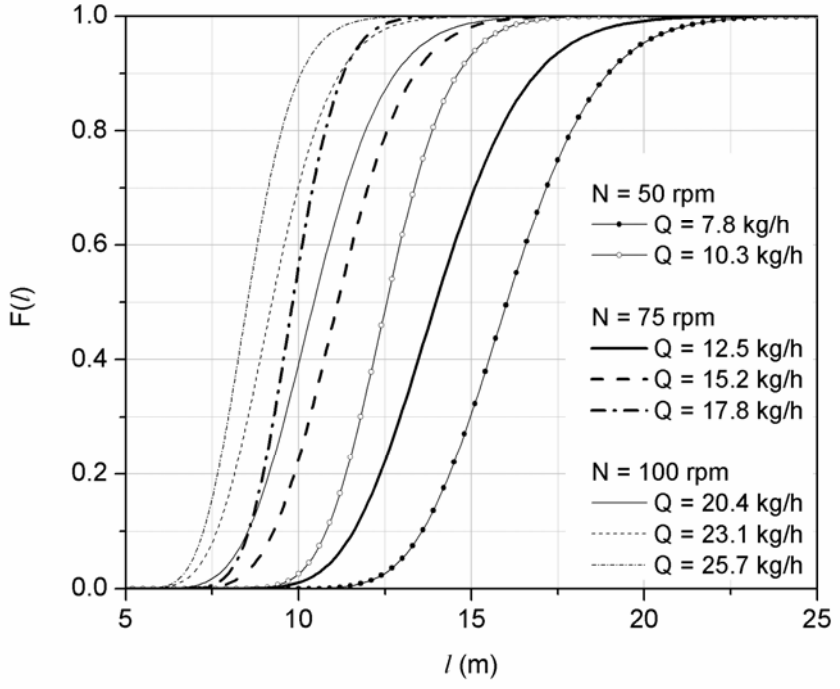

Figure 6–16. Operating conditions effect on TLD.

Figure 6–16 shows the effect of the operating conditions on the cumulative distribution function $F(l)$. The effect of the flow rate becomes less noticeable as the screw speed increases. The distribution becomes narrower at high screw speeds and high flow rates as well.

As with the RTD, a mean trajectory length l_m and a variance σ_l^2 can be determined by using the value of l instead of t in **Equation 6.7** and **Equation 6.8** respectively. Additionally, a macromixing index M can be defined from l_m and a characteristic dimension L of the system (Villermaux, 1996) such as

$$M = \frac{l_m}{L} \tag{6.16}$$

A large value of M corresponds to an efficient macromixing as fluid elements cover long distances with respect to the system size before exiting. In the case of plug flow in a straight tube $M = 1$ because there is no macromixing.

Two characteristic dimensions are of interest in the Co-Kneader: the axial distance along the screw L_{ax} and the down channel distance or helical distance L_h. The helical distance is the length that the fluid elements would cover if the screw channels were completely closed (*i.e.* an equivalent single screw). **Table 6-6** shows the calculated values of the mean trajectory length and the macromixing index calculated with both characteristic dimensions. We can see that the mean trajectory length is larger at low flow rates and at low screw speeds. The macromixing indexes follow the same trend. An interesting result is that the value of M_{ax} is much larger than the value of M_h. Particles cover approximately 20 times the axial length of the Co-Kneader and 3 times more distance than in a closed channel single screw. This result confirms that the mixing in the Co-Kneader is mainly the result of axial flows through the slices.

Table 6-6. Results of mean trajectory length, variance and macromixing index.

Run No.	N (rpm)	Q (kg/h)	l_m (m)	σ_l^2	Helical distance		Axial distance	
					L_h (m)	M_h	L_{ax} (m)	M_{ax}
1	50	7.8	16.34	4.74	3.36	4.86	0.505	32.36
2	50	10.3	12.66	1.86	3.36	3.77	0.505	25.06
3	75	12.5	13.96	3.79	3.36	4.16	0.505	27.65
4	75	15.2	11.35	2.35	3.36	3.38	0.505	22.49
5	75	17.8	9.93	1.24	3.36	2.95	0.505	19.66
6	100	20.4	10.75	2.76	3.36	3.20	0.505	21.29
7	100	23.1	9.37	1.75	3.36	2.79	0.505	18.56
8	100	25.7	8.60	1.25	3.36	2.56	0.505	17.04

Having performed the injection of particles in three different planes according to the sections of the screw gave us the opportunity to examine and compare the characteristics of each type of element. **Figure 6–17** shows that compared with the conveying sections (EZ-1, EZ-2), the mixing section (KE) has the longest trajectory length and broadest distribution. If the trajectory length is normalized relative to L_{ax} (**Figure 6–18**) the mixing section still has the longest trajectory, approximately 5 times longer than the conveying sections. This was an expected result since the mixing element has more screw slices than the conveying elements. As a consequence of this there is more backflow and the particles cover more distance before reaching the exit plane. On the other hand, when we compare the trajectory length relative to L_h (**Figure 6–19**) the conveying sections show a much wider distribution and a longer trajectory than the mixing section. This may be due to the fact that the conveying element only has one slice, compared to the three of the mixing element; therefore the particles must go down-channel with the flow. Additionally it can be observed in **Figure 6–19** that since the ratio of l/L_h is higher than 1, the conveying element has some degree of down-channel mixing. This is probably caused by the cross-channel velocity created by the oscillating motion of the Co-Kneader.

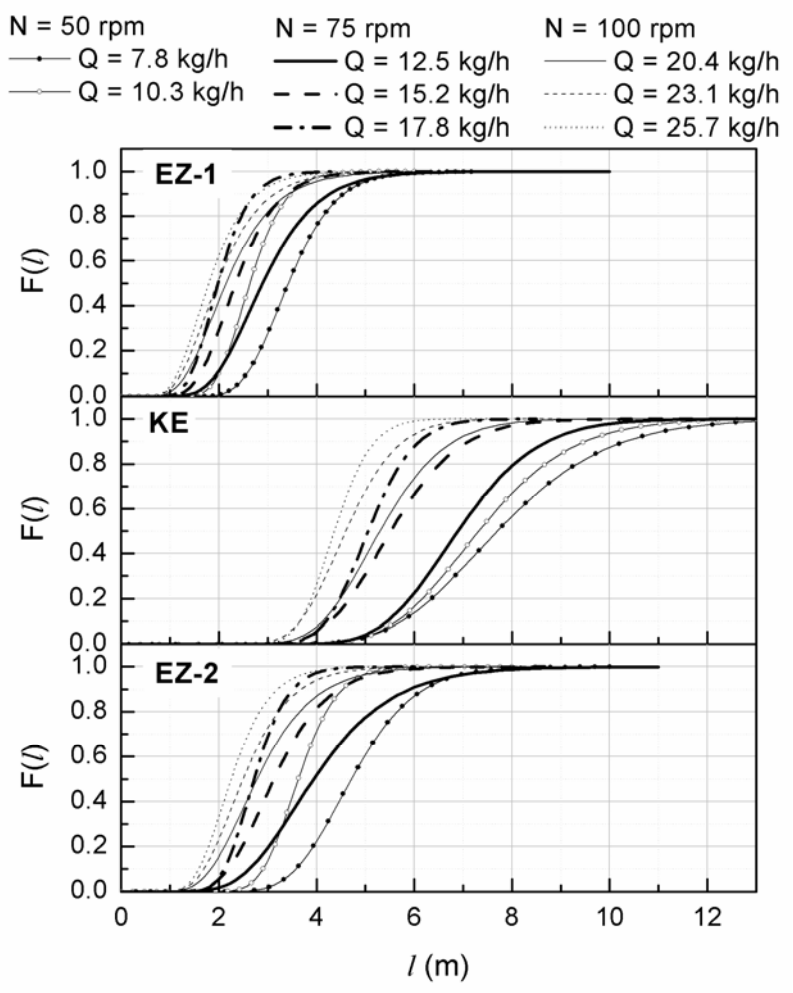

Figure 6–17. Cumulative distribution functions for the different screw sections.

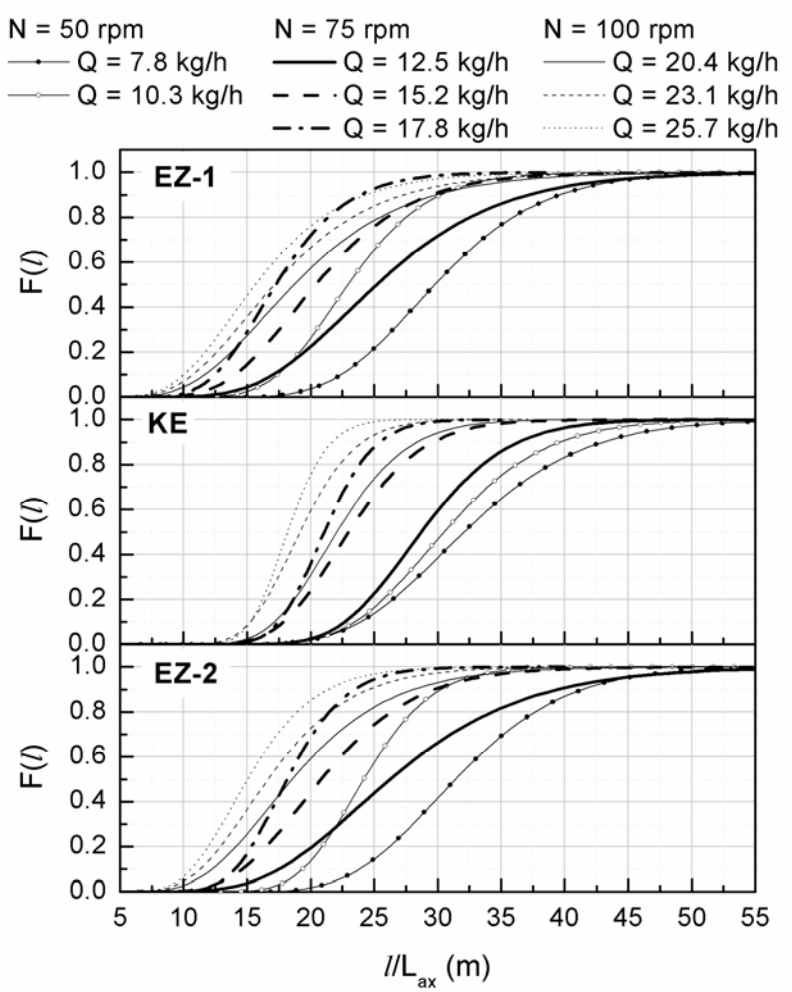

Figure 6–18. Cumulative distribution functions for the different screw sections compared with L_{ax}.

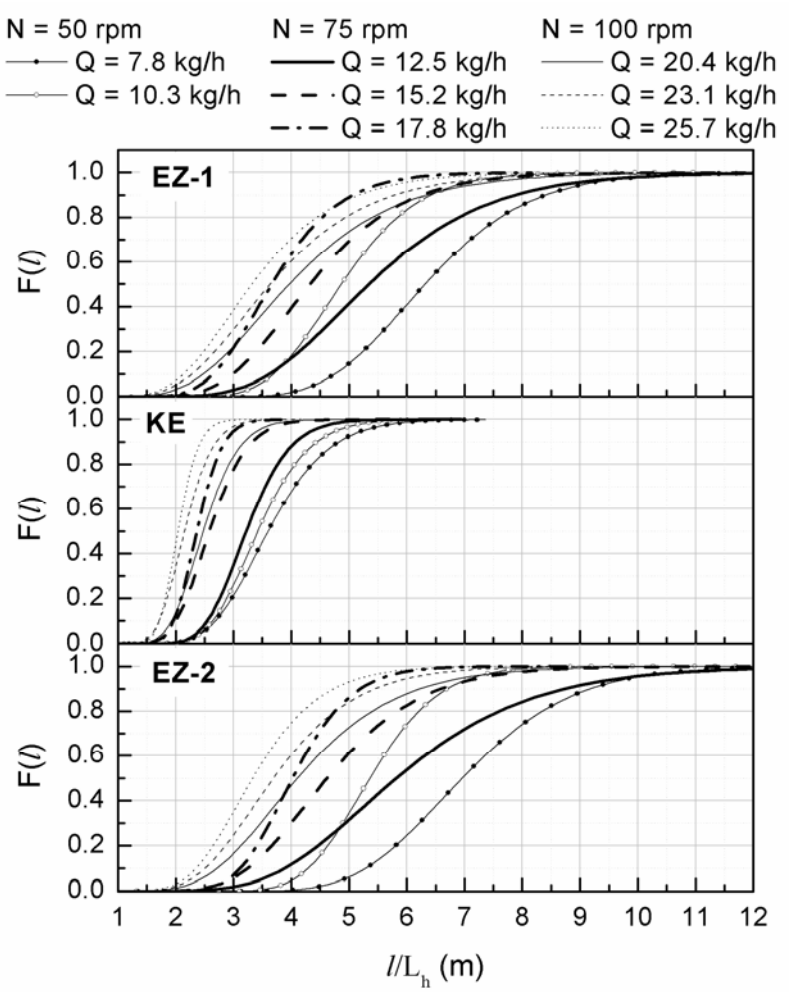

Figure 6–19. Cumulative distribution functions for the different screw sections compared with L_h.

6.6 Conclusions

Newtonian simulations performed with a 3D MINI-based VFEM were done in order to predict the flow inside a Co-Kneader. The calculations took into account both the presence of the pins and the screw oscillation. The numerical results were verified by experimental pressure measurements and prove to be in good agreement. Pressure profiles along the screw were obtained and the different pumping capabilities of the screw elements were observed, that of the KE element being the lower. Velocity fields showed that the presence of the pins is crucial in the overall mixing performance of the Co-Kneader since they disrupt the steady flow in the screw

channel and without them the split and recombination effect could not take place. By means of particle tracking, RTD and TLD curves were obtained. The numerical RTD results were in good agreement with the experimental measurements. Previously reported effects of operating conditions on the residence time were confirmed. The analysis of TLD showed that the different screw elements contribute differently to the mixing capacity of the Co-Kneader. The mixing element produces axial mixing while the conveying element yields down-channel mixing. A more localized analysis (*i.e.* element by element) should be performed in order to confirm these observations. The TLD analysis was performed on an extruder for the first time and it proved to be a complementary tool in the study of the mixing mechanisms in the Co-Kneader.

6.7 Acknowledgements

The financial support of the National Science and Engineering Research Council of Canada (NSERC) and of TOTAL is greatly acknowledged. Thanks are also directed to CONACYT (Mexico) for the financial support of M. Brito-Bazan.

6.8 Notation

δ	Relative error	%
θ	Dimensionless time	Dimensionless
μ	Newtonian viscosity	Pa s
ρ	Density	kg/m^3
σ^2	Variance	s^2
σ_l^2	Length variance	m^2
φ	Flight angle	°
ω	Oscillation frequency	1/s

A	Area	m^2
D	Diameter	m
D_b	Inside diameter of barrel	mm
D_o	Outside diameter of screw	mm
e	Flight thickness	mm
H	Screw channel depth	mm
h	Bin width	Dimensionless
N	Screw speed	rpm
n	Number of data points	Dimensionless
L_{ax}	Axial length	m
L_e	Length of screw element	mm
L_h	Helical or down-channel length	m
l	Trajectory length	m
l_m	Mean trajectory length	m
M	Mixing index	Dimensionless
P	Pressure	Pa
Q	Flow rate	kg/h
R	Radius	m
S_0	Amplitude of screw stroke	mm
s	Width of screw slice	mm
t	Time	s
t_m	Mean residence time	s
V	Volume	m^3
W	Screw channel width	mm

6.9 References

Arnold, D., Brezzi, F., & Fortin, M. (1984). A stable finite element for the stokes equations. *Calcolo, 21*(4), 337-344.

Bertrand, F., Tanguy, P. A., & Thibault, F. (1997). A three-dimensional fictitious domain method for incompressible fluid flow problems. *International Journal for Numerical Methods in Fluids, 25*(6), 719-736.

Booy, M. L., & Kafka, F. Y. (1987). *Isothermal Flow of Viscous Liquids in the Mixing Section of a Buss Kneader*, Los Angeles, CA, USA.

Bravo, V. L., Hrymak, A. N., & Wright, J. D. (2004). Study of particle trajectories, residence times and flow behavior in kneading discs of intermeshing co-rotating twin-screw extruders. *Polymer Engineering and Science, 44*(4), 779-793.

Brzoskowski, R., Kumazawa, T., & White, J. L. (1989). *Modelling flow in mixing section of a KoKneader (Buss)*, New York, NY, USA.

Campolo, M., Sbrizzai, F., & Soldati, A. (2003). Time-dependent flow structures and Lagrangian mixing in Rushton-impeller baffled-tank reactor. *Chemical Engineering Science, 58*(8), 1615-1629.

Coesnon, B., Heniche, M., Devals, C., Bertrand, F., & Tanguy, P. A. (2008). A fast and robust fictitious domain method for modelling viscous flows in complex mixers: The example of propellant make-down. *International Journal for Numerical Methods in Fluids, 58*(4), 427-449.

Elemans, P. H. M., & Meijer, H. E. H. (1990). On the modeling of continuous mixers. Part II. The cokneader. *Polymer Engineering and Science, 30*(15), 893-904.

Fangary, Y. S., Barigou, M., Seville, J. P. K., & Parker, D. J. (2000). Fluid trajectories in a stirred vessel of non-Newtonian liquid using positron emission particle tracking. [Article]. *Chemical Engineering Science, 55*(24), 5969-5979.

Fradette, L. (1999). *Etude de dispersion dans un melangeur statique Sulzer SMX.* Ph.D., Ecole Polytechnique, Montreal (Canada), Canada.

Freedman, D., & Diaconis, P. (1981). On the histogram as a density estimator: L_2 theory. *Probability Theory and Related Fields, 57*(4), 453-476.

Glowinski, R., Pan, T. W., & Periaux, J. (1994). A Fictitious Domain Method for Dirichlet Problem and Applications. *Computer Methods in Applied Mechanics and Engineering, 111*(3-4), 283-303.

Heniche, M., & Tanguy, P. A. (2006). A new element-by-element method for trajectory calculations with tetrahedral finite element meshes. *International Journal for Numerical Methods in Engineering, 67*(9), 1290-1317.

Heniche, M., Tanguy, P. A., Reeder, M. F., & Fasano, J. B. (2005). Numerical investigation of blade shape in static mixing. *AIChE Journal, 51*(1), 44-58.

Ishikawa, T., Amano, T., Kihara, S.-I., & Funatsu, K. (2002). Flow patterns and mixing mechanisms in the screw mixing element of a co-rotating twin-screw extruder. *Polymer Engineering and Science, 42*(5), 925-939.

Kiared, K., Larachi, F., Guy, C., & Chaouki, J. (1997). Trajectory length and residence-time distributions of the solids in three-phase fluidized beds. *Chemical Engineering Science, 52*(21-22), 3931-3939.

Levenspiel, O. (1999). *Chemical reaction engineering* (3rd ed.). New York: Wiley.

Lyu, M.-Y., & White, J. L. (1995). Models of Flow and Experimental Studies on a Modular List/Buss Kokneter. *International Polymer Processing, 10*(4), 305-313.

Lyu, M.-Y., & White, J. L. (1996). Modelling of a Viscous Non-Newtonian Polymer Melt in a List/Buss Kneader and Comparison to Experiment. *International Polymer Processing, 11*(3), 208-221.

Lyu, M.-Y., & White, J. L. (1997a). Non-isothermal non-Newtonian analysis of flow in a modular list/buss kneader. *Journal of Reinforced Plastics and Composites, 16*(16), 1445-1460.

Lyu, M.-Y., & White, J. L. (1997b). Simulation of linear viscoelastic flow behavior in the Buss Kneader. *Polymer Engineering and Science, 37*(3), 623-635.

Lyu, M.-Y., & White, J. L. (1997c). Simulation of Non-Isothermal Flow in a Modular Buss Kneader and Comparison with Experiment. *International Polymer Processing, 12*(2), 104-109.

Lyu, M.-Y., & White, J. L. (1998). Residence time distributions and basic studies of flow and melting in a modular Buss Kneader. *Polymer Engineering and Science, 38*(9), 1366-1377.

Lyu, M.-Y., & White, J. L. (2000). Simulation of non-linear viscoelastic flow behavior in the Buss Kneader. *Journal of Reinforced Plastics and Composites, 19*(10), 756-791.

Mehranpour, M., Nazokdast, H., & Dabir, B. (2002a). Computational study of the velocity field in the conveying element of a Ko-Kneader with CFD method. *International Polymer Processing, 17*(2), 108-114.

Mehranpour, M., Nazokdast, H., & Dabir, B. (2002b). Estimation of residence time distribution in two elements of a Ko-Kneader. *International Polymer Processing, 17*(1), 22-25.

Mehranpour, M., Nazokdast, H., & Dabir, B. (2003a). Computational study of velocity field in the KE element of a modular Ko-Kneader with CFD method. *International Polymer Processing, 18*(4), 330-337.

Mehranpour, M., Nazokdast, H., & Dabir, B. (2003b). Prediction of residence time distribution in EZ and KE element of a Ko-Kneader by using CFD method. *International Polymer Processing, 18*(4), 327-329.

Mehranpour, M., Nazokdast, H., & Dabir, B. (2004). Prediction of residence time distribution for different screw configurations of a Ko-Kneader by using a cluster model. *International Polymer Processing, 19*(1), 13-15.

Nauman, E. B. (1991). On residence time and trajectory calculations in motionless mixers. *Chemical engineering journal, 47*(3), 141-148.

Nauman, E. B., & Buffham, B. A. (1983). *Mixing in continuous flow systems*. New York: Wiley.

Rauwendaal, C. (1991). Mixing in single-screw extruders. In C. Rauwendaal (Ed.), *Mixing in polymer processing* (pp. 129-239). New York: Marcel Dekker.

Rauwendaal, C. (1994). *Polymer Extrusion* (3rd ed.). New York: Hanser.

Shimazaki, H., & Shinomoto, S. (2007). A Method for Selecting the Bin Size of a Time Histogram. *Neural Computation, 19*(6), 1503-1527.

Tadmor, Z., & Gogos, C. G. (1979). *Principles of polymer processing*. U.S.: John Wiley & Sons.

Villermaux, J. (1996). Trajectory Length Distribution (TLD), a novel concept to characterize mixing in flow systems. *Chemical Engineering Science, 51*(10), 1939-1946.

Wand, M. P. (1997). Data-based choice of histogram bin width. *The American Statistician, 51*(1), 59.

Yao, W. G., Tanifuji, S., Takahashi, K., & Koyama, K. (2001). Mixing efficiency in a pin mixing section for single-screw extruders. *Polymer Engineering & Science, 41*(6), 908-917.

CHAPTER 7
MIXING ANALYSIS OF TWO SCREW ELEMENTS OF A CO-KNEADER BY A CFD METHOD

Magdalena Brito-Bazan, Mourad Heniche, Louis Fradette, Philippe A. Tanguy

URPEI, CREPEC, Department of Chemical Engineering, Ecole Polytechnique de Montreal.
P.O Box 6079, Station Centre-Ville, Montreal, Que., Canada H3C 3A7

7.1 Presentation of the article

This article was submitted to the Advances in Polymer Technology Journal.

This article tackles the third and last of the specific objectives which was to better characterize the hydrodynamics and mixing abilities of each type of screw element.

The article presents a mixing analysis on each type of screw element which includes extensional efficiency coefficients, shear rate characterization using the Metzner-Otto relationship and particle distributions along the Co-Kneader.

Keywords: Co-Kneader, CFD, screw elements, shear rate, RTD, extensional efficiency

7.2 Abstract

The mixing and conveying elements of a Co-Kneader have been characterized by means of a 3D CFD flow model that included the oscillation of the screw as well as the presence of the pins. Numerical results were validated by means of experimental pressure data. The results for each screw element include dimensionless characteristic curves, extensional efficiency parameters and RTD. It is showed that the pins in the barrel promote extensional flows in the screw channel. For the first time, the shear rate relationship of Metzner-Otto was used in order to obtain the constant of proportionality K_s for each type of element. The cross-section and axial mixing evolution along a mixing section has been studied by means of particle tracking.

7.3 Introduction

A Co-Kneader is a type of extruder that incorporates a reciprocating motion with the standard rotating movement of a single screw extruder. The screw has interrupted flights and is fitted in a barrel that has three rows of stationary pins. The rotational and reciprocating motions of the Co-Kneader cause the pins to move relative to the screw, in a sinusoidal way through the flight clearances of the screw. Interchangeable modular screw elements assembled into a shaft give the flexibility to change the screw configuration. However, contrary to twin-screws extruders, there are no general guidelines as to how to assemble a screw profile according to the application.

Since its invention (List, 1950), there have been relatively few studies on the Co-Kneader compared to single screw and twin screw extruders. The first studies focused on compounding applications using the machine (Stade, 1977, 1978; Todd, 1987). Work aimed at understanding the flow inside the Co-Kneader began by modelling the flow of one passing pin between two screw flights (Booy & Kafka, 1987; Brzoskowski *et al.*, 1989). The results in both studies revealed low pressure values and flow recirculation behind the pin. It was also found that the maximum shear rate value occurred between the pin and the flight when the clearance became the smallest.

Characterization of the different screw elements began by determining their pumping capacities by means of experiments and flow models. Elemans & Meijer (1990) obtained experimental throughput versus pressure characteristic curves with Newtonian model fluids for conveying, mixing and closed-channel mixing elements. They found that conveying elements had a much larger pumping capacity than the two mixing elements. Also, they concluded that the presence of the pins affected very little the pumping abilities of all the screw elements. The authors also developed a flow model which only considered the rotational motion of the screw. Lyu & White (1995, 1996, 1997b) developed flow models and calculated dimensionless screw characteristic curves for three different types of screw elements: conveying, mixing and restriction ring. The Newtonian flow model (Lyu & White, 1995) showed that the conveying and mixing elements were able to develop pressure but not the restriction ring element. Results obtained with a Power Law flow model (Lyu & White, 1996) indicated that the pumping capacity of all screw elements was less than for Newtonian fluids. In the same manner, a linear viscoelastic fluid flow model (Lyu & White, 1997b) showed that the deviation from the Newtonian behaviour was more important for long relaxation times.

Shear rate results obtained by the Finite Volume technique have been reported for the conveying and mixing elements of the Co-Kneader. It has been found that the reciprocating action of the screw has a much stronger effect than the down channel flow on both the extent and distribution of shear rate in the mixing element (Mehranpour *et al.*, 2003a). On the contrary, this effect is not observed on the conveying element, where the reciprocating action only increases the shear rate at the upper part of the screw channel (Mehranpour *et al.*, 2002a). The computer simulations incorporated the oscillation of the screw; however they excluded the pins on the barrel wall.

Another useful tool to describe continuous flow systems is the analysis of Residence Time Distributions (RTD). Mehranpour *et al*. has determined the individual RTD of a conveying and a mixing element by following an analytical method (2002b) and by CFD (2003b). However the pins on the barrel wall were also omitted in the models.

Other characterizations performed on Co-Kneader screw elements include the calculation of leakage flows through the slices in each screw element and results from a non-isothermal flow model. Lyu & White (1996) found that the amount of backflow in both the conveying and mixing element is a function of the forward and backward motions of the screw, and that it was larger in the mixing element. The mixing element also showed to have the lowest temperature rise compared to the conveying and restriction ring elements (Lyu & White, 1997c).

The screw configuration of the Co-Kneader has proven to have an impact on fiber breakage in compounding glass fiber-reinforced thermoplastics (Shon & White, 1999) and also on the development of phase morphology on an immiscible polymer blend (Shon *et al.*, 2008). It is thus clear that a more complete characterization of the screw elements of the Co-Kneader is needed in order to design the appropriate screw profile according to the needs of each particular application. The characterization should also be based on models that take into account both the oscillation of the screw and the presence of the pins.

In this study we present a mixing analysis performed on the conveying and mixing elements of the Co-Kneader. The analysis is based on flow fields obtained from validated numerical simulations which were performed using a 3D fictitious domain finite element method that incorporates the oscillation of the screw as well as the pins in the barrel. The presented results include dimensionless characteristic curves for each type of element, extensional efficiency coefficients, and a shear rate characterization using the Metzner-Otto relationship. Residence time distributions and particle tracking results are also reported. The objective is to better characterize the hydrodynamics and mixing abilities of each type of screw element in order to facilitate the implementation of new screw profiles.

7.4 Description of the Co-Kneader

This study is based on a laboratory-scale Co-Kneader. The internal diameter of the barrel D_b is 50.8 mm and it has a length to diameter ratio L/D_b equal to 11. Along the length of the barrel there are three rows of pins. Each pin is cylindrical with a diameter of 4.2 mm and a length of 7.4 mm. In this work, conveying and mixing elements were studied (**Figure 7–1**). The conveying element (EZ element) has a single flight, one screw slice and one pin in each of two rows. The mixing element (KE element) has two flights, three screw slices and two pins in each of the three rows. Detailed dimensions of the screw elements are summarized in **Table 7-1**.

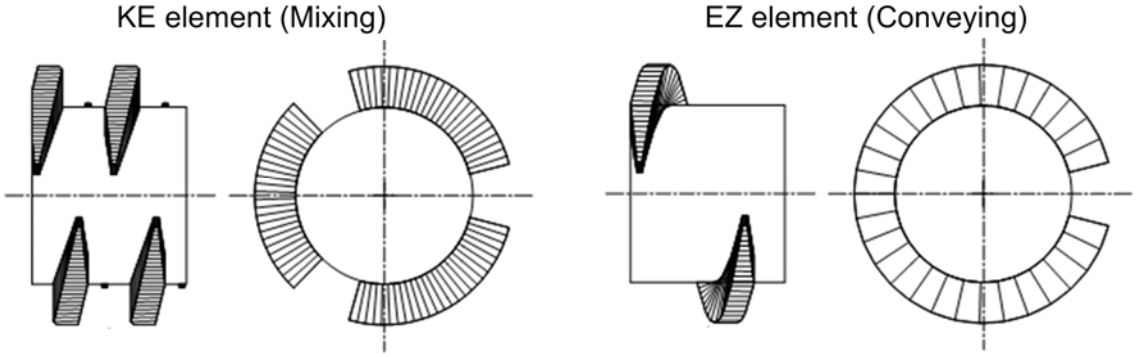

Figure 7–1. Screw elements.

Table 7-1. Geometrical configuration of the screw elements.

[Unit: mm]	KE	EZ
Inside diameter of barrel, D_b	50.80	50.80
Outside diameter of screw, D_o	50.20	50.20
Screw channel width, W	10.56	21.33
Screw channel depth, H	8.20	8.20
Length of one element, L_e	30	30
Flight angle, φ	9.37	9.37
Width of slice, s	8.53	8.53
Flight thickness, e	4.32	4.32
Number of flights	2	1
Number of slices	3	1

While the screw rotates, it also goes back and forth once per complete turn. **Figure 7–2a** shows the angular position at which the screw is at the minimum and maximum axial displacement. In this study the amplitude of oscillation S_0 is equal to 7.5 mm. The rotational and reciprocating motions cause the pins to move, relative to the screw flights, in a sinusoidal fashion. As shown in **Figure 7–2b**, every 120° the pins in the mixing elements return to the initial position (i.e. between the screw slices).

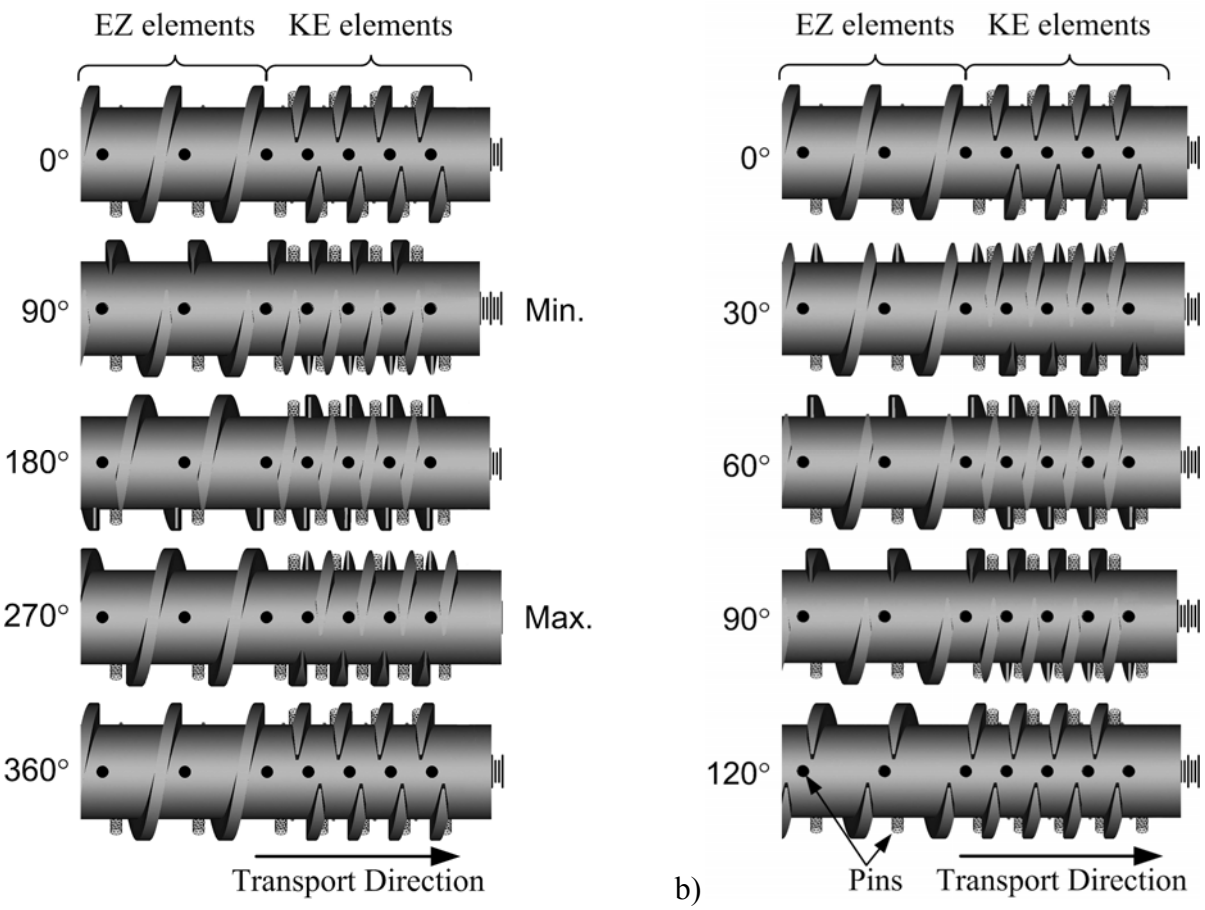

Figure 7–2. Screw angular positions. **a)** Axial displacement. **b)** Pin passage through screw channel.

7.5 Methodology

7.5.1 Numerical methodology

The unsteady three-dimensional flow field in the Co-Kneader was obtained by solving the incompressible Navier-Stokes equations with a finite element method.

$$\rho\left(\frac{\partial \mathbf{v}}{\partial t} + \mathbf{v}\cdot\nabla\mathbf{v}\right) + \nabla p + \nabla\cdot\tau = f \qquad (7.1)$$

$$\nabla\cdot\mathbf{v} = 0 \qquad (7.2)$$

The 5-node P1+-P1 (MINI) tetrahedral element was used to approximate the velocity and the pressure (Arnold *et al.*, 1984). An Eulerian frame of reference was used with the purpose of simplifying the boundary conditions, which are difficult to impose due to the complex movement of the Co-Kneader. In order to do so, a fictitious domain method known as virtual finite element method (VFEM) was employed. Within the VFEM framework, a unique mesh is required during the computations and the screw is represented by a set of moving control points that act like kinematic constraints (Bertrand *et al.*, 1997; Glowinski *et al.*, 1994). MINI-based VFEM has been showed as a suitable strategy for simulating complex mixing systems since the accuracy obtained is comparable with that given by other more costly elements (Coesnon *et al.*, 2008).

The simulated geometry was based on the Co-Kneader described earlier. The 3D mesh which represented the fluid field was an annulus section in which the shape of the pins was subtracted (**Figure 7–3a**). The inlet and the outlet of the system were accounted for by two short pipe sections placed perpendicularly on each end of the main part and facing opposite directions. The final 3D unstructured mesh required about 1 million elements (**Figure 7–3a**), yielding a system of nearly half a million equations.

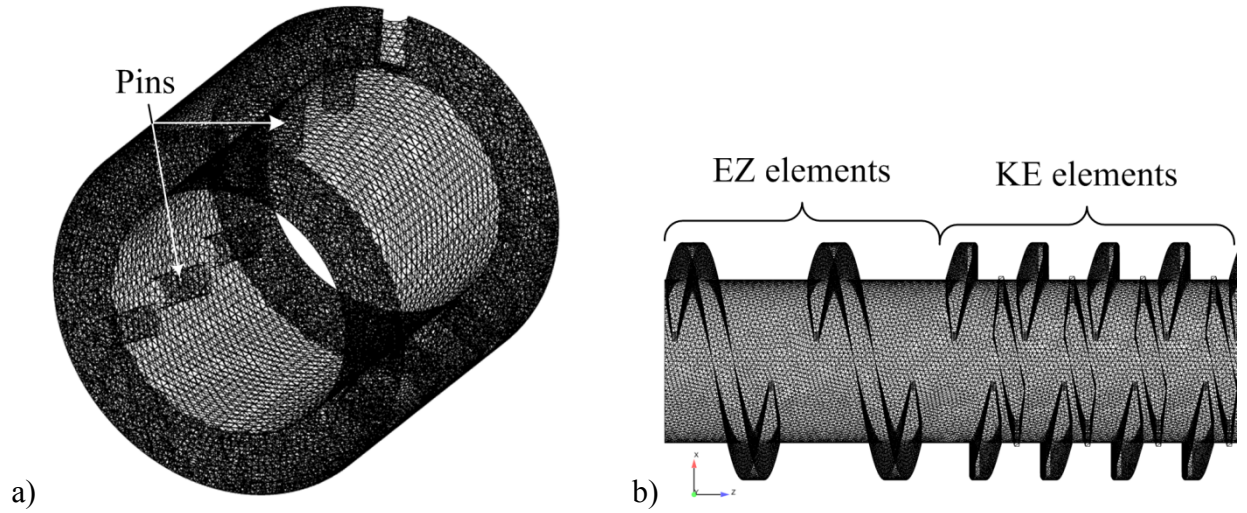

Figure 7–3. Section of the finite element meshing of the Co-kneader. **a)** 3D mesh of the barrel and pins, **b)** surface grid of the screw elements.

Flow simulations were obtained for the screw configuration shown in **Figure 7–4**. It comprises two conveying sections of 5 elements each and a mixing section of 8 elements. A portion of the surface grid used to generate the control points that represent the screw (virtual object) is shown in **Figure 7–3b**. The complete screw profile (**Figure 7–4**) was constituted by approximately 135 000 control points. Both the 3D and the surface mesh were generated on I-DEAS (EDS) software, and post-processing visualization was done with Ensight (CEI).

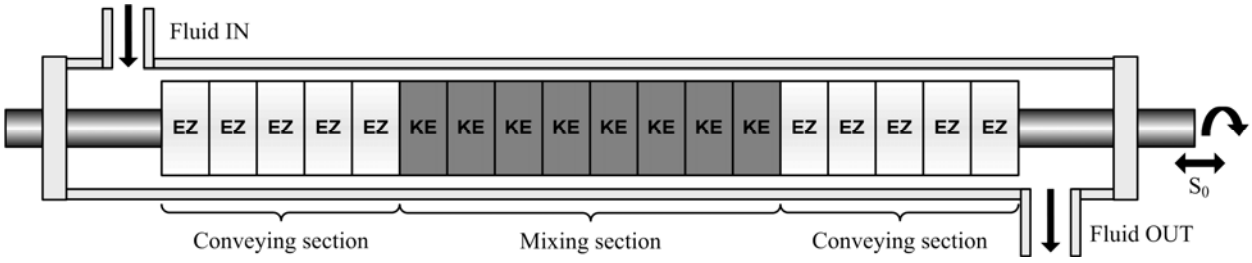

Figure 7–4. Screw profile.

Cartesian coordinates (*x, y, z*) were used as reference frame in the numerical model. The screw is oriented along the *z*-axis, the barrel cross-section is defined in the *x*-*y* plane, and the inlet and

outlet cross-sections are defined in the *x-z* plane. The set of boundary conditions employed were the following:

- Laminar velocity profile in the axial direction at the fluid inlet: $v_x = v_z = 0$ and v_y given by **Equation 7.3** in cylindrical coordinates ($r,\ \theta,\ y$), where Q is the mass flow rate and $R=\sqrt{(x^2+z^2)}$ is the radius of the inlet pipe.

$$v_y = \frac{2Q}{\rho\pi R^2}\left[1-\left(\frac{r}{R}\right)^2\right] \tag{7.3}$$

- At the exit $v_x = v_z = 0$
- No slip condition at the barrel wall: $\mathbf{v} = 0$
- Imposed velocity on the control points is given by **Equation 7.4** and **Equation 7.5**, where S_0 is the amplitude of the oscillation and the frequency ω is $2\pi N/60$.

$$v = \pi DN + \frac{dS(t)}{dt} \tag{7.4}$$

$$S(t) = \frac{S_0}{2}\sin\omega t \tag{7.5}$$

The simulated fluid has a Newtonian viscosity of 0.2 Pa·s and a density of 1270 kg/m^3. The operating conditions studied are listed in **Table 7-2**. Calculations were done at each 3° of screw rotation, which corresponds to 120 time steps to complete a single screw turn and its corresponding back and forth cycle. It was observed that the solutions were periodic after the first screw turn. All simulations were run on an IBM P690 cluster and each required approximately 70

hours of CPU time. The problem was resolved using a Newton-Raphson iterative scheme available in the commercial 3D finite element software POLY3D™ (Rheosoft, Inc.).

Table 7-2. Investigated operating conditions.

Run no.	N (rpm)	Q (kg/h)
1	50	7.8
2	75	12.5
3	75	15.2
4	75	17.8
5	100	23.1

7.5.2 Particle tracking

The RTD and the particle distributions results presented in this work were obtained by the particle tracking technique, where the motion of massless particles is dominated only by the flow field. The path followed by a particle is obtained by the following equation

$$\mathbf{v}(\mathbf{x}) = \frac{d\mathbf{x}}{dt} \tag{7.6}$$

where $\mathbf{v}(\mathbf{x})$ is the velocity vector, $\mathbf{x}$ is the vector position and t is the time. We used an element-by-element approach coupled with a predictor-corrector shooting scheme that do not need the use of any time steps (Heniche & Tanguy, 2006). This method has been successfully applied to the complex geometries of static mixers (Heniche *et al.*, 2005). An important parameter when using this approach is the number of shootings, on which the accuracy of the computed trajectories depends. The trajectories used for the analyses presented in this work were obtained using 300 shootings per element.

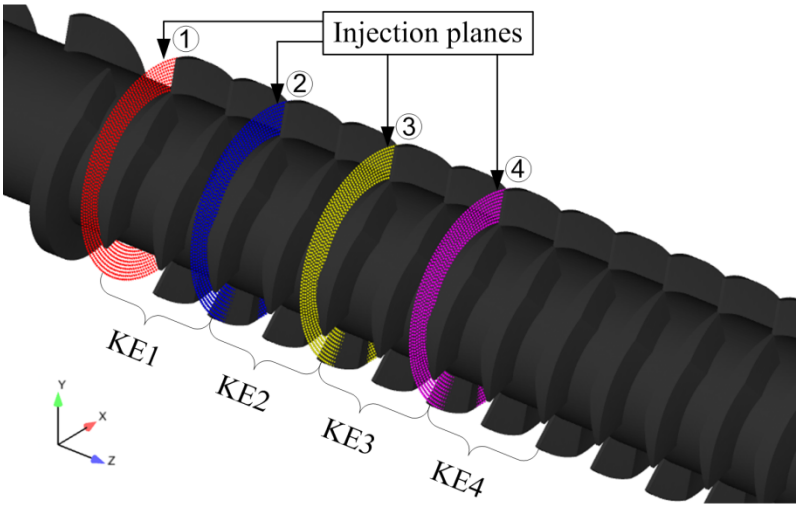

Figure 7–5. Location of injection planes for the mixing section.

To minimize the particle loss due to zero velocity near the walls, the injected particles were positioned leaving a small gap from the wall. All subsequent analyses were then performed based on the number of particles arriving at the exit plane. The injection of particles was done following the screw cross section plane *x*-*y*. Individual mixing elements were studied by injecting 1000 particles at each of the four planes depicted in **Figure 7–5**. In the analysis of consecutive elements, 1500 particles were injected at plane 1. A similar approach was used for the conveying elements.

7.5.2.1 Residence Time Distributions

Residence time analysis is based on the fact that depending on the geometry and hydrodynamics of the system, fluid elements spend different amounts of time to pass through the system. The distribution of these times of passage is called the residence time distribution of the fluid and is denoted by $E(t)$ (Levenspiel, 1999). Experimentally, this function is the direct response to a tracer impulse and it is obtained by normalizing the output concentration by the total amount of tracer injected. The mean residence time t_m of the distribution is defined by

$$t_m = \sum_{0}^{\infty} t \cdot E(t) \Delta t \qquad (7.7)$$

The variance σ^2, which gives a measure of the spread of the distribution around the mean, is obtained by

$$\sigma^2 = \sum_0^\infty (t - t_m)^2 \cdot E(t) \cdot \Delta t \tag{7.8}$$

From the material balance of the system, a theoretical mean residence time can be calculated as

$$t_m = \frac{V}{Q} \tag{7.9}$$

Additionally, a cumulative distribution function $F(t)$ can be defined such as

$$F = \int_0^t E dt \tag{7.10}$$

By determining the time t_i taken by each of the massless tracer particles to get from the injection point to the exit plane, a numerical RTD could be constructed. According to Nauman & Buffham (1983), a fraction of the volumetric flow rate ΔQ_i has to be associated to each particle. This fraction is approximated by

$$\Delta Q_i = V(r_i) \cdot \Delta A_i \tag{7.11}$$

where $V(r_i)$ is the velocity at the point of entry which varies according to the position $r_i(x,y)$, and ΔA_i is a small area element determined by

$$\Delta A_i = \frac{A}{N_{particles}} \tag{7.12}$$

where A is the injection plane area and $N_{particles}$ is the number of particles that reached the exit plane. Paired values of ΔQ_i and t_i can then be used to construct a histogram, which once normalized will become the $E(t)$ function defined as the fraction of the volumetric flow which has a residence time between t and $t+dt$. The following RTD results are based on histograms constructed with the bin width obtained from the Freedman-Diaconis Rule (1981) which is defined as

$$h = 2\frac{IQR(x)}{n^{1/3}} \tag{7.13}$$

where h is the bin width, n is the number of data points and IQR is the interquartile range of the data which is equal to the difference between the third and first quartiles.

7.6 Results and discussion

7.6.1 Model validation with experimental pressure gradients

In order to verify the accuracy of the numerical model, pressure gradient results obtained across the screw length are first compared with experimental values (**Figure 7–6**). The experimental results were obtained using a laboratory Co-Kneader setup having the same dimensions, screw configuration and fluid properties as the numerical model. The relative error calculated between the experimental and the numerical results in all cases is less than 8%. Knowing that the pressure is the most sensitive numerical variable to match flow rate, we can conclude that we have a good agreement between the simulated and the experimental flows.

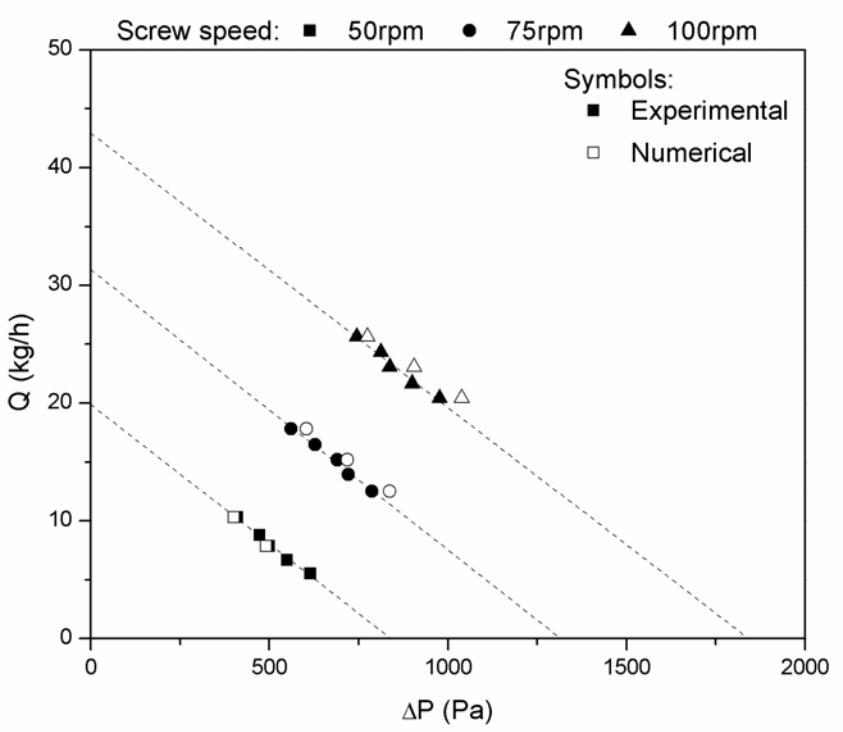

Figure 7–6. Comparison of experimental and numerical results.

7.6.2 Characteristic curves

As part of a more comprehensive look into the fluid dynamics of the Co-Kneader, characteristic curves for each type of element were obtained. **Figure 7–7** shows the dimensionless characteristic curve for the conveying EZ element and the mixing KE element.

The dimensionless flow rate Q^* is defined as

$$Q^* = \frac{Q}{Q_{\max}} = \frac{2Q}{HWv_x} \tag{7.14}$$

where Q is the imposed flow rate of the simulation, Q_{max} is the maximum theoretical flow of a single screw, H and W are geometrical parameters and v_x is the down channel velocity component of the screw speed obtained by

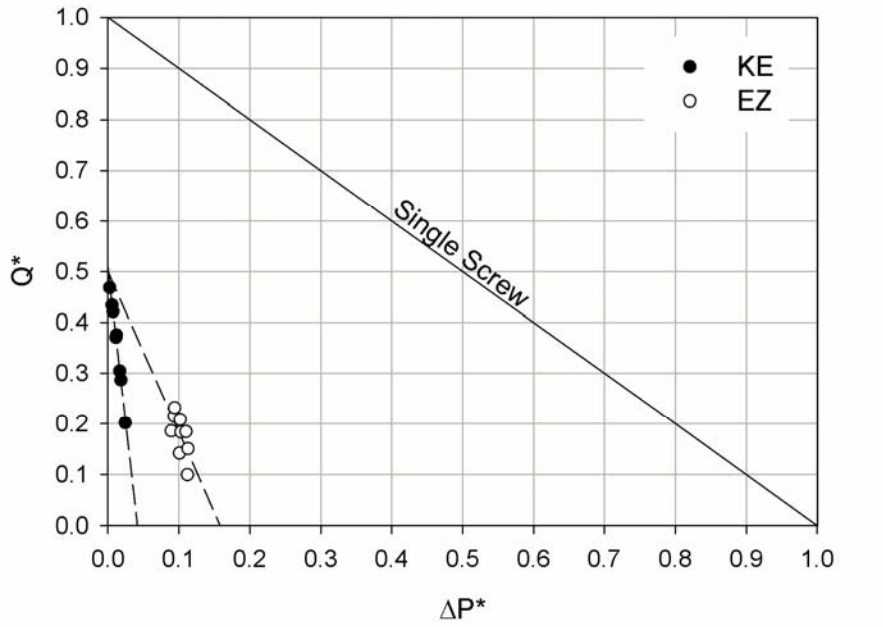

Figure 7–7. Dimensionless characteristic curve for the different screw elements.

$$v_x = \pi D_s N \cos\varphi \tag{7.15}$$

The pressure gradient ΔP is equal to P_2-P_1, where P_1 is the pressure at the inlet of each element and P_2 the pressure at the exit of that same element. The numerical results of P_1 and P_2 are average values of all the calculated time steps. The dimensionless pressure gradient ΔP^* is defined by

$$\Delta P^* = \frac{\Delta P}{\Delta P_{\max}} \frac{\Delta P H^2}{6\mu L_h v_x} \tag{7.16}$$

where ΔP_{max} is the maximum theoretical pressure gradient of a single screw and L_h is the channel length of each screw element; 0.16 m for the EZ element and 0.32 m for the double flighted KE element. The intersection with the y-axis gives the maximum flow rate value (when $\Delta P = 0$) and the intersection with the x-axis represent the maximum pressure that the screw can generate at closed discharge ($Q = 0$). We can see that even if the maximum flow reached with both elements

is the same, the pressure-generating capacity is different. The conveying element has a greater pumping capacity than the mixing element; however, compared with a theoretical single screw both elements have very little pumping capacity. This is why in practice, the Co-Kneader is coupled with a crosshead screw extruder (Rauwendaal, 1991a). The main reason why the Co-Kneader screw elements have a poor pumping capacity is the presence of the slices in the flights. **Figure 7–8** shows the unrolled screw channels of both types of screw elements. If we compare the length of the slices L_s relative to the length of the channel L_h we found that for the EZ element the slices represent about 16% of the total channel length, whereas in the KE element they represent 48%.

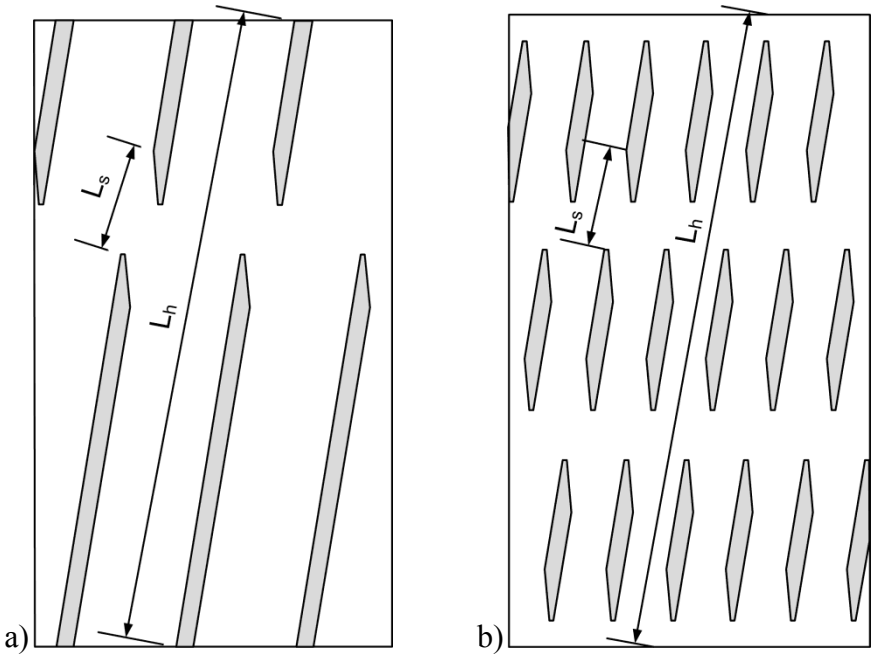

Figure 7–8. Unrolled screw channel: **a)** EZ conveying element, **b)** KE mixing element.

The results found in this section are qualitatively in agreement with the ones previously reported by Elemans & Meijer (1990) and Lyu & White (1995). However a quantitative comparison is difficult to perform due to the fact that Elemans & Meijer do not present their results in a dimensionless form and Lyu & White performed their calculations using an analytical model that considered only the oscillating nature of the screw but not the presence of the pins.

7.6.3 Extensional efficiency

In order to evaluate the dispersive mixing efficiency of the flow inside the Co-Kneader we obtained the extensional efficiency α as defined by Manas-Zloczower (1994):

$$\alpha = \frac{\left|\dot{\underline{\underline{\gamma}}}\right|}{\left|\dot{\underline{\underline{\gamma}}}\right| + \left|\underline{\underline{\omega}}\right|} \tag{7.17}$$

where $\left|\dot{\underline{\underline{\gamma}}}\right|$ is the norm of the rate of deformation tensor and $\left|\underline{\underline{\omega}}\right|$ is the norm of the vorticity tensor.

In this manner, the parameter α quantifies the elongational and rotational flow components of the velocity field. The base for using α as a tool to evaluate dispersive mixing comes from the conclusion that elongational flows are more effective than simple shear flows in the dispersion of liquids and solid agglomerates into liquids (Manas-Zloczower, 1994). The extensional efficiency coefficient is equal to 0 for pure rotation, 0.5 for simple shear flows and 1 for pure elongation.

It should be highlighted that this criterion, being dependent of $\left|\underline{\underline{\omega}}\right|$, is not frame invariant (Rauline *et al.*, 1998). However, since in this study the reference frame is kept constant, the value of α can be used for comparative purposes.

The extensional efficiency along the Co-Kneader at different angular positions of the screw is shown in **Figure 7–9**. The abscissa represents the axial length of the mixer. The plotted value of α corresponds to the average extensional efficiency at the cross-section plane located at a given distance along the Co-Kneader. The peaks at the start and at the end of the screw are due to the entrance and exit effects of the flow. We can see that the mixing section has a higher value of α compared to the conveying sections.

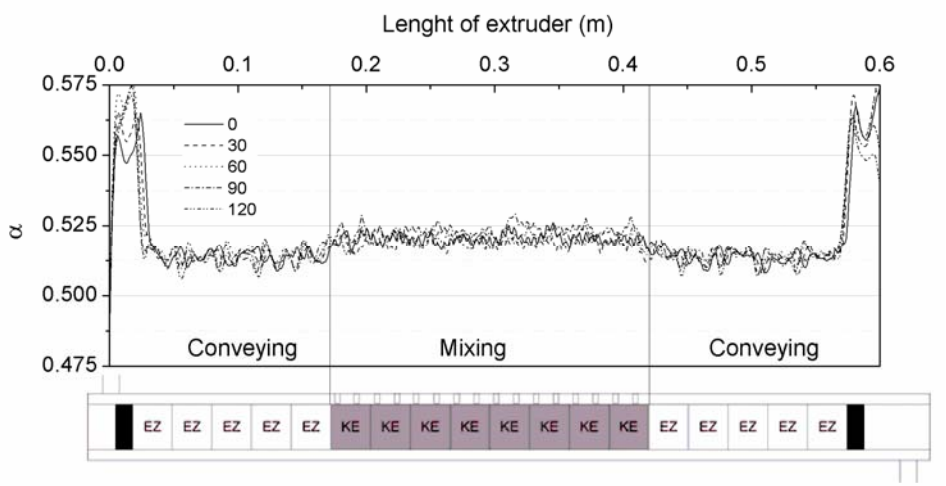

Figure 7–9. Extensional efficiency along the Co-Kneader. N = 75rpm, Q = 15.2 kg/hr.

By analysing each separate section of the screw, we can calculate a mean value of α for the conveying and the mixing screw elements as a function of the screw angular position (**Figure 7–10**). In addition to the mixing element having a higher value of α_m than the conveying element, we observe that α_m is more sensitive to the screw position in the mixing element that in the conveying element. Also, the maximum and minimum values of α_m in each element are reached at different screw positions. The maximum for the conveying element is reached at 60°, 180° and 300°, when the pin is closer to the screw flight. The minimum is located at 120° when the pin is located between the screw slices, and 240° when the pin is in the middle of the screw channel. For the mixing element, the maximum is reached at 90° and 210° when the pin is closer to the screw flight. As with the conveying element, the minimum values correspond to screw positions in which the pins are located between the screw slices or in the middle of the channel. The screw speed also has a larger impact on the mixing element than on the conveying element. In terms of magnitude there is not a significant difference between $\alpha_{m-\mathrm{KE}}$ and $\alpha_{m-\mathrm{EZ}}$, both being between 0.51 and 0.53.

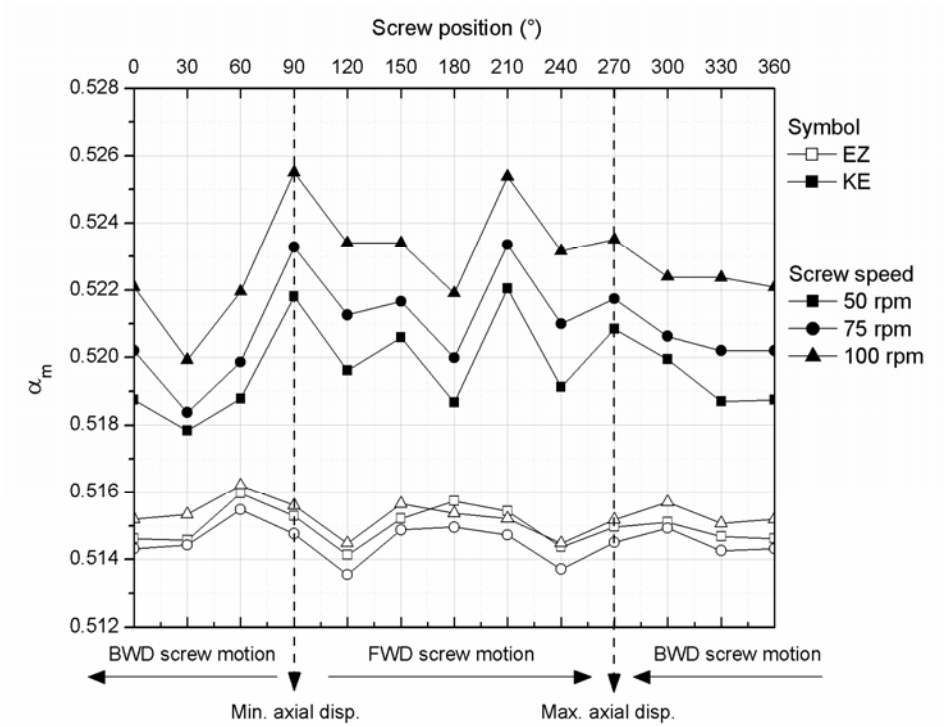

Figure 7–10. Mean extensional efficiency of the EZ and KE elements as a function of screw position and screw speed.

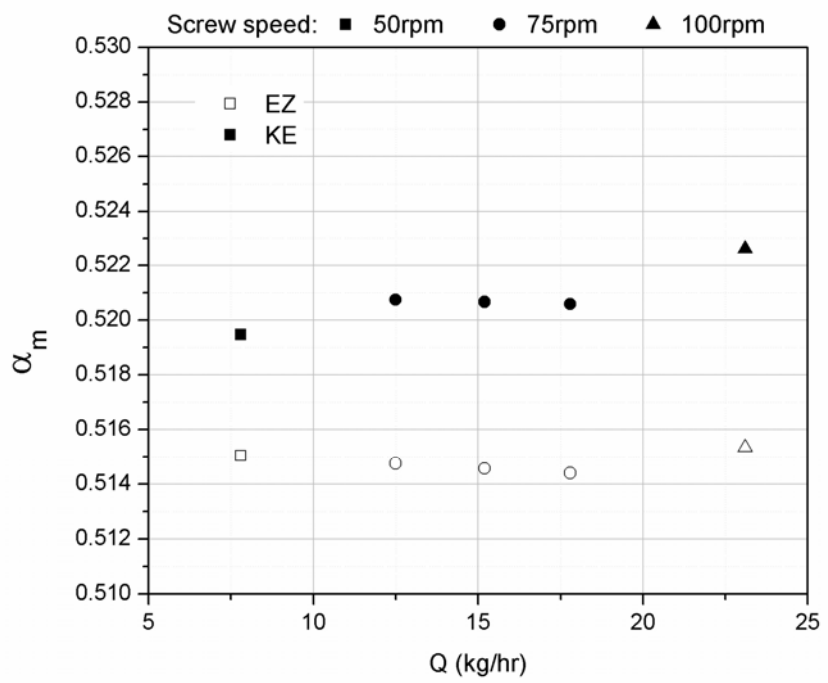

Figure 7–11. Mean extensional efficiency of the EZ and KE elements as a function of operating conditions.

The effect of the flow rate on α_m is showed in **Figure 7–11**. We can see that the value of $\alpha_{m-\mathrm{KE}}$ and of $\alpha_{m-\mathrm{EZ}}$ remains fairly constant when varying the flow rate at the same screw speed.

In order to evaluate the efficiency of different flow fields for mixing, not only the values of the coefficient α have to be considered, but also the magnitude and distribution of shear stresses τ in the flow field (Manas-Zloczower, 1994). **Figure 7–12** shows the spatial distribution of α projected on a cylindrical surface placed at mid-channel distance from the screw root. We can see that the flow is mainly shear flow ($\alpha = 0.5$) between the flights of both types of screw elements. However, around the pin in the mixing element and at the tips of the screw flight in the conveying element α takes values of ~0.8. If we look at the distribution of shear stresses for the same operating condition (**Figure 7–13**) we found that it is only around the pins and not at the tips of the screw flights where τ has larger values. This fact confirms that it is the pins that generate the dispersive mixing action in the Co-Kneader.

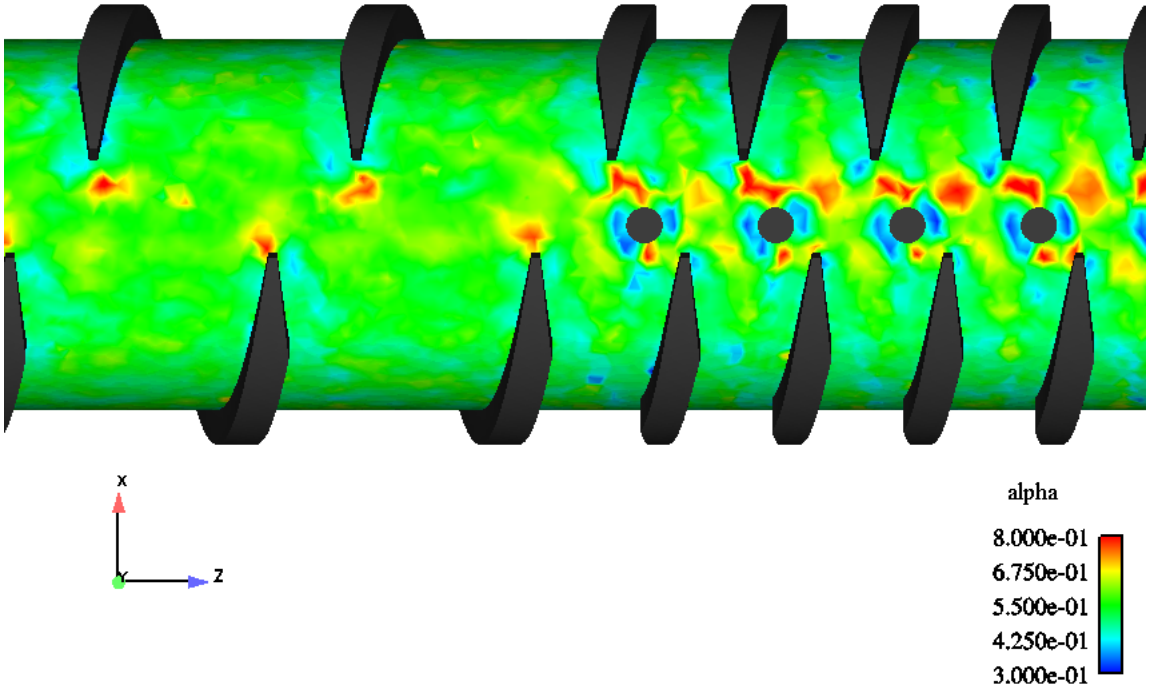

Figure 7–12. Distribution of the extensional efficiency coefficient. N = 100rpm, Q = 23.1kg/h.

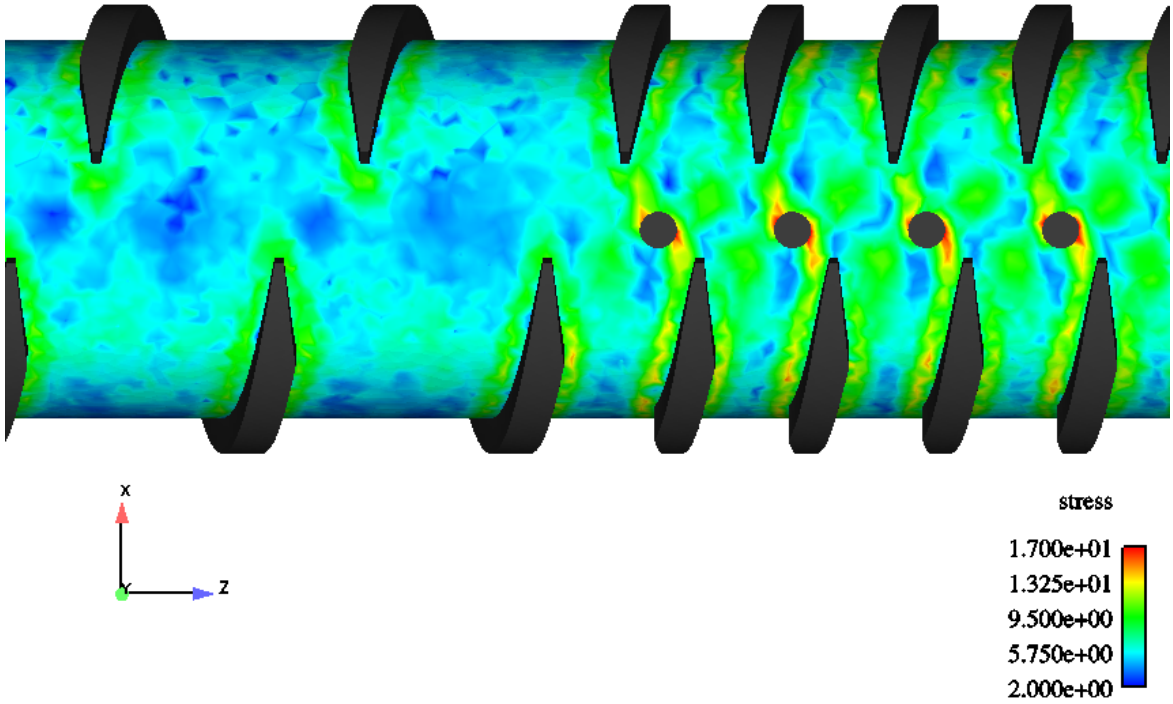

Figure 7–13. Distribution of shear stresses. N = 100rpm, Q = 23.1 kg/h.

7.6.4 Shear rate

In the same manner as for the extensional efficiency, the shear rate $\dot{\gamma}$ along the Co-Kneader was obtained for different positions of the screw. **Figure 7–14** shows the values depending on the pin position relative to the screw flights.

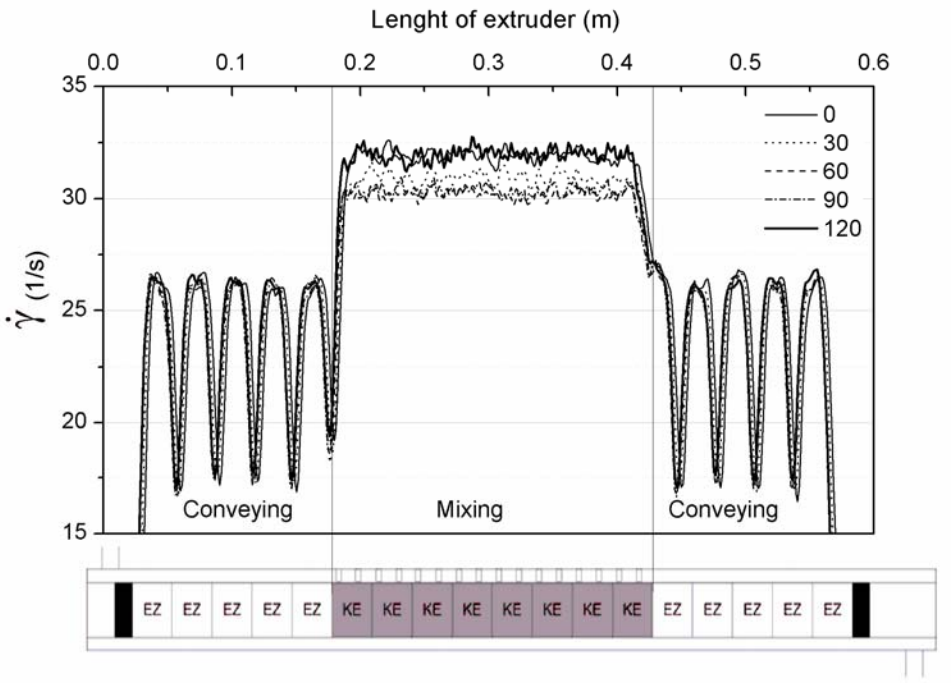

Figure 7–14. Shear rate along the extruder in different screw angular positions. N = 75rpm, Q = 15.2 kg/hr.

The differences between elements are clearly showed in this plot. The mean shear rate is higher in the mixing elements and it remains constant along all the mixing section. On the contrary, on the conveying sections there are large oscillations, where the higher values correspond to the location of the only pin found on each element. Another interesting feature is the variation of $\dot{\gamma}$ in the mixing zone according to the relative position of the pin with respect to the screw flight. To analyse this variation, the mean value of $\dot{\gamma}$ for each section was plotted as a function of the angular position of the screw (**Figure 7–15**). We can see that the value of $\dot{\gamma}_m$ in the mixing element is higher when the pin is at the initial position of 0° (*i.e.* between the screw slices) and it

decreases as the pin travels between the screw flights. It then reaches again the maximum value when it has completed its passage (120°). The cycle is repeated three times, which correspond to the three pins and the three slices in the flights found on the mixing element. Because the conveying element only has one pin, the value of $\dot{\gamma}_m$ is not affected as much by the position of the screw.

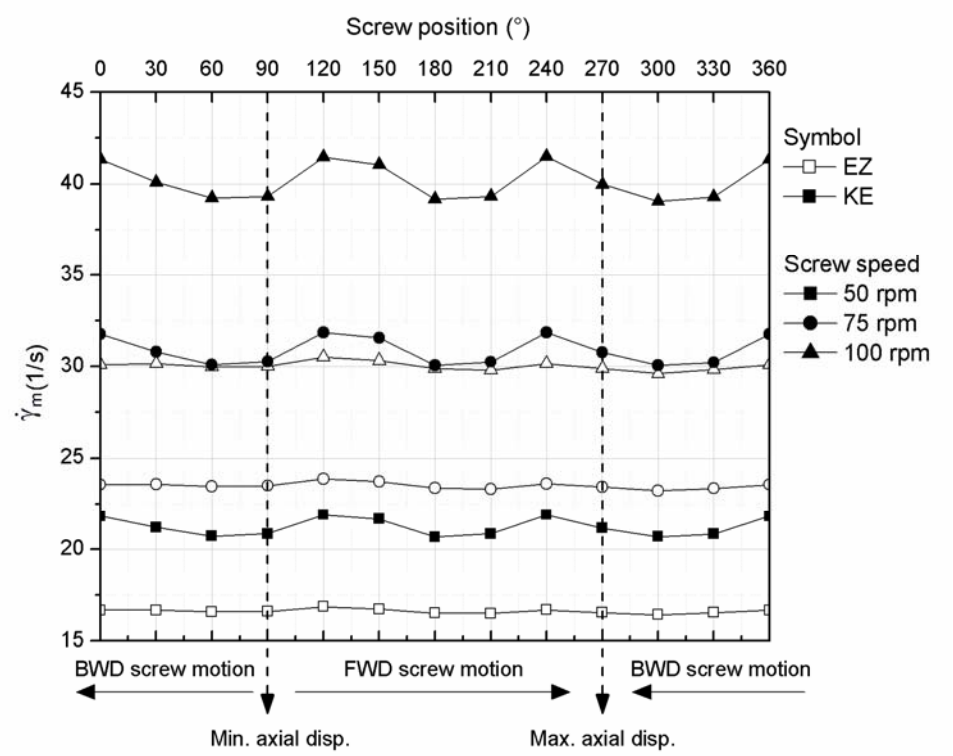

Figure 7–15. Mean shear rate of the EZ and KE element as a function of screw position and screw speed.

Figure 7–16 shows the effect of the operating conditions on the mean shear rate. We see that only the screw speed has an impact on the shear rate value, which indicates that the level of shear rate that can be obtained depends only on the geometry of the extruder and the rotational speed.

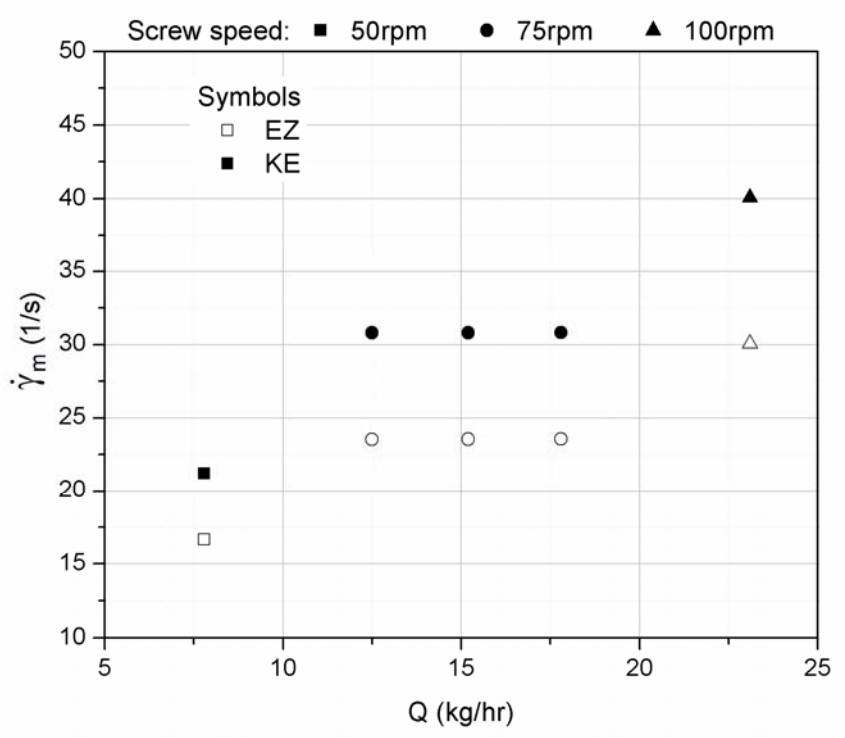

Figure 7–16. Mean shear rate of the EZ and KE elements as a function of operating conditions.

Determination of shear rate based only on geometrical parameters already exists for single screws (Rauwendaal, 1994). The shear rate in the screw channel of a single screw can be approximated by

$$\dot{\gamma}_{ch} = \pi\left(\frac{D_o}{H} - 2\right)N = K_{ch}N \tag{7.18}$$

According to the manufacturer, the maximum shear rate in the Co-Kneader can be obtained by

$$\dot{\gamma} = \pi\left(\frac{D_o}{s_z}\right)N = K_{pin}N \tag{7.19}$$

where s_z is the gap width between the stationary pin and the passing screw flight. However shear rates values obtained with this formula are generated only when the screw flight is passing near

the pin. A more practical average value of the shear rate produced in each screw element can be obtained by using the Metzner-Otto relationship (Metzner & Otto, 1957). This definition is well known and widely used in agitated vessels and static mixers. It is based on the assumption that the fluid motion in an agitated tank can be represented by an average or effective shear rate. The shear rate is then proportional to the impeller speed with the constant of proportionality K_s,

$$\dot{\gamma} = K_s N \tag{7.20}$$

This function depends only on the geometry. With the K_s and a viscosity-shear rate curve for a non-Newtonian fluid, an effective or process viscosity can be determined.

The values of K_s for the conveying and the mixing elements were obtained using the data from **Figure 7–16**. **Table 7-3** lists the calculated K_s as well as the constants obtained from **Equation 7.18** and **Equation 7.19**. The values of K_{ch} and K_{pin} are the same for both screw elements since they do not consider particular geometrical features of each screw element. Since the values of K_s were obtained from the simulations, we can consider that the interactions of the pins and the screw oscillation are taken into account. Therefore a higher value of K_s for the mixing element was to be expected since it has more pins passing through. The difference between the Co-Kneader and a similar single screw is also evidenced; the value of K_{ch} being 38% lower than the K_s value of the EZ element and 77% lower than the K_s of the KE element.

Table 7-3. Values of K_s and other geometric constants for the EZ and KE screw elements.

	EZ element	KE element
K_{ch}	13	13
K_{pin}	315	315
K_s	18	23

7.6.5 Residence Time Distributions

Figure 7–17 shows the calculated mean residence time for each type of element after a given number of consecutive screw elements. Theoretical values obtained from **Equation 7.9** are presented as well. We can see that the results obtained for the conveying elements present a very small deviation from the theoretical values. On the other hand, the mixing elements exhibit a greater deviation from the theoretical values as the number of screw elements increase. The difference increases with the screw speed as well. This difference can be attributed to a greater number of lost particles in the mixing element. Also, the lost particles are often those with long residence times. The higher relative error between numerical and theoretical values in the mixing element is 16%.

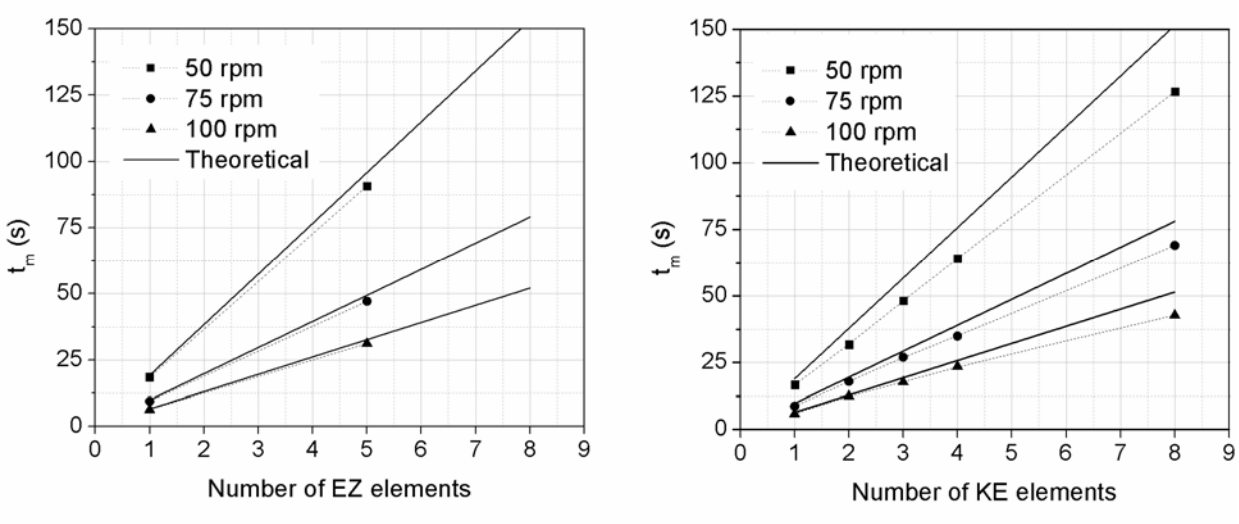

Figure 7–17. Calculated and theoretical mean residence time.

The numerical values of σ^2 are presented in **Figure 7–18**. We see that the spread of the residence time distributions increases as the number of consecutive mixing elements increases, however the relationship is not linear. Also, the variance increases as a function of screw speed and flow rate.

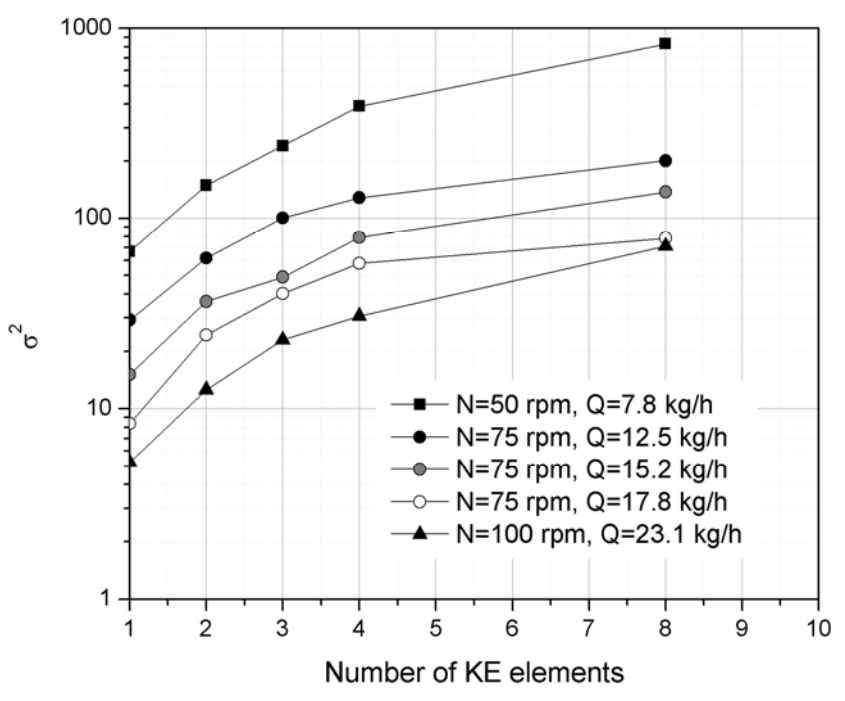

Figure 7–18. Calculated variance as a function of the number of consecutive mixing elements.

By fitting the data to the axial dispersion model (ADM) (Levenspiel, 1999)

$$E(\theta) = \frac{1}{2}\sqrt{\frac{Pe}{\pi\theta}}\exp^{\left[-\frac{Pe(1-\theta)^2}{4\theta}\right]} \tag{7.21}$$

we can obtain the axial Peclet number *Pe* defined as

$$Pe = \frac{uL}{D_{ax}} \tag{7.22}$$

where u is the mean axial velocity of the flow, L the axial length and D_{ax} the axial dispersion coefficient. At *Pe* higher than 100, this model approximates plug flow behavior. On the other hand, a *Pe* approaching 0 indicates fully mixed flow (Nauman, 2008).

Figure 7–19 shows the fitting of the calculated results to the axial dispersion model after a given number of mixing elements. The values of the adjusted R^2 show that the ability of the model to fit the results depends on the number of screw elements; after more mixing elements the model predicts the RTD curve better. The same pattern was observed for the other operating conditions.

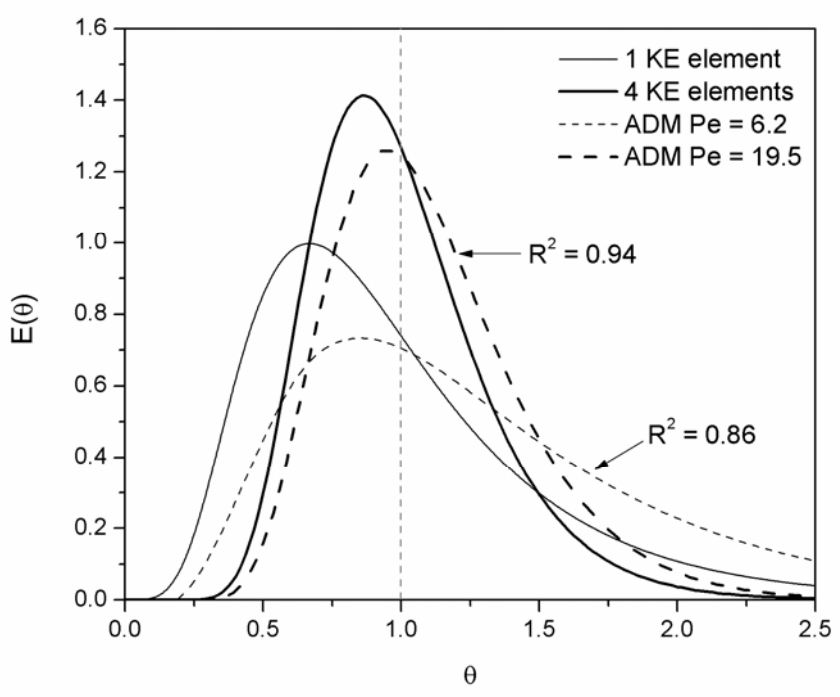

Figure 7–19. Fitting of results with the ADM. N = 50 rpm, Q = 7.8 kg/h.

The evolution of the *Pe* with the number of consecutive mixing elements is shown in **Figure 7–20**. A linear relationship is observed, however the rate at which the *Pe* number increases appears to be dependent on the operating conditions. At high screw speeds and high flow rates the *Pe* number increases more rapidly with each mixing element.

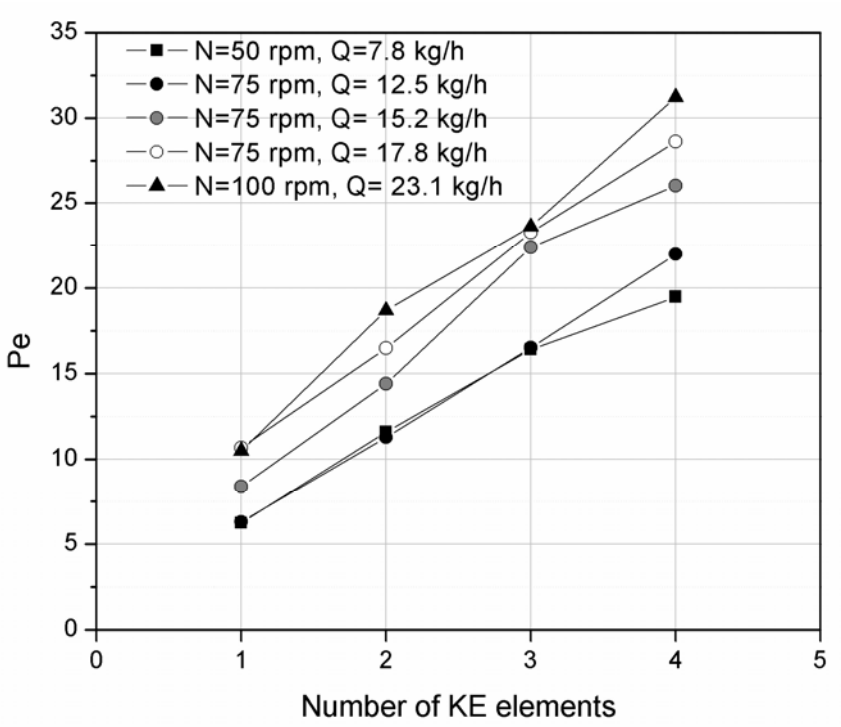

Figure 7–20. Peclet number as a function of consecutive mixing elements.

With the purpose of characterizing the geometry of each screw element type, individual RTD curves for each conveying and mixing elements were obtained. **Figure 7–21** shows the cumulative distribution functions obtained for each of the first four elements of the mixing and conveying sections, expressed in terms of the dimensionless time θ

$$\theta = \frac{t}{t_m} \tag{7.23}$$

The curves of the conveying elements display a small variation in spread depending on the position of the element. However, when we compared with other operating conditions, no clear trend regarding the position and the width of the distribution could be discern. On the other hand, there is no difference in the RTD of the mixing elements, which indicates that the flow develops very quickly in this geometry.

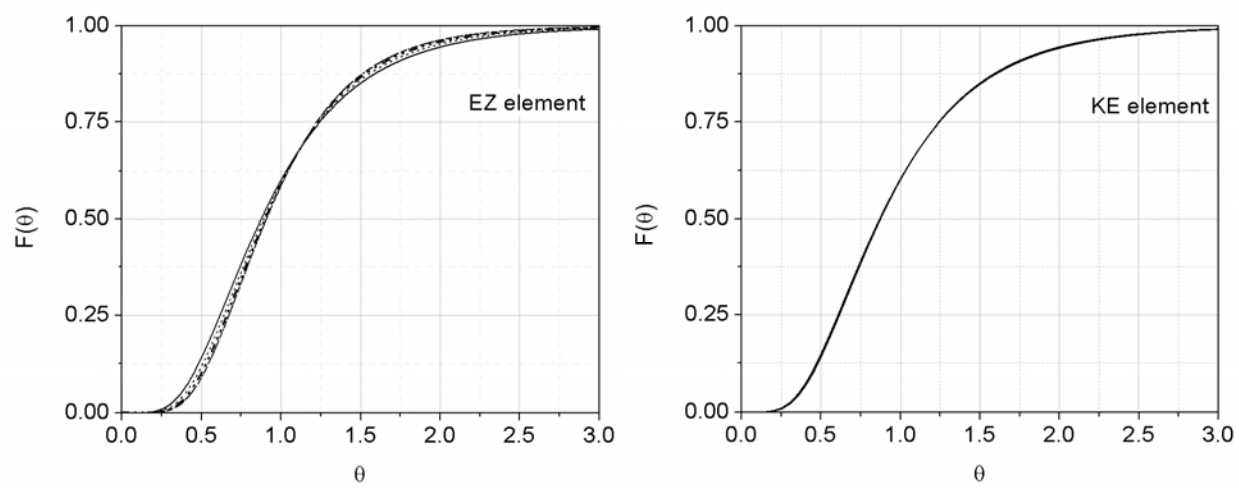

Figure 7–21. Cumulative distribution functions obtained individually for the first 4 screw elements of each type. N = 75rpm, Q = 12.5kg/h.

Mean residence times for each type of element at different operating conditions are presented in **Figure 7–22**. As the screw speed increases the difference between the two elements decreases, the conveying element having the longer mean residence time. The variance was calculated as well (**Figure 7–23**), showing that the mixing element has a broader distribution. Following previous trends, the distribution in both elements becomes narrower with high speeds and higher flow rates.

We compared the values of t_m and σ^2 obtained directly from the calculations of consecutive mixing elements with those obtained from adding the values of t_m and σ^2 obtained from a single element (**Figure 7–24**). The difference between the values of t_m increases as the number of consecutive mixing elements increase, the higher relative error being 17%. In the case of σ^2, the deviation is greater and the relative error varies between 17% and 40%.

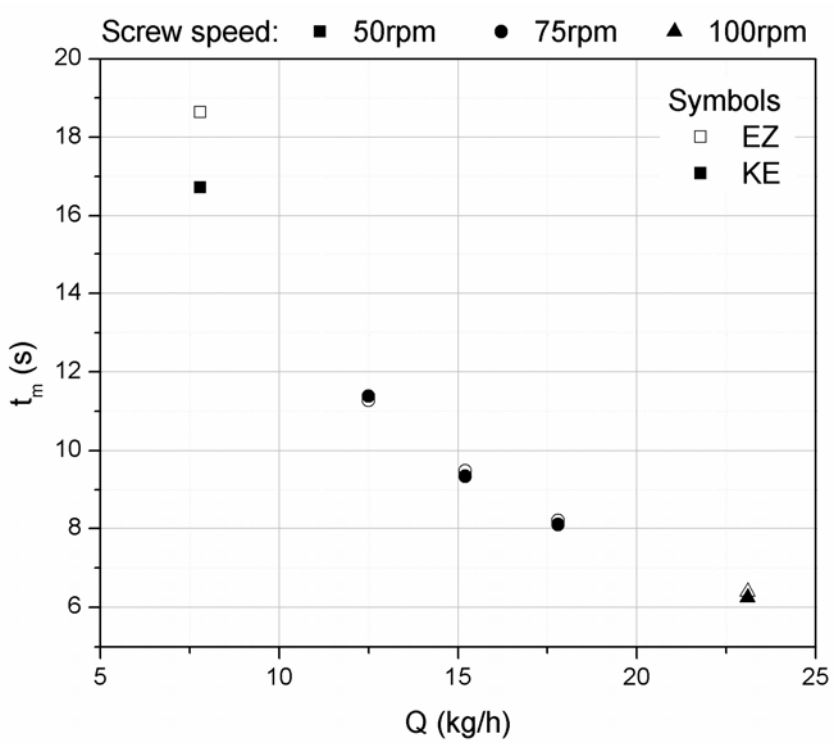

Figure 7–22. Mean residence time of individual mixing and conveying elements.

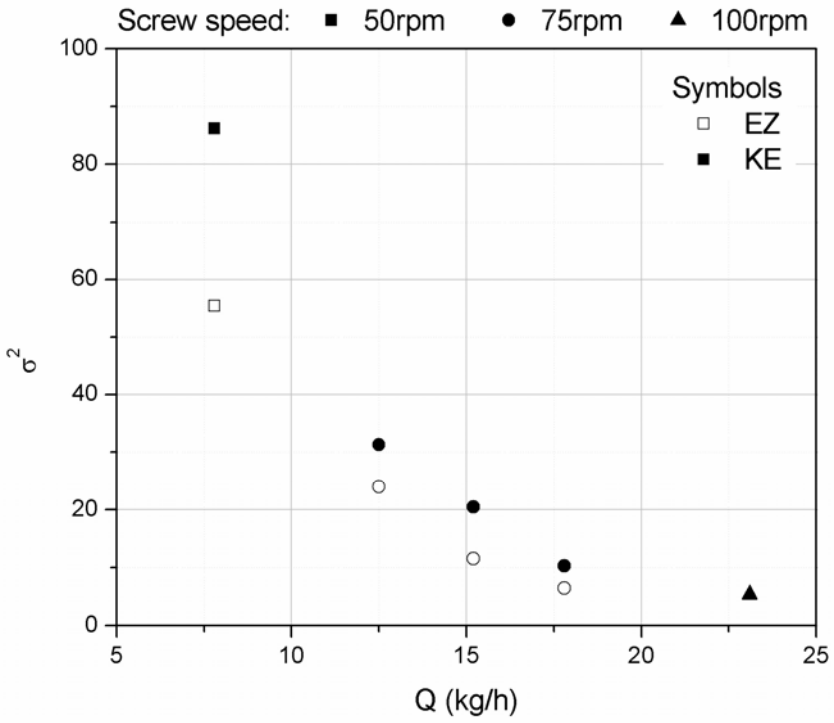

Figure 7–23. Variance of individual mixing and conveying elements.

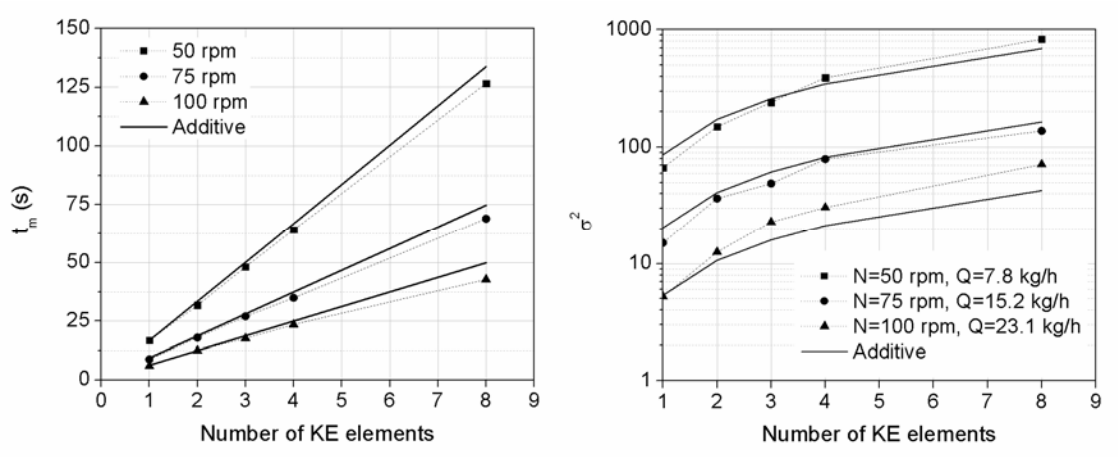

Figure 7–24. Comparison of calculated t_m and σ^2 with additive rule.

7.6.6 Particle distribution

Poincaré sections at the exit of the first four mixing elements of the Co-Kneader are shown in **Figure 7–25**. In addition to the injection plane defined in **Figure 7–5**, the injection of particles concentrated on the upper portion of the cross section was also studied.

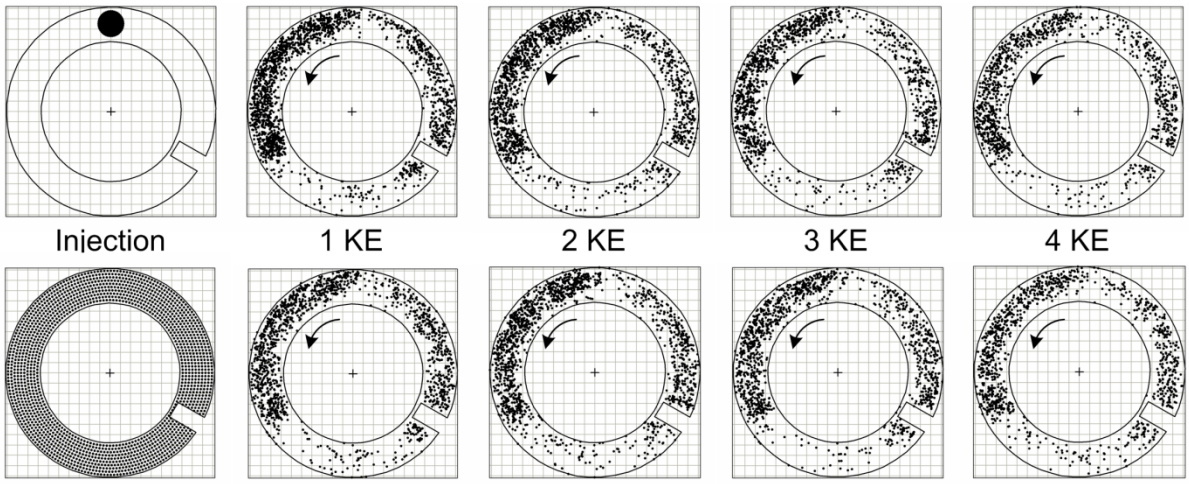

Figure 7–25. Poincaré sections at exit of first 4 mixing elements. N = 75 rpm, Q = 17.8 kg/h.

We can see that the initial position of the particles does not have an impact on the spatial distribution at the exit of the mixing elements. This confirms the fact that the velocity profile is quickly developed. Also, we can see that a constant spatial distribution in the cross section is attained after only one mixing element. In all cases, the particles are concentrated on the upper left side of the cross section, with some particles in the upper right side and very little in the lower region. In a single screw extruder, particles only on the upper left side would be expected because the plane would cut in the middle of a closed screw channel and the particles would have nowhere to go but in the down channel direction. In the case of the Co-Kneader the screw channel is opened, therefore particles can be found in other locations in the cross-section. The same observations were made for the other operating conditions.

In **Figure 7–26** we present the mixing evolution of the particles injected in the upper portion of the mixing element. At 0.5 s we can clearly see how the pin splits the flow and promotes backflow of the particles. In 5 seconds the particles are evenly distributed along the screw axis.

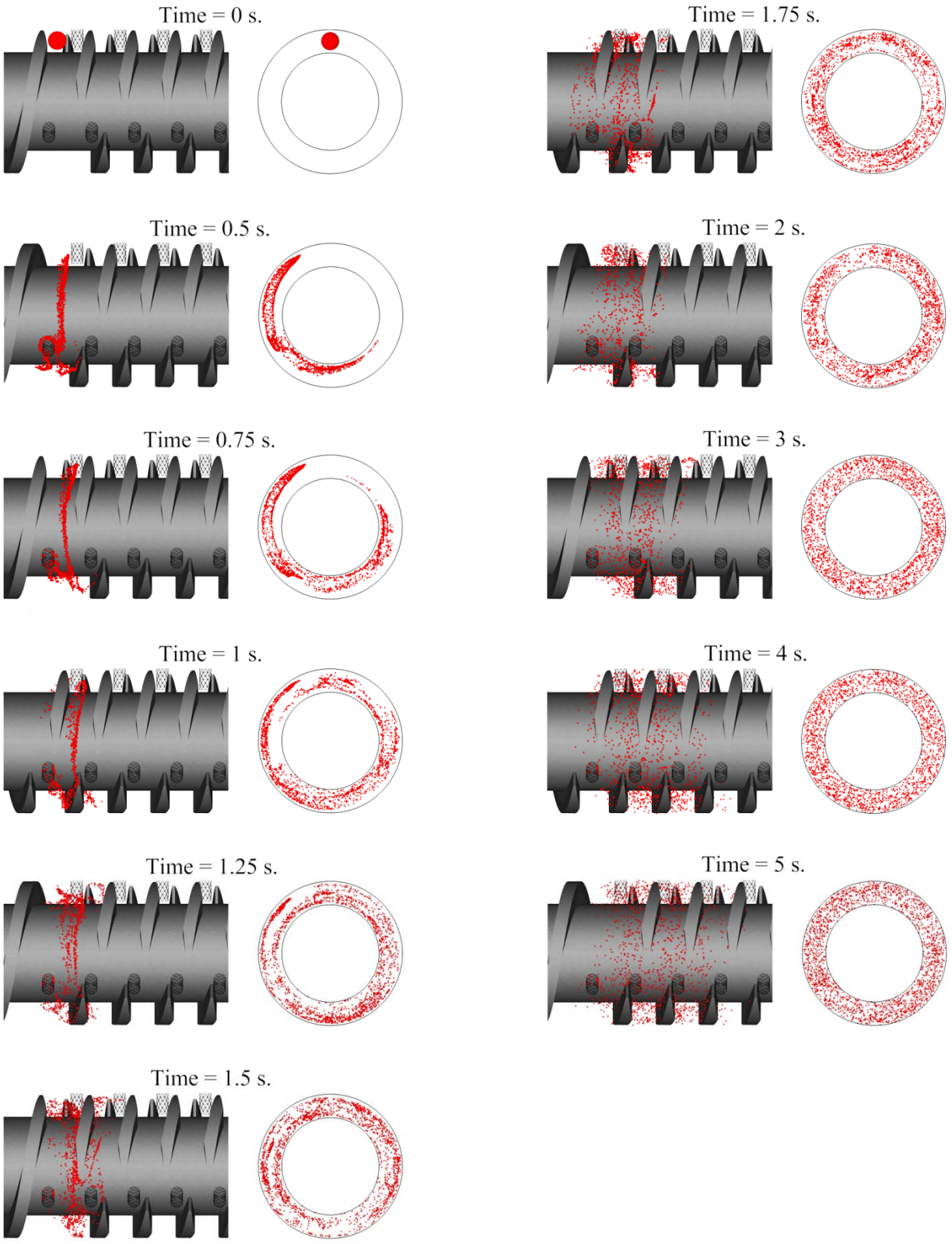

Figure 7–26. Evolution of mixing in the mixing section of the Co-Kneader. N = 75 rpm, Q = 17.8 kg/h.

7.7 Conclusions

In this work we have investigated the mixing characteristics of two screw elements of the Co-Kneader extruder. The results were obtained by means of a validated 3D CFD model that included the oscillation of the screw as well as the pins in the barrel. Dimensionless characteristic curves were presented, and the pumping capacity of each element was compared to that of a similar single screw extruder. Extensional efficiency results showed that the conveying element had a lower mean value than the mixing element. Also, it was demonstrated that the pins promote extensional flows in the screw channel. It was possible to obtain for each type of screw element the constant of proportionality K_s by using the Metzner-Otto relationship. This gives the possibility to obtain the effective shear rate value given by each screw element as only a function of the screw speed. It was found that the mean residence time of an array of elements can be obtained by adding the individual mean times within an error of 17%; however the error in the variance obtained in the same manner is doubled. Finally, by visualization of particle distributions we could reaffirm the performance of the Co-Kneader as a continuous mixer.

7.8 Acknowledgements

The financial support of the National Science and Engineering Research Council of Canada (NSERC) and of TOTAL is greatly acknowledged. Thanks are also directed to CONACYT (Mexico) for the financial support of M. Brito-Bazan.

7.9 Notation

α	Extensional efficiency	Dimensionless
$\dot{\gamma}$	Shear rate	1/s
θ	Dimensionless time	Dimensionless

μ	Newtonian viscosity	Pa s
ρ	Density	kg/m^3
σ^2	Variance	s^2
τ	Shear stress	Pa
φ	Flight angle	°
ω	Oscillation frequency	1/s
A	Area	m^2
D	Diameter	m
D_b	Inside diameter of barrel	mm
D_o	Outside diameter of screw	mm
e	Flight thickness	mm
H	Screw channel depth	mm
h	Bin width	s
K_{ch}	Shear rate constant from single screw channel	Dimensionless
K_{pin}	Shear rate constant from pin-flight gap	Dimensionless
K_s	Shear rate constant from Metzner-Otto relationship	Dimensionless
L_{ax}	Axial length	m
L_e	Length of screw element	mm
L_h	Helical or down-channel length	m
L_s	Length of flight slices	mm
l	Trajectory length	m
l_m	Mean trajectory length	m
N	Screw speed	rpm
n	Number of data points	Dimensionless
P	Pressure	Pa
P^*	Dimensionless pressure	Dimensionless
Q	Flow rate	kg/h
Q^*	Dimensionless flow rate	Dimensionless
R	Radius	m

S_0	Amplitude of screw stroke	mm
s	Width of screw slice	mm
s_z	Gap between pin and screw flight	mm
t	Time	s
t_m	Mean residence time	s
u	Mean axial velocity	m/s
V	Volume	m^3
v	Velocity	m/s
W	Screw channel width	mm

7.10 References

Arnold, D., Brezzi, F., & Fortin, M. (1984). A stable finite element for the stokes equations. *Calcolo, 21*(4), 337-344.

Bertrand, F., Tanguy, P. A., & Thibault, F. (1997). A three-dimensional fictitious domain method for incompressible fluid flow problems. *International Journal for Numerical Methods in Fluids, 25*(6), 719-736.

Booy, M. L., & Kafka, F. Y. (1987). Isothermal Flow of Viscous Liquids in the Mixing Section of a Buss Kneader. *SPE ANTEC Tech. Papers*, 140-145.

Brzoskowski, R., Kumazawa, T., & White, J. L. (1989). Modelling flow in mixing section of a KoKneader (Buss). *SPE ANTEC Tech. Papers*, 54-58.

Coesnon, B., Heniche, M., Devals, C., Bertrand, F., & Tanguy, P. A. (2008). A fast and robust fictitious domain method for modelling viscous flows in complex mixers: The example of propellant make-down. *International Journal for Numerical Methods in Fluids, 58*(4), 427-449.

Elemans, P. H. M., & Meijer, H. E. H. (1990). On the modeling of continuous mixers. Part II. The cokneader. *Polymer Engineering & Science, 30*(15), 893-904.

Freedman, D., & Diaconis, P. (1981). On the histogram as a density estimator: L_2 theory. *Probability Theory and Related Fields, 57*(4), 453-476.

Glowinski, R., Pan, T. W., & Periaux, J. (1994). A Fictitious Domain Method for Dirichlet Problem and Applications. *Computer Methods in Applied Mechanics and Engineering, 111*(3-4), 283-303.

Heniche, M., & Tanguy, P. A. (2006). A new element-by-element method for trajectory calculations with tetrahedral finite element meshes. *International Journal for Numerical Methods in Engineering, 67*(9), 1290-1317.

Heniche, M., Tanguy, P. A., Reeder, M. F., & Fasano, J. B. (2005). Numerical investigation of blade shape in static mixing. *AIChE Journal, 51*(1), 44-58.

Levenspiel, O. (1999). *Chemical reaction engineering* (3rd ed.). New York: Wiley.

List, H. (1950). US Patent No. 2 505 125. U. S. P. Office.

Lyu, M.-Y., & White, J. L. (1995). Models of Flow and Experimental Studies on a Modular List/Buss Kokneter. *International Polymer Processing, 10*(4), 305-313.

Lyu, M.-Y., & White, J. L. (1996). Modelling of a Viscous Non-Newtonian Polymer Melt in a List/Buss Kneader and Comparison to Experiment. *International Polymer Processing, 11*(3), 208-221.

Lyu, M.-Y., & White, J. L. (1997a). Simulation of linear viscoelastic flow behavior in the Buss Kneader. *Polymer Engineering & Science, 37*(3), 623-635.

Lyu, M.-Y., & White, J. L. (1997b). Simulation of Non-Isothermal Flow in a Modular Buss Kneader and Comparison with Experiment. *International Polymer Processing, 12*(2), 104-109.

Manas-Zloczower, I. (1994). Studies of mixing efficiency in batch and continuous mixers. *Rubber Chemistry and Technology, 67*(3), 504-528.

Mehranpour, M., Nazokdast, H., & Dabir, B. (2002a). Computational study of the velocity field in the conveying element of a Ko-Kneader with CFD method. *International Polymer Processing, 17*(2), 108-114.

Mehranpour, M., Nazokdast, H., & Dabir, B. (2002b). Estimation of residence time distribution in two elements of a Ko-Kneader. *International Polymer Processing, 17*(1), 22-25.

Mehranpour, M., Nazokdast, H., & Dabir, B. (2003a). Computational study of velocity field in the KE element of a modular Ko-Kneader with CFD method. *International Polymer Processing, 18*(4), 330-337.

Mehranpour, M., Nazokdast, H., & Dabir, B. (2003b). Prediction of residence time distribution in EZ and KE element of a Ko-Kneader by using CFD method. *International Polymer Processing, 18*(4), 327-329.

Metzner, A. B., & Otto, R. E. (1957). Agitation of non-newtonian fluids. *Chemical Engineering Progress, 3*(1), 3-10.

Nauman, E. B. (2008). Residence Time Theory. *Industrial & Engineering Chemistry Research, 47*(10), 3752-3766.

Nauman, E. B., & Buffham, B. A. (1983). *Mixing in continuous flow systems*. New York: Wiley.

Rauline, D., Tanguy, P. A., Le Blévec, J. M., & Bousquet, J. (1998). Numerical investigation of the performance of several static mixers. *The Canadian Journal of Chemical Engineering, 76*(3), 527-535.

Rauwendaal, C. (1991). Mixing in single-screw extruders. In C. Rauwendaal (Ed.), *Mixing in polymer processing* (pp. 129-239). New York: Marcel Dekker.

Rauwendaal, C. (1994). *Polymer Extrusion* (3rd ed.). New York: Hanser.

Shon, K., Bumm, S. H., & White, J. L. (2008). A comparative study of dispersing a polyamide 6 into a polypropylene melt in a Buss Kneader, continuous mixer, and modular intermeshing corotating and counter-rotating twin screw extruders. *Polymer Engineering & Science, 48*(4), 756-766.

Shon, K., & White, J. L. (1999). Comparative study of fiber breakage in compounding glass fiber-reinforced thermoplastics in a Buss Kneader, modular co-rotating and counter-rotating twin screw extruders. *Polymer Engineering & Science, 39*(9), 1757-1768.

Stade, K. (1977). Techniques for Compounding Glass Fiber-Reinforced Thermoplastics. *Polymer Engineering & Science, 17*(1), 50-57.

Stade, K. (1978). Production of Glass Fiber-Reinforced Poly(Butylene Terephthalate) on a Continuous Kneader. *Polymer Engineering & Science, 18*(2), 107-113.

Todd, D. B. (1987). Mixing Mechanisms for Polyoxymethylene. *SPE ANTEC Tech. Papers*, 128-132.

CHAPTER 8
GENERAL DISCUSSION AND CONCLUSIONS

The work presented in this thesis was divided in three parts. The first step was devoted to the development of a visualization technique that allowed for the mixing in the Co-Kneader to be evidenced. The second stage involved the development of a three dimensional numerical model that included both the oscillation of the screw and the pins in the barrel. The final stage aimed at the better characterization of the hydrodynamics and mixing abilities of the conveying and mixing screw elements.

8.1 Experimental Flow Visualization and Residence Time Distributions

This work reports for the first time flow visualization experiments performed in a fully transparent laboratory-scale Co-Kneader. In order to analyze the results, an image analysis technique usually used in stirred tanks was also applied for the first time in a continuous mixer. As expected, mixing curves are a function of the operational conditions; as the rotational speed increases, mixing time decreases. The mixing curves obtained as a result of the image analysis present very small variations between experiment repetitions, which mean that the technique is as robust for continuous systems as for stirred tanks. From the experimental mixing curves three different regions which are related to the different sections of the screw were clearly identified; two conveying sections with a mixing section in between. By performing a mathematical fitting analysis of the mixing curves, an axial mixing rate, defined as the increase in axial mixed area in time for each section, was estimated. The results clearly suggest that there is a sharp change of the mixing rate depending on the screw section and the flow rates. It has been found that the image analysis technique, for the first time applied to continuous systems, gives new insight into the macro-mixing mechanism of the Co-Kneader and may be used as a simple experimental method to quantify the degree of backmixing

Analysis of the RTD showed an expected trend, as the feed rate and screw speed increase, the mean residence time decreases. Similar behavior was observed regarding the spread of the distributions, as the feed rate and screw speed increased, the variance decreased. The axial dispersion model allowed for an estimation of the axial dispersion coefficient. It was found that for a fully filled system, the dispersion coefficient increased linearly with the flow rate and the screw speed. By comparing the RTD with that of a single screw extruder it was found that the pins and the slices in the Co-Kneader generate evenly and distributed residences times. Compared to a static mixer the Co-Kneader has a broader residence time distribution.

8.2 Numerical Flow Simulation

Newtonian simulations that took into account for the first time both the oscillation of the screw and the pins were performed with a 3D MINI-based VFEM. In order to verify the accuracy of the numerical model, pressure gradient as a function of flow rate results were obtained across the screw length and compared with experimental values. The CFD results were found to be in good agreement with the experimental results. The relative error calculated between the experimental and the numerical results in all cases is less than 8%.

The local effect of the pins was analyzed from CFD velocity fields. It was found that the flow is split and recombined from one channel to another when a pin is located between the slices of the screw, thus promoting backflow and distributive mixing. However, when there is no pin between the slices, the flow simply continues down channel. In the same way, the regular down channel flow between the screw flights is disrupted when there is a pin in the channel. Furthermore, it was shown that the flow appears to accelerate more between adjacent pins than it does when there are no pins.

The RTD and TLD analysis presented in this work were obtained by a particle tracking technique, where the motion of massless particles is dominated only by the flow field. The numerical RTD results were in good agreement with experimental measurements. TLD showed that the mixing element yields axial mixing whereas the conveying element causes down-channel mixing. The TLD analysis was performed on an extruder for the first time and it proved to be a complementary tool in the study of the mixing mechanisms in the Co-Kneader.

8.3 Mixing Analysis of Screw Elements

Dimensionless characteristic flow curves were generated from numerical simulations. It was shown that the conveying element has a greater pumping capacity than the mixing element; however, compared with a theoretical single screw both elements have very little pumping capacity. These results may explain why in practice, the Co-Kneader is coupled with a crosshead screw extruder. Results from this work confirm that the poor pumping capacity of the Co-Kneader is due to the presence of the slices in the flights.

In order to evaluate the dispersive mixing efficiency of the flow inside the Co-Kneader, the extensional efficiency, α was obtained. This parameter quantifies the elongational and rotational flow components of the velocity field. It was shown that the mixing section has a slightly higher value of α compared to the conveying sections. In terms of magnitude there was not a significant difference between $\alpha_{m-\mathrm{KE}}$ and $\alpha_{m-\mathrm{EZ}}$, both being between 0.51 and 0.53. Furthermore, it was found that the value of $\alpha_{m-\mathrm{KE}}$ and of $\alpha_{m-\mathrm{EZ}}$ remains fairly constant when varying the flow rate at the same screw speed. CFD results suggest that the pins in the barrel promote extensional flows in the screw channel.

In the same manner as for the extensional efficiency, the shear rate $\dot{\gamma}$ along the Co-Kneader was obtained for different positions of the screw. The differences between elements were clearly showed; the mean shear rate is higher in the mixing elements and it remains constant along all the

mixing section. On the contrary, on the conveying sections there are large oscillations, where the higher points correspond to the location of the only pin found on each element. It was found that the mean value of the shear rate $\dot{\gamma}_m$ is higher when the pin is at the initial position of 0° (*i.e.* between the screw slices) and it decreases as the pin travels between the screw flights, reaching the maximum value when it has completed its passage (120°). Because the conveying element only has one pin, the value of $\dot{\gamma}_m$ is not affected as much by the position of the screw. In order to deal with geometrical and operational variables and its impact on the shear rate, an average value of $\dot{\gamma}$ produced in each screw element was obtained by using the classical Metzner-Otto approach. The estimated values of K_s. for the conveying and the mixing elements were 18 and 23 respectively. A higher value of K_s for the mixing element is explained since it has more pins passing through. To the best knowledge of the authors, this is the first time that a shear rate characterization for a Co-Kneader as complete as possible has been shown.

Additionally it was found that the mean residence time of an array of elements can be obtained by adding the individual mean times within an error of 17%; however the error in the variance obtained in the same manner is doubled. Finally, by visualization of particle distributions the performance of the Co-Kneader as a continuous mixer was reaffirmed.

8.4 General Conclusions

The main objective of this project was to obtain a reliable description of the flow mechanisms and mixing in the Co-Kneader and to clarify how process variables impact the mixing capacity of the machine in order to facilitate the implementation of tailored screw profiles according to the application. In light of the obtained results the following can be concluded:

- Novel techniques aimed at characterize and quantify mixing mechanisms such as TLD analysis and the acid-base discoloration method coupled with the image analysis technique, were successfully applied for the first time in a continuous mixer. They

allowed for the description of the mixing mechanism in the Co-Kneader, which was found to be mainly in the axial direction, as well as the clarification of how process variables impacted axial mixing and backflow.

- By means of the 3D CFD model which incorporated all geometrical and mechanical characteristics of the Co-Kneader, it was possible to better assess the impact provided by the pins in the overall flow and mixing capabilities of the machine. It was found that besides making the flow split and recombine in the screw channels, they also promote extensional flow where otherwise there would only be shear flow.

- The characterization of commonly used screw elements was achieved by analyzing the RTD and shear rate produced by each individual screw element. This information can then be used towards the design of new screw profiles specially created for the needs of a particular application.

Overall, the experimental and CFD results suggest that the Co-Kneader screw extruder can be better designed and operated. The strategy followed allows for a detailed analysis of the Co-Kneader hydrodynamic performance. This analysis will then help identify and investigate suitable measures, such as different screw profiles or optimal operating conditions, for product design and process improvement.

CHAPTER 9
RECOMMENDATIONS FOR FUTURE RESEARCH

9.1 Experimental Flow Visualization

- This is the first time that the acid-base discoloration technique and image analysis method are applied in continuous systems. More experiments at different operating conditions, tracer concentrations and fluid viscosities are needed to investigate the capabilities of this methodology.
- The flow visualization analysis proved to be helpful towards the evaluation of the degree of backmixing. Well-known geometries like single-screw extruders in which the backmixing is known to be minimal should be investigated in order to have a reference point and corroborate the results.
- Application of the acid-base discoloration technique and image analysis to higher viscosity fluids as well as non-Newtonian fluids, pastes, etc.
- Investigation of the effect of rheological behavior on the axial mixing rate.
- Application of the acid-base discoloration technique and image analysis in other continuous systems like twin screw extruders or static mixers, as well as other Co-Kneader screw configurations.

9.2 Numerical Flow Simulation

- When the screw flight travels near the pins small gaps are created. Refinement of the mesh surrounding the pins is necessary in order to have higher resolution on the flow field in these gaps and better predict extreme shear rate values found in this area.
- Take advantage of the particle tracking technique to obtain trajectory length distributions and perform mixing analysis on other continuous systems.

- Simulations performed with non-Newtonian fluid properties.

9.3 Screw Profiles

- Optimization of existing screw profiles or conceptualization of new ones. The manufacturer of the Co-Kneader recommends a standard screw profile for all applications. However, given the flexibility that this mixer has, it seriously limits the scope of applications in which it can perform. The flow and mixing characterization of the conveying and mixing screw elements presented in this thesis can be used in order to optimize or design new screw configurations for different applications. These new screw configurations should be investigated and evaluated relative to the requirements of each particular application (*e.g.*, High shear rate, short residence time).

REFERENCES

Arnold, D., Brezzi, F., & Fortin, M. (1984). A stable finite element for the stokes equations. *Calcolo, 21*(4), 337-344.

Ascanio, G., Brito-Bazan, M., Brito-De La Fuente, E., Carreau, P. J., & Tanguy, P. A. (2002). Unconventional configuration studies to improve mixing times in stirred tanks. *Canadian Journal of Chemical Engineering, 80*(4), 558-565.

Bertrand, F., Tanguy, P. A., & Thibault, F. (1997). A three-dimensional fictitious domain method for incompressible fluid flow problems. *International Journal for Numerical Methods in Fluids, 25*(6), 719-736.

Bigio, D., & Baim, W. (1991). Study of the mixing abilities of the NITSE using a Newtonian fluid. *SPE ANTEC Tech. Papers*, 146-148.

Bigio, D., & Stry, W. (1990). Measures of mixing in laminar flow. *Polymer Engineering & Science, 30*(3), 153-161.

Bonnot, S., Cabaret, F., Fradette, L., & Tanguy, P. A. (2007). Characterization of mixing patterns in a coaxial mixer. *Chemical Engineering Research and Design, 85*(8 A), 1129-1135.

Booy, M. L., & Kafka, F. Y. (1987). Isothermal Flow of Viscous Liquids in the Mixing Section of a Buss Kneader. *SPE ANTEC Tech. Papers*, 140-145.

Bravo, V. L., Hrymak, A. N., & Wright, J. D. (2004). Study of particle trajectories, residence times and flow behavior in kneading discs of intermeshing co-rotating twin-screw extruders. *Polymer Engineering & Science, 44*(4), 779-793.

Brown, D. A. R., Jones, P. N., & Middleton, J. C. (2004). Experimental Methods. In E. L. Paul, V. A. Atiemo-Obeng & S. M. Kresta (Eds.), *Handbook of Industrial Mixing: Science and Practice* (pp. 145-256). Hoboken, N.J.: John Wiley & Sons.

Brzoskowski, R., Kumazawa, T., & White, J. L. (1989). Modelling flow in mixing section of a KoKneader (Buss). *SPE ANTEC Tech. Papers*, 54-58.

Brzoskowski, R., Kumazawa, T., & White, J. L. (1991). A Model of Flow in the Mixing Section of the List Kokneader. *International Polymer Processing, 6*(2), 136-142.

Cabaret, F., Bonnot, S., Fradette, L., & Tanguy, P. A. (2007). Mixing time analysis using colorimetric methods and image processing. *Industrial and Engineering Chemistry Research, 46*(14), 5032-5042.

Campolo, M., Sbrizzai, F., & Soldati, A. (2003). Time-dependent flow structures and Lagrangian mixing in Rushton-impeller baffled-tank reactor. *Chemical Engineering Science, 58*(8), 1615-1629.

Carneiro, O. S., Poulesquen, A., Covas, J. A., & Vergnes, B. (2002). Visualisation and analysis of the flow along the kneading block of a twin-screw extruder. *International Polymer Processing, 17*(4), 301-308.

Coesnon, B., Heniche, M., Devals, C., Bertrand, F., & Tanguy, P. A. (2008). A fast and robust fictitious domain method for modelling viscous flows in complex mixers: The example of propellant make-down. *International Journal for Numerical Methods in Fluids, 58*(4), 427-449.

Danckwerts, P. V. (1953). Continuous-flow systems. Distribution of residence times. *Chemical Engineering Science, 2*(1), 1-13.

Elemans, P. H. M. (2009). Modelling of the Co-Kneader. In I. Manas-Zloczower (Ed.), *Mixing and compounding of polymers: theory and practice* (2nd ed., pp. 419-448). Munich: Hanser.

Elemans, P. H. M., & Meijer, H. E. H. (1990). On the modeling of continuous mixers. Part II. The cokneader. *Polymer Engineering & Science, 30*(15), 893-904.

Fangary, Y. S., Barigou, M., Seville, J. P. K., & Parker, D. J. (2000). Fluid trajectories in a stirred vessel of non-Newtonian liquid using positron emission particle tracking. [Article]. *Chemical Engineering Science, 55*(24), 5969-5979.

Fradette, L. (1999). *Étude de dispersion dans un mélangeur statique Sulzer SMX.* Ph.D., École Polytechnique de Montréal, Canada.

Freedman, D., & Diaconis, P. (1981). On the histogram as a density estimator: L_2 theory. *Probability Theory and Related Fields, 57*(4), 453-476.

Glowinski, R., Pan, T. W., & Periaux, J. (1994). A Fictitious Domain Method for Dirichlet Problem and Applications. *Computer Methods in Applied Mechanics and Engineering, 111*(3-4), 283-303.

Guntzburger, Y., Fradette, L., Farhat, M., Heniche, M., Tanguy, P. A., & Takenaka, K. (2009). Effect of the geometry on the performance of the Maxblend impeller with viscous Newtonian fluids. *Asia-Pacific Journal of Chemical Engineering, 4*(5), 528-536.

Heniche, M., & Tanguy, P. A. (2006). A new element-by-element method for trajectory calculations with tetrahedral finite element meshes. *International Journal for Numerical Methods in Engineering, 67*(9), 1290-1317.

Heniche, M., Tanguy, P. A., Reeder, M. F., & Fasano, J. B. (2005). Numerical investigation of blade shape in static mixing. *AIChE Journal, 51*(1), 44-58.

Hoppe, S., Detrez, C., & Pla, F. (2002). Modeling of a cokneader for the manufacturing of composite materials having absorbent properties at ultra-high-frequency waves. Part 1: Modeling of flow from residence time distribution investigations. *Polymer Engineering & Science, 42*(4), 771-780.

Iranshahi, A., Devals, C., Heniche, M., Fradette, L., Tanguy, P. A., & Takenaka, K. (2007). Hydrodynamic characterization of the Maxblend impeller. *Chemical Engineering Science, 62*(14), 3641-3653.

Ishikawa, T., Amano, T., Kihara, S.-I., & Funatsu, K. (2002). Flow patterns and mixing mechanisms in the screw mixing element of a co-rotating twin-screw extruder. *Polymer Engineering & Science, 42*(5), 925-939.

Jaffer, S. A., Bravo, V. L., Wood, P. E., & Hrymak, A. N. (2000). Experimental validation of numerical simulations of the kneading disc section in a twin screw extruder. *Polymer Engineering & Science, 40*(4), 892-901.

Jakopin, S., & Franz, P. (1983). *Flow behavior in continuous kneader and its effect on mixing.* AIChE Annual Meeting, Washington, DC, USA.

Joo, J. W., & Kwon, T. H. (1993). Analysis of residence time distribution in the extrusion process including the effect of 3-d circulatory flow. *Polymer Engineering & Science, 33*(15), 959-970.

Kiared, K., Larachi, F., Guy, C., & Chaouki, J. (1997). Trajectory length and residence-time distributions of the solids in three-phase fluidized beds. *Chemical Engineering Science, 52*(21-22), 3931-3939.

Levenspiel, O. (1999). *Chemical reaction engineering* (3rd ed.). New York: Wiley.

List, H. (1950). US Patent No. 2 505 125. U. S. P. Office.

Lyu, M.-Y., & White, J. L. (1995). Models of Flow and Experimental Studies on a Modular List/Buss Kokneter. *International Polymer Processing, 10*(4), 305-313.

Lyu, M.-Y., & White, J. L. (1996). Modelling of a Viscous Non-Newtonian Polymer Melt in a List/Buss Kneader and Comparison to Experiment. *International Polymer Processing, 11*(3), 208-221.

Lyu, M.-Y., & White, J. L. (1997a). Non-isothermal non-Newtonian analysis of flow in a modular list/buss kneader. *Journal of Reinforced Plastics and Composites, 16*(16), 1445-1460.

Lyu, M.-Y., & White, J. L. (1997b). Simulation of linear viscoelastic flow behavior in the Buss Kneader. *Polymer Engineering & Science, 37*(3), 623-635.

Lyu, M.-Y., & White, J. L. (1997c). Simulation of Non-Isothermal Flow in a Modular Buss Kneader and Comparison with Experiment. *International Polymer Processing, 12*(2), 104-109.

Lyu, M.-Y., & White, J. L. (1998). Residence time distributions and basic studies of flow and melting in a modular Buss Kneader. *Polymer Engineering & Science, 38*(9), 1366-1377.

Lyu, M.-Y., & White, J. L. (2000). Simulation of non-linear viscoelastic flow behavior in the Buss Kneader. *Journal of Reinforced Plastics and Composites, 19*(10), 756-791.

Ma, X., Geng, X., & Zhu, L. (2003). Study on the characteristic of axial circular flow field in co-rotating twin screw extrusion. *SPE ANTEC Tech. Papers*, 142-146.

Manas-Zloczower, I. (1994). Studies of mixing efficiency in batch and continuous mixers. *Rubber Chemistry and Technology, 67*(3), 504-528.

Manas-Zloczower, I. (2009). Continuous process visualization: visual observation, on-line monitoring, model-fluid extrusion and simulation. In I. Manas-Zloczower (Ed.), *Mixing and compounding of polymers: theory and practice* (2nd ed., pp. 473-576). Munich: Hanser.

Mavros, P. (2001). Flow visualization in stirred vessels - A review of experimental techniques. *Chemical Engineering Research & Design, 79*(A2), 113-127.

Mehranpour, M., Nazokdast, H., & Dabir, B. (2002a). Computational study of the velocity field in the conveying element of a Ko-Kneader with CFD method. *International Polymer Processing, 17*(2), 108-114.

Mehranpour, M., Nazokdast, H., & Dabir, B. (2002b). Estimation of residence time distribution in two elements of a Ko-Kneader. *International Polymer Processing, 17*(1), 22-25.

Mehranpour, M., Nazokdast, H., & Dabir, B. (2003a). Computational study of velocity field in the KE element of a modular Ko-Kneader with CFD method. *International Polymer Processing, 18*(4), 330-337.

Mehranpour, M., Nazokdast, H., & Dabir, B. (2003b). Prediction of residence time distribution in EZ and KE element of a Ko-Kneader by using CFD method. *International Polymer Processing, 18*(4), 327-329.

Mehranpour, M., Nazokdast, H., & Dabir, B. (2004). Prediction of residence time distribution for different screw configurations of a Ko-Kneader by using a cluster model. *International Polymer Processing, 19*(1), 13-15.

Metzner, A. B., & Otto, R. E. (1957). Agitation of non-newtonian fluids. *Chemical Engineering Progress, 3*(1), 3-10.

Nauman, E. B. (1991). On residence time and trajectory calculations in motionless mixers. *Chemical Engineering Journal, 47*(3), 141-148.

Nauman, E. B. (2008). Residence Time Theory. *Industrial & Engineering Chemistry Research, 47*(10), 3752-3766.

Nauman, E. B., & Buffham, B. A. (1983). *Mixing in continuous flow systems*. New York: Wiley.

Pinto, G., & Tadmor, Z. (1970). Mixing and Residence Time Distribution in Melt Screw Extruders. *Polymer Engineering & Science, 10*(5), 279-288.

Rauline, D., Tanguy, P. A., Le Blévec, J. M., & Bousquet, J. (1998). Numerical investigation of the performance of several static mixers. *The Canadian Journal of Chemical Engineering, 76*(3), 527-535.

Rauwendaal, C. (1991a). Mixing in single-screw extruders. In C. Rauwendaal (Ed.), *Mixing in polymer processing* (pp. 129-239). New York: Marcel Dekker.

Rauwendaal, C. (1994). *Polymer Extrusion* (3rd ed.). New York: Hanser.

Rauwendaal, C. (1998a). *Polymer mixing: a self-study guide*. New York: Hanser.

Rauwendaal, C. (1998b). *Understanding extrusion*. Munich: Hanser.

Rauwendaal, C. (2009). Mixing in Single-Screw Extruders. In I. Manas-Zloczower (Ed.), *Mixing and compounding of polymers: theory and practice* (2nd ed., pp. 853-945). Munich: Hanser.

Rauwendaal, C. (Ed.). (1991b). *Mixing in Polymer Processing*. New York: Marcel Dekker.

Sakai, T. (2009). Intermeshing Twin Screw Extruders. In I. Manas-Zloczower (Ed.), *Mixing and compounding of polymers: theory and practice* (2nd ed., pp. 981-1017). Munich: Hanser.

Sanchez, R., Bigio, D. I., & Karnik, S. (1997). Mixing of a low molecular weight additive in a co-rotating twin screw extruder: Visualization of the flow path. *SPE ANTEC Tech. Papers*, 3724-3729.

Shimazaki, H., & Shinomoto, S. (2007). A Method for Selecting the Bin Size of a Time Histogram. *Neural Computation, 19*(6), 1503-1527.

Shon, K., Bumm, S. H., & White, J. L. (2008). A comparative study of dispersing a polyamide 6 into a polypropylene melt in a Buss Kneader, continuous mixer, and modular intermeshing corotating and counter-rotating twin screw extruders. *Polymer Engineering & Science, 48*(4), 756-766.

Shon, K., Chang, D., & White, J. L. (1999). A comparative study of residence time distributions in a kneader, continuous mixer, and modular intermeshing co-rotating and counter-rotating twin screw extruders. *International Polymer Processing, 14*(1), 44-50.

Shon, K., Liu, D., & White, J. L. (2005). Experimental studies and modeling of development of dispersion and fiber damage in continuous compounding. *International Polymer Processing, 20*(3), 322-331.

Shon, K., & White, J. L. (1999). Comparative study of fiber breakage in compounding glass fiber-reinforced thermoplastics in a Buss Kneader, modular co-rotating and counter-rotating twin screw extruders. *Polymer Engineering & Science, 39*(9), 1757-1768.

Stade, K. (1977). Techniques for Compounding Glass Fiber-Reinforced Thermoplastics. *Polymer Engineering & Science, 17*(1), 50-57.

Stade, K. (1978). Production of Glass Fiber-Reinforced Poly(Butylene Terephthalate) on a Continuous Kneader. *Polymer Engineering & Science, 18*(2), 107-113.

Tadmor, Z., Broyer, E., & Gutfinger, C. (1974). Flow analysis network (FAN)—A method for solving flow problems in polymer processing. *Polymer Engineering & Science, 14*(9), 660-665.

Tadmor, Z., & Gogos, C. G. (1979). *Principles of polymer processing*. U.S.: John Wiley & Sons.

Tadmor, Z., & Gogos, C. G. (2006). *Principles of polymer processing* (2nd ed.). Hoboken, N.J.: Wiley-Interscience.

Todd, D. B. (1987). Mixing Mechanisms for Polyoxymethylene. *SPE ANTEC Tech. Papers*, 128-132.

Troelstra, E. J. (1998). *The Buss Kneader as Polymerization Reactor for Acrylates.* PhD, University of Groningen, The Netherlands.

Troelstra, E. J., Van Lune, J., Van Dierendonck, L. L., & Janssen, L. P. B. M. (2002). Modeling of a Buss-Kneader as a polymerization reactor for acrylates. Part I: Model validation. *Polymer Engineering & Science, 42*(1), 230-239.

Villermaux, J. (1996). Trajectory Length Distribution (TLD), a novel concept to characterize mixing in flow systems. *Chemical Engineering Science, 51*(10), 1939-1946.

Wand, M. P. (1997). Data-based choice of histogram bin width. *The American Statistician, 51*(1), 59.

White, J. L., & Lyu, M.-Y. (1998). Development of the modern Buss Kneader and the study of its flow and mixing mechanisms. *Polymer - Plastics Technology and Engineering, 37*(3), 385-410.

White, J. L., Potente, H., & Berghaus, U. (2003). *Screw extrusion: science and technology*. Munich ; Cincinnati: Hanser.

Yao, W. G., Takahashi, K., Koyama, K., & Dai, G. C. (1997). Design of a new type of pin mixing section for a screw extruder based on analysis of flow and distributive mixing performance. *Chemical Engineering Science, 52*(1), 13-21.

Yao, W. G., Tanifuji, S., Takahashi, K., & Koyama, K. (2001). Mixing efficiency in a pin mixing section for single-screw extruders. *Polymer Engineering & Science, 41*(6), 908-917.

APPENDIX 1

DESIGN AND CONFIGURATION DRAWINGS

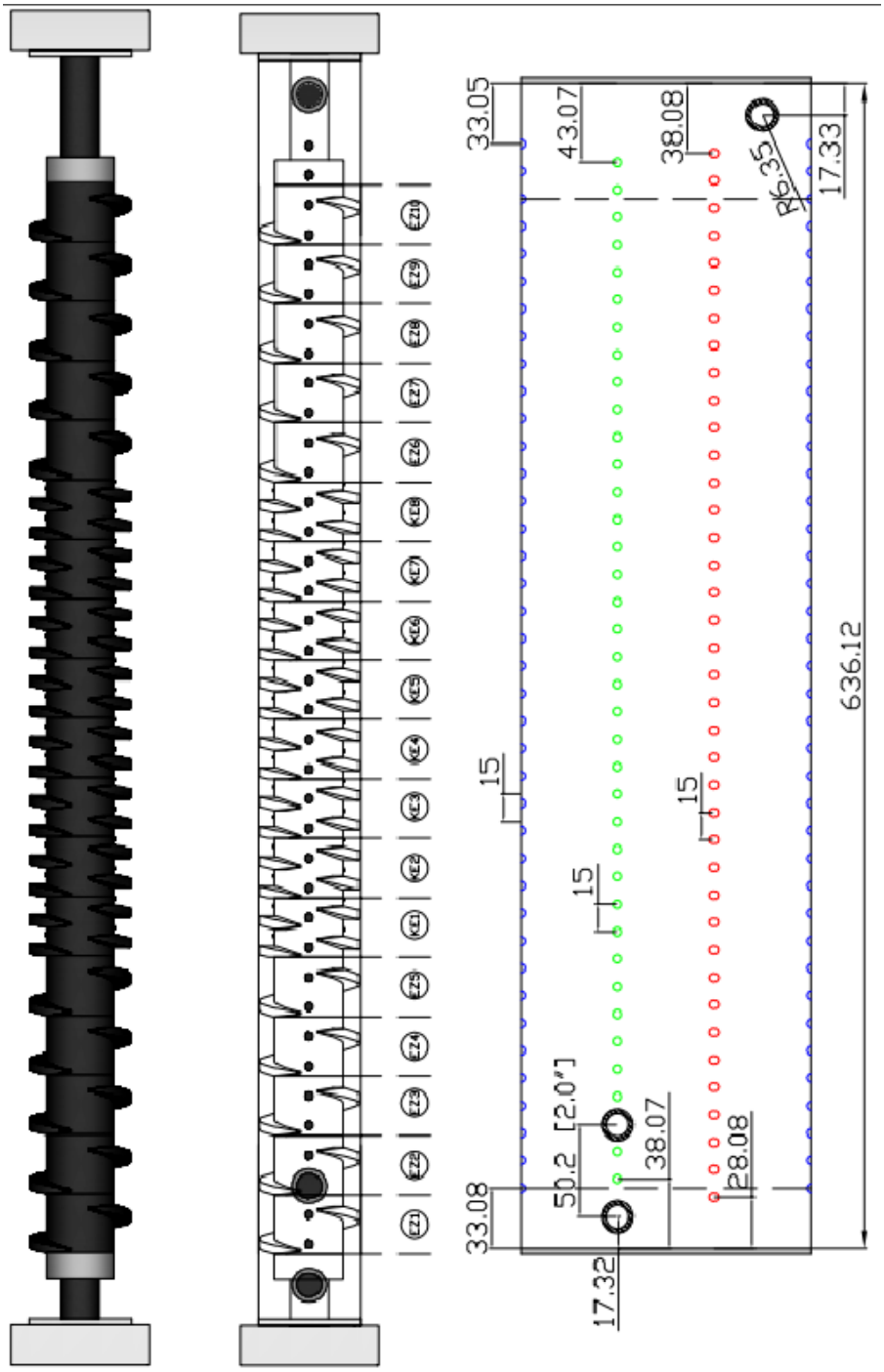

Figure A1- 1. Screw profile with unrolled barrel showing pin perforations.

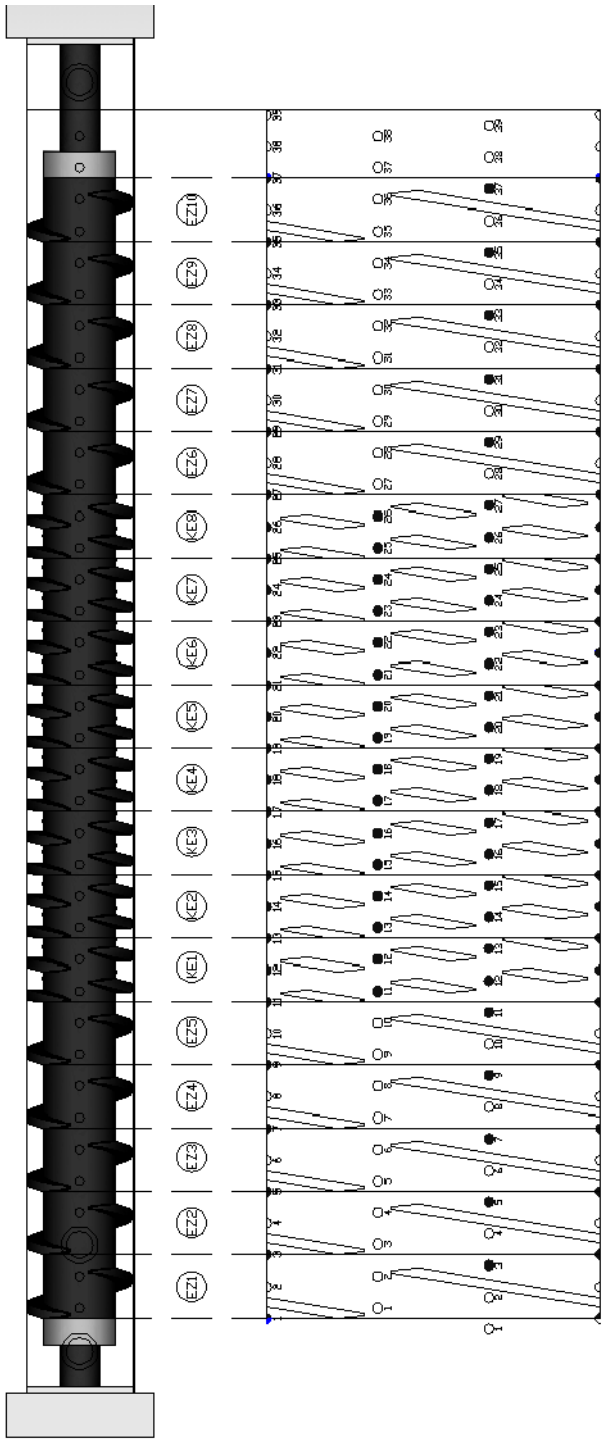

Figure A1- 2. Pins configuration.